PhD Dissertation
307

LOCATING AND PARAMETER RETRIEVAL OF INDIVIDUAL TREES FROM TERRESTRIAL LASER SCANNER DATA

Gábor Béla Brolly

The University of West Hungary (Sopron)
Roth Gyula Doctoral School of Forestry and Wildlife Management Sciences
Course Forest Assets Management (E3)

Supervisor: associate professor Dr. Kornél Czimber
Inst. of Geomatics and Civil Engineering
Dept. of Surveying and Remote Sensing

Sopron
2013

LOCATING AND PARAMETER RETRIEVAL OF INDIVIDUAL TREES FROM TERRESTRIAL LASER SCANNER DATA

Értekezés doktori (PhD) fokozat elnyerése érdekében

Írta:
Brolly Gábor Béla

Készült a Nyugat-magyarországi Egyetem Roth Gyula Erdészeti és Vadgazdálkodási Tudományok Doktori Iskola Erdővagyon-gazdálkodás programja keretében

Témavezető: Dr. Czimber Kornél egyetemi docens

Elfogadásra javasolom (igen / nem)

(aláírás)

A jelölt a doktori szigorlaton …......... % -ot ért el,

Sopron,…................................

a Szigorlati Bizottság elnöke

Az értekezést bírálóként elfogadásra javasolom (igen / nem)

Első bíráló (Dr. …...................... …..................) igen /nem

(aláírás)

Második bíráló (Dr. …...................... …..................) igen /nem

(aláírás)

(Esetleg harmadik bíráló (Dr. …...................... …..................) igen /nem

(aláírás)

A jelölt az értekezés nyilvános vitáján…...........% - ot ért el

Sopron,

………………………...
a Bírálóbizottság elnöke

A doktori (PhD) oklevél minősítése…................................

………………………..
Az EDT elnöke

Table of contents

Abstract / Kivonat

The thesis introduces algorithms developed by the author allowing highly automated processing of terrestrial laser scanner data recorded in uneven-aged, temperate forests with multiple canopy layers and undergrowth. The extraction of tree positions is achieved in irregular as well as in regular data structures of two and three dimensions using a clustering technique and the concept of disconnected image objects. The two-dimensional methods deliver the parametric models of the stems' cross-section, while the three-dimensional ones reveal the complete tree structure through a regular grid model. The models provide means for the estimation of essential tree metrics, such as stem diameter at breast height, tree height and horizontal crown projection area. The algorithms were validated with laser scans captured in stands of close-to-nature conditions. The algorithms provide a tool for tree locating and parameter retrieval even in the presence of low vegetation; furthermore, the mapping can be extended to the juvenile trees within the regeneration patches. The algorithms have potential in supporting forest inventories and in providing an objective data pool for scientific studies on forest dynamics.

Az értekezés olyan saját fejlesztésű eljárásokat mutat be, melyek többkorú, szintezett, aljnövényzettel rendelkező faállományokban is lehetővé teszik földi lézeres letapogatással felmért fák adatainak magas fokon automatizált feldolgozását. A faegyedek azonosítása síkbeli és térbeli, valamint szabályos és szabálytalan adatmodelleken történik az adatok particionálásával, valamint nem folytonos képi objektumokon végzett alakfelismeréssel. A síkbeli eljárások az azonosított faegyedek törzsének keresztmetszetének parametrikus leírását szolgáltatják, míg a térbeliek a fa szerkezetének térbeli rácsmodelljét (voxel modelleket). A modellek alapján a mellmagassági átmérő, a famagasság, és a koronavetületet mint a faegyedek legfontosabb mennyiségi állapotjellemzői határozhatók meg. Az eljárások tesztelése természetszerű állapotú faállományokban készült felmérések adatain történt. A javasolt eljárásokkal a fák térképezése aljnövényzet jelenlétében is hatékonyan elvégezhető, továbbá kiterjeszthető az újulati foltokban található egyedekre is. Az eljárások hatékonyan segíthetik az erdőleltározást, valamint objektív alapadatokat nyújthatnak az erdődinamikai vizsgálatokhoz.

1. Introduction

Tree maps depict the location of trees in a cartographic projection system and optionally other attributes at an individual level, resulting in a combination of spatial and biophysical features in a geographic information system. Tree models can be regarded as the extension of tree maps as they resemble the size and shape of the objects in addition to their positions, allowing direct estimation of structure-related tree metrics. Tree maps and tree models are increasingly used in fields of applications as diverse as forest inventory, forest monitoring, civil engineering, as well as the simulation of forest dynamics. However, the surveying of vegetation introduces many specific requirements, and thus data acquisition and processing is still challenging over forested areas.

Terrestrial laser scanning is an active remote sensing technology that provides coordinates of the surface of objects by laser range finding in a regular pattern with a high sampling density. It has the ability to acquire some millions of surface point coordinates with positional accuracy of a few millimetres within an area of 0.01−1 hectare per scanning positions in forested environment. Because of 3D data acquisition principle, the processing workflow can be automated to a high degree. Efficient data acquisition in combination with automatic processing offers a powerful solution for tree mapping and parameter retrieval. Automated processing protocols have the additional advantage of being objective and repeatable, which makes them promising for forest inventory and monitoring systems of regional scale. As the laser scans provide data on tree structure with high sampling density, structural parameters can be achieved that exceed the possibilities of the present dendrometric devices. Consequently, the use of terrestrial laser scanner data has good prospects for describing complex forest structures, such as close-to-nature stands, and forest reserves. Nevertheless, commercially available software packages have been developed for extracting models of artificial objects within urbanized environments, but have limitations in processing the laser scanner data recorded in forested areas. In order to exploit the advantages of terrestrial laser scanning in tree mapping, specific algorithms need to be optimised for the detection and modelling of trees.

This thesis introduces algorithms developed by the author, which aim to automate tree locating and individual tree parameter retrieval from terrestrial laser scans. The algorithms are optimized for diverse structural characteristics, such as uneven-aged, multi-layered, mixed stands including regrowth patches. In addition to the survey of old-growth trees and the assessment of standard parameters (stem diameter and tree height), algorithms for detecting juvenile trees and for estimates of individual crown projection area are presented. The algorithms resulted in 2D parametric models of stem cross-sections and 3D grid models of the complete trees, from which the positions and biophysical attributes can be directly estimated. The performance of the algorithms in terms of detection reliability and estimation accuracy was validated on test sites established in Hungarian forests with diverse stand structure.

2. Literature overview

2.1. Laser scanning

Laser scanning or LiDAR (Light Detection and Ranging) is an active remote sensing technology using laser range findings in regular pattern for data capture. Laser beam is characterized by high emission power, narrow beam width, well-defined frequency (monochromatic) and coherent radiation which allows for directional illumination and short pulse duration. As a result, the range finding systems have the ability of high accuracy and high measuring frequency. The wavelength used for the distance measurement is in the domain of visible light and near infrared electromagnetic radiation. The laser beam illuminates the surface of the target objects in an elliptical area called footprint. The distance between the instrument and the object can be calculated through the two-path runtime of the reflected signal. Measuring the polar and azimuthal direction of the emitted laser beam, the 3D coordinates of the reflection can be allocated in the sensor's own coordinate system.

Laser scanners are data capture devices composed of two principal components: the range finding system and the beam deflection unit. In the course of the data acquisition, the scanner samples the target object with high frequency (10–1000 kHz) measurements that resulted in a high density and spatially explicit description of the object surfaces. Spectral parameters (e.g. intensity, amplitude, beam width) can be recorded additionally that characterize the reflectance properties of the target object. The platform of the sensor can be a fixed tripod, motor vehicle, aircraft or satellite; upon which ground based or terrestrial (TLS), mobile, airborne (ALS) and spaceborne laser scanning systems are distinguished (*Figure 2-1*).

Laser scanning is subdivided further according to the ranging principle and the footprint size. The sensor alternatively records the round trip time of the pulse, the incident phase of a continuous wave, the full waveform of the reflected signal, or angles at widened laser illumination upon which pulse ranging, phase comparison, waveform analysis and triangulation-based ranging principles are distinguished (Pfeifer and Briese, 2007). In case of small footprint laser scanning, the footprint size is usually smaller than the surface of the target object. At large footprint laser scanning, the footprint radius is in the order of some ten meters so the laser beam illuminates multiple targets that cannot be separated. Spaceborne laser scanning is characterized by typically full waveform and large footprint technique, while airborne laser scanning utilizes small footprint and either pulse ranging or full waveform recording. Terrestrial laser scanners generally belong to the group of small footprint sampling instruments using pulse ranging or phase comparison principle, although some recent sensor digitize the full waveform as well. Scanners using the triangulation principle are ground-based. As they are restricted in ranging to a few metres, they are used principally indoor. The typical configurations of laser scanner systems regarding to the platform, ranging principle and footprint size are given in *Table 2-1*.

Table 2-1. Typical configurations of laser scanning systems.

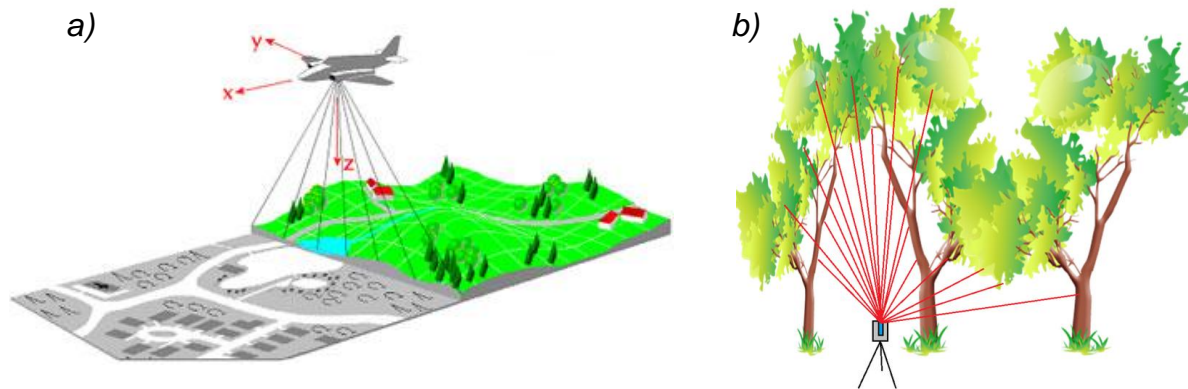| Platform	Ranging principle			Footprint	
	Pulse ranging	Phase shift	Full-waveform	Small	Large
Spaceborne			*		*
Airborne	*		*	*	
Terrestrial	*	*		*	

Figure 2-1. Examples on laser scanning from a) airborne and b) terrestrial platforms.(www.toposys.com, www.avf.forst.uni-goettingen.de)

The primary output of laser scanning is referred to as point cloud (*Figure 2-2*) containing 3D coordinates and optionally descriptive data about the reflectance properties of the target surface. The point cloud is defined in the sensor's coordinate system. If the point measurements are required to be located in a geodetic projection system or the spatial integration of data from different scans is needed, the transformation of the point cloud becomes necessary. The point cloud lacks any kind of spatial structure or explicit thematic information. The absence of the spatial structure means that the point cloud is stored as a sequential list without any explicit information on the neighbourhood relations. As a result, the number, the shape and size of the surveyed objects are unknown. In the absence of thematic information, the semantic meaning cannot be specified i.e. what the object is from which the laser beam was reflected. The point cloud is a kind of model that holds data on every surveyed object without regarding its relevance for the mapping purpose. One of the main goals in the data processing is to filter the members of the point cloud focusing on the thematic class of the targets to be mapped. The modelling of the target objects takes place following the classification procedure. The range of possible model types involves colour coded point clouds, triangulated meshes, grid models, composition of parametric surface patches, and 3D object models constructed of solid primitives. Due to the high sampling density, the models are generated ordinarily through the approximation of the point measurements. Beyond the surveying of topography, the accurate and spatially explicit models allows for revealing the structure of complex constructions and vegetated areas as well as their temporal changes (e.g. Wulder et al. (2007), Lovas et al., (2009)). Lovas et al. (2012) provide comprehensive overview on laser scanning and its applications in Hungarian.
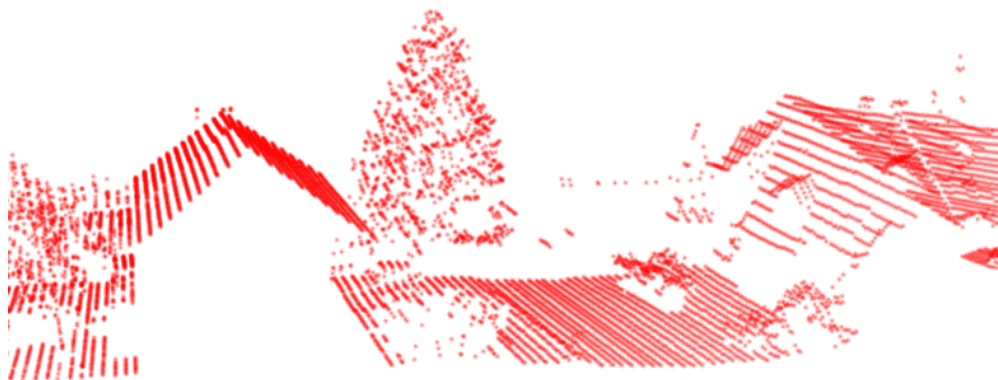

Figure 2-2. Point cloud from small footprint airborne laser scanning. (Source data: Sopron, Hungary, 2007. Captured by GEOService Ltd. Figure compiled by the author.)

9

Terrestrial laser scanning is an active remote sensing technique operating from fixed ground based position and using laser range finding with high measuring frequency to obtain directly 3D coordinates (and optionally reflectance data) of high spatial density and high accuracy from object surfaces. The general processing of the point cloud data essentially covers the georeferencing of the point measurements, filtering data with regard to the objects to be mapped, and creation of spatially detailed models with high accuracy.

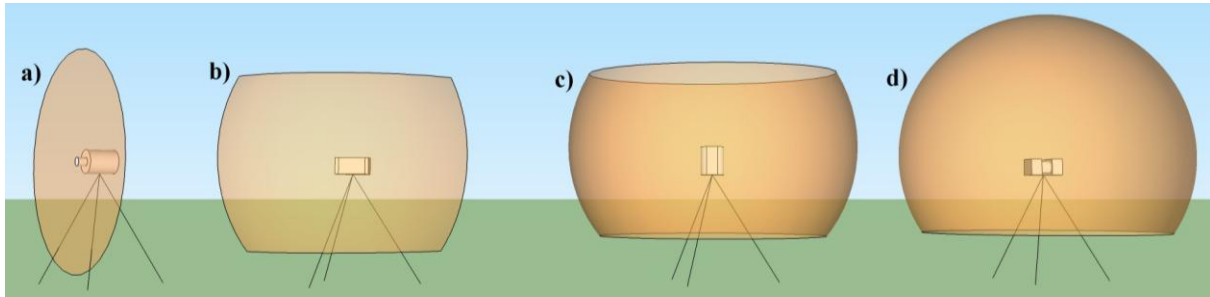## 2.2. Terrestrial laser scanners

Terrestrial laser scanners composed of two main parts: the laser range finding system and the beam deflection unit. Concerning the measurement range, object scanners and surveying scanners can be differentiated. Only the latter meets the requirements of forest-mapping purposes allowing ranging in a distance of up to some hundred meters or even more.

The widely used surveying terrestrial laser scanners use either pulse ranging or phase comparison as a range finding principle. Pulse ranging systems calculate the distance by the time span between the emission and the detection of the laser signal assuming constant propagation of the laser light. At the phase comparison technique, the emitted laser signal is a continuous wave modulated on frequency. The distance of the reflection within the range of the modulated wavelength is determined through measuring the incident phase. Range measures exceeding the wavelength of modulation are ambiguous. Practically, the instruments utilize multiple modulation wavelengths for the extension of the effective range: The incident phase of the longer wavelengths is used to resolve the phase ambiguity of the shorter ones, which resulted in accurate distance even at long-range measurements. The distinct ranging principles resulted in differences in the effective range, precision, and scanning frequency. Pulse ranging commonly provides longer effective ranging while the phase comparison technique delivers higher precision and higher measurement frequency. However, the performance of recent laser scanners using different ranging principles has been converging. Waveform digitization has not become widespread in terrestrial laser scanners so far, although a few examples are already exists. Waveform digitizing systems record the complete backscattered waveform at constant time intervals during the acquisition. It has the advantage that additional descriptive data can be derived from the reconstructed signal (Wagner, 2005). The temporal position of the target with respect to the transmitted pulse gives the absolute target range. The width of the echo provides information on the surface roughness or the direction of the target surface, while the amplitude of the echo is proportional to the target's reflectance. When the laser beam contacts with multiple targets, each of them results a peak in the recorded signal (multiple echoes).

Frölich (2004) distinguishes three types of beam deflection units with respect to sensor's field of view (*Figure 2-3*). Present classification of the instruments is limited to the typical constructions, although hybrid variants also exist.

1. Line scanners or profiling systems emit laser beams only in one direction and allocate them by a rotating mirror in the plane round about the axis. To produce a 3D point cloud, the sensor has to be moved along the direction of the axis so instruments of these types are rather applicable at mobile mapping, traffic security applications and vehicle control systems.
2. Camera view systems (frame scanners) are equipped with two oscillating or rotating mirrors, deflecting the laser light in horizontal and in vertical plane with a field of view about 60 degrees in both direction. The allocation of the laser beam in the vertical plane is called line scanning, while the horizontal one is called frame scanning.

3. Devices used to date at static terrestrial data capture are of panoramic view. Scanners of this type use similar technique for line scanning as the camera view systems, but the frame scanning is achieved by a slower rotation of the whole sensor body round about the polar instrument axis. The angle of view is full around in horizontal plane and 270–320 degree in vertical plane. Instruments having limited zenith angle enable the polar axis to be tilt in order to capture data from arbitrary part of the upper hemisphere. *Figure 2-4* illustrates the main components of a (panoramic view) laser scanner system on the example of Riegl LMS Z420i.

Figure 2-3. Scanners' field of view: (a) line scanner (b) frame scanner (c) panoramic scanner with limited upper zenith angle (d) panoramic scanner with full view over the upper hemisphere. (Illustrated by the author)

Terrestrial laser scanners optionally record spectral data characterizing the reflectivity of the target surface. The most common descriptive feature is the intensity of the reflected pulse. State-of-art instruments digitize the full waveform of the emitted and reflected laser signal. Following the waveform decomposition, multiple returns can be distinguished and the accuracy of the ranging can be enhanced by post-processing analysing of the signal waveform. In addition, the amplitude and echo width can be derived for each reflection. Numerous scanners capture RGB data simultaneously with the ranging. Some earlier devices have mount points for external digital camera, while the newer ones contain built-in camera. External cameras generally deliver images of higher quality, although they are more eccentric relative to the laser sensor. The range of the further optional extra supplies involves internal memory for on-board data recording, GNSS receiver, biaxial inclination sensor and compass for direct georeferencing, various standard interfaces (incl. WLAN, USB, Fire-wire, etc.), and colour touch screen.

1. Ranging unit
2. Laser beam
3. Rotating / oscillating mirror
4. Beam deflection unit
5. TCP/IP interface
6. Laptop
7. High resolution digital camera
8. Ethernet cable
9. Processing software
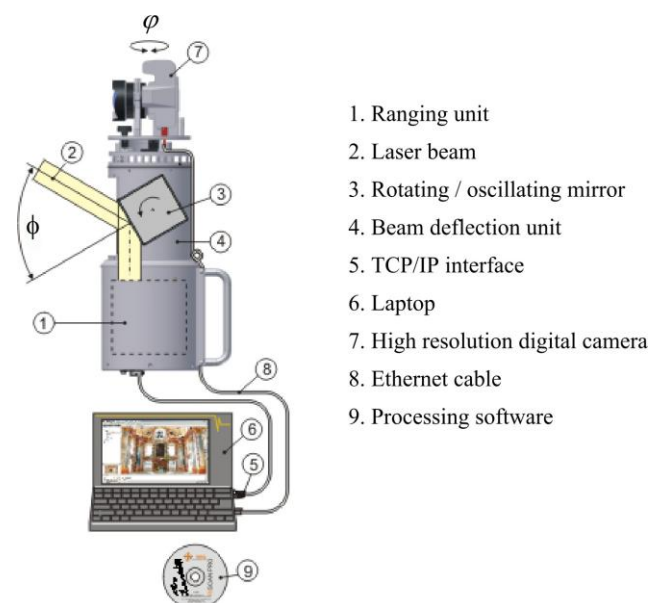
Figure 2-4. The main components of laser scanner system on the example of Riegl LMS Z420i (www.riegl.com).

Table 2-2 introduces the technical parameters of three recent TLS devices depicted in *Figure 2-5*. The sample data for the evaluation of the algorithm described in this thesis were collected using an instrument Riegl LMS Z420i that stood for a state-of-art laser scanner around 2005. The VZ 400 belongs to the subsequent generation of pulse ranging Riegl scanners. The development of the past years can be noted on the example of these two instruments through the extension of full-waveform digitization capacity, increase of the measurement rate in the order of one magnitude, the reduction in weight by 40% and the integration of GNSS receiver as well as internal memory. The third instrument, the Leica HDS 7000 is an example to an up-to-date scanner using phase comparison ranging technique. Its technical parameters reflect the main characteristic features of the phase comparison ranging principle: the higher scanning rate and the limited effective range. The precision is slightly better as it is at the pulse ranging instruments. All the instruments use eye-safe class laser so no additional equipment for protection is needed for the operation.

a)   *b)*   *c)*
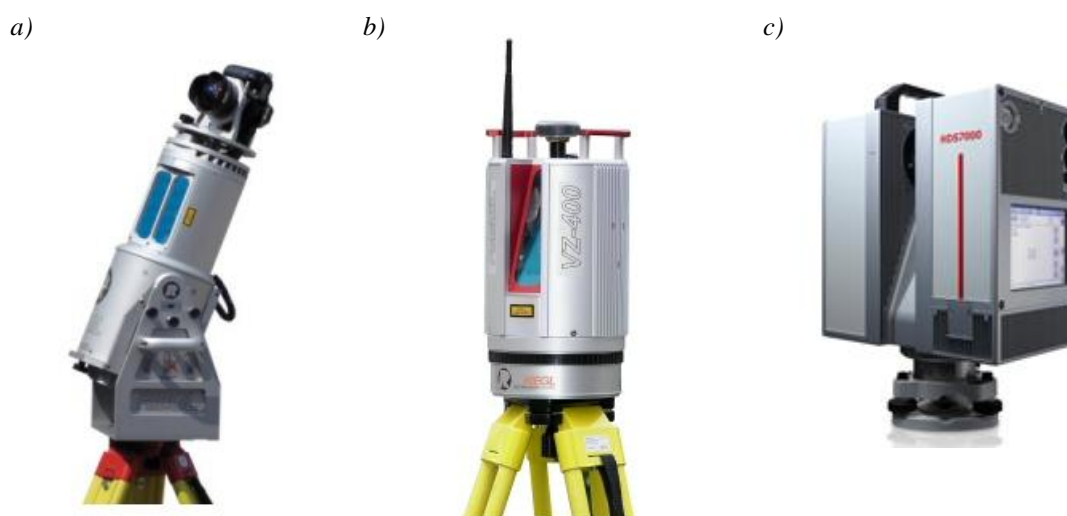
Figure 2-5. Examples on recent terrestrial laser scanners a) Riegl LMS-Z 420i (pulse ranging) b) Riegl VZ400 (pulse ranging with full waveform digitization) c) Leica HDS7000 (phase shift) (www.riegl.com, www.leica-geosystems.com).

Table 2-2. Examples on the technical parameters of recent terrestrial laser scanners (www.riegl.com, www.leica-geosystems.com).

	Riegl LMS Z420i	Riegl VZ 400	Leica HDS7000
Ranging method	Pulse ranging	Pulse ranging (full-waveform)	Phase shift
Max. Measurement range [m]	350 - 1000[1]	280 - 600[1]	187
Precision [mm]	4	3	1-3[2]
Accuracy [mm]	10	5	5
Beam divergence [mrad]	0,25	0,3	<0,3
Footprint size at 100 m [mm]	25	30	<30
Measurement rate [kHz]	8 - 11	42 - 122	1016
Line scan angle range [deg]	80	100	320
Weight [kg]	16	9.6	9.8

1: Depending on target reflectivity

2: At 50 m distance, depending on target reflectivity

From the viewpoint of forestry-related applications of terrestrial laser scanning, attention should be paid for the reduction in the effective range by up to 50% resulting from the low reflectivity and rough surface of tree bark (www.riegl.com). Scanners with effective range of at least 50 meter are required for individual tree locating. Thin twigs and leaves may cause multiple echoes that result in invalid point measurements (ghost points) in the point cloud (Bienert et al, 2006). In addition, the reflections from trees beyond the ambiguity interval of the instruments using phase comparison ranging principle raise the proportion of measurement noise. Instruments with ranging accuracy in the order of 1 cm deemed appropriate for forestry applications, which is fulfilled by almost any of the recent scanners. A more crucial parameter is the scanning rate: Trees from afar of the sensor can be interpreted better as well as the tree tops can be located with higher accuracy in a dense point cloud data. Furthermore, the higher scanning rate reduces the time of data collection that resulted in fewer ghost points at the tree crowns moved by the wind (Henning and Radtke, 2006a). Ducey et al. (2013) found that the smaller footprint size leads to better penetration through the understory vegetation, although the larger footprint size is better suited for the identification of tree tops. To provide complete sampling of the tree crown, instruments of those should be preferred that enable data capture from the entire upper hemisphere without changing the tilt angle of the polar axis. RGB data have the advantage at interpretation aiming at species classification. Additionally, low weight, built-in power supply and compact design are necessary for the effective and convenient use over rural circumstances.

Full-waveform laser scanning holds great promise for forestry applications. Echo amplitude was found to be diagnostic feature in full-waveform airborne laser scans at the estimate of mixture rate of conifers and deciduous trees in leaf-less state (Brolly and Király, 2009b). It is expected that the spectral data of the terrestrial waveform recording systems can be similarly sufficient in distinguishing groups of tree species. Beside the amplitude, the echo width has potential in tree species classification through the quantification of bark roughness. Multiple targets that are close to each other cause invalid (ghost) points because the echoes are superposed and their average range is returned. This issue may occur regardless to the type of laser ranging. Using full-waveform digitization, the echo shape indicates whether an echo originates from a single target or multiple targets, thus the number of ghost points can be suppressed. As low vegetation produce multiple echoes as well, this capability can also be efficient in their automatic filtering. Moreover, waveform digitization enables the detection of multiple echoes per pulse if the distance between the targets exceeds the minimum of multi-target resolution. With regard to forestry, multiple echo detection is prosperous for describing the fine structure of branching in the canopy. Studies on the benefit of full-waveform digitization in the field of forestry are required to verify these assumptions.

2.3. Transformation of the point cloud

The point cloud is defined by spherical coordinates (r, φ, ϕ) in the scanner's own coordinate system, where r denotes the range, φ and ϕ describe the orientation of the directed laser beam in azimuthal and polar directions respectively (*Figure 2-6*). Although the raw observables deliver polar coordinates, most software packages provide rectangular coordinates (x, y, z) as output. The relationship between the raw observables and the rectangular coordinates can be expressed as follows (Reshetyuk, 2009):

$$\begin{bmatrix} x \\ y \\ z \end{bmatrix} = r \cdot \begin{bmatrix} \cos \varphi \cdot \cos \phi \\ \sin \varphi \cdot \cos \phi \\ \sin \phi \end{bmatrix} \qquad (2\text{-}1)$$

Each point cloud is defined in the scanner's own coordinate system, so transformations are needed to combine scans recorded from different positions and to locate the merged point cloud in a superior coordinate system (e.g. Hungarian Projection System EOV). The process of transforming each local coordinate system into a common coordinate system is generally referred to as relative orientation or specifically in case of terrestrial laser scans; registration. The subsequent transformation of the combined point cloud into an earth-fixed coordinate system is achieved through the process of absolute orientation or georeferencing (Pfeifer and Briese, 2007).
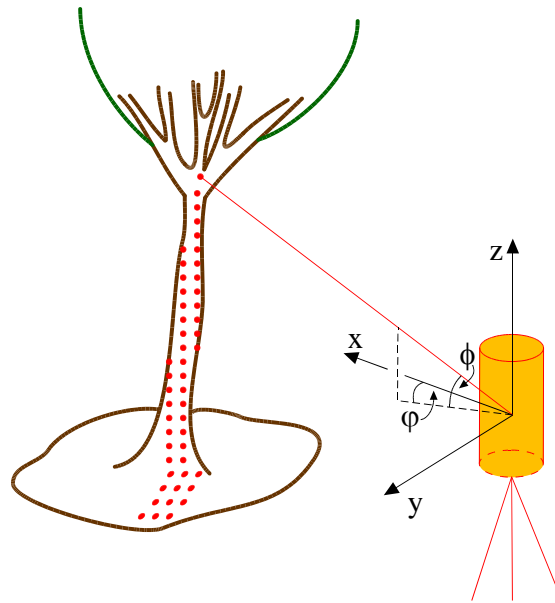

Figure 2-6. Raw observables in the sensor's own coordinate system.

Both type of orientations realized as congruency transformation that preserves the distance and angle between any of the point pairs within the same scan. The number of parameters is six including a $\mathbf{t}(\Delta x, \Delta y, \Delta z)$ translation vector and $(\omega, \varphi, \kappa)$ rotation angles around each axis of the local sensor coordinate system. Let denote $\mathbf{p_i}(x_i, y_i, z_i)$ local coordinates of the i-th element in the point cloud, $\mathbf{p_i}$ the coordinates in the target reference system, $\mathbf{R}$ the rotation matrix and $\mathbf{t}$ the translation vector. The formula for the transformation is the following (Henning and Radtke, 2007):

$$\mathbf{p_i} = \mathbf{R} \cdot \mathbf{p_i} + \mathbf{t} \qquad (2\text{-}2)$$

In the course of registration, the parameters $\mathbf{R}$ and $\mathbf{t}$ are computed by tie points i.e. matching point pairs from the overlapping regions of the scans. The minimal number of tie points is three, but the more points are included in the registration the higher reliability can be achieved. The object function, according to the least squares adjustment, is the following:

$$\sum_{i=1}^{n} \left| \mathbf{p_i} - \mathbf{q_i} \right|^2 = MIN \tag{2-3}$$

Where $n(\geq 3)$ denotes the number of tie point pairs, and $\mathbf{q_i}$ denotes the i-th matched point in the target coordinate system. Tie points are represented by artificial reflectors or characteristic objects that can be identified in different point clouds.

Reflectors are special markers with circular, cylindrical or spherical shape and high reflectivity (*Figure 2-7*). The measurements on the reflectors can be detected automatically by selecting the points with extremely high intensity. Alternatively, markers with spherical shape are available that can be identified automatically through their geometric features. Applying least squares surface fitting, the shape of the reflector can be modelled accurately allowing the exact location of its centre. Reflectors have to be established at the overlapping area of the scans in evenly distributed arrangement prior the data collection. Registration via reflectors can be applied almost under all circumstances including forest surveys. The drawback of this method is that the reflectors are accessible only up to a few meters height above the ground, thus they unable to guarantee alignment in the higher regions of the crown.
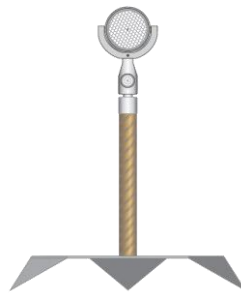
Figure 2-7. Target object for registration of scans. (www.riegl.com)

The other group of registration methods extracts matching points automatically from the overlapping part of two point clouds. The most popular algorithm for the calculation of the registration parameters is the Iterative Closest Point Algorithm (ICP, *Figure 2-8*) that minimizes the sum of squared distance between the closest points of two scans (Agca, 2007). The groups of corresponding points are unknown beforehand so coarse registration is needed as an initialization. The algorithm involves new matching point groups in each of the iterations, refines the registration parameters then transforms the point cloud to be adjusted using the updated parameters. The corresponding point groups are extracted by searching for planar surfaces or similarities in the intensity values. The recently used variants of the ICP accomplish local plane fitting at first and continue minimizing the discrepancy between the points and the corresponding planes. Using hierarchic approach, by selecting the appropriate planar surfaces in coarse-to-fine manner, speeds up the process. The ICP is a powerful technique therefore; it is implemented in many of the point cloud processing software packages. Although, its use is limited in forested scenes, especially at the height of tree crowns due to the difficulties of extracting appropriate planar surfaces within the canopy.

Object-based registration procedures are evolved from the ICP algorithm so they can be regarded as its extension. These algorithms recognize the corresponding point groups as edges, corners, cylindrical, conical or spherical surfaces. The orientation parameters are calculated through iterative alignment of the corresponding objects. Object-based registration can be utilized in scenes where most of the scanned objects are artificial constructions with smooth surface and regular shape. The use of classic object-based registration techniques have strong limitations over forested areas as the algorithm can not match the surface points of

trees (piLine, 2009). Henning and Radtke (2007), and Huang et al (2011) developed automatic object-based registration methods optimized for forest scenes. The algorithms detect point measurements from the stem surfaces in each scan. The stem points were split into 1 m height intervals, which resulted in horizontal stem slice sections. A circle was fitted by least squares adjustment onto each stem slice section. The matching circles were selected upon the similarity in diameter. The orientation parameters were calculated through the ICP algorithm using the corresponding circle centres as input data. This approach resulted in precise image alignments up to approximately 20 meters above the ground, with an average post-registration error of 0.16 cm.
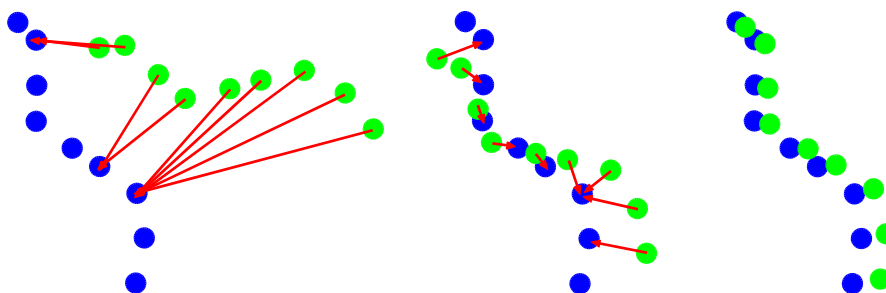
Figure 2-8. Concept of the ICP algorithm illustrated in three iterative steps. (Adapted from Pfeifer, 2007)

The process of georeferencing is similar to that of the registration in the sense it computes the parameters of a congruency transform as well. The indirect solution of georeferencing needs control points with coordinates defined in the superior reference system. The control points are marked in the field with the same type of reflectors as it was mentioned at the tie points. Direct georeferencing can be applied with instruments that have the ability to locate the absolute position, azimuth and inclination of the sensor. The position and attitude of the scanner is measured by a GNSS receiver coupled with biaxial inclination sensor. The azimuth can be estimated by compass or using a pair of GNSS sensors equipped on a fixed base. Deviation of the stand axis from the vertical, defined by the local gravity field, may be observed and corrected with an electronic spirit level. Although direct georeferencing has the highest degree of automation, it has not come into wide use so far because of its limited accuracy (Berényi, 2011). However, this technique could be convenient for applications in forested areas where surveying base points are usually not available near the scanner position.

2.4. Data structures

2.4.1. Dimensions and data types

Models represent objects with respect to relevant aspects. Our models aimed at describing the components of a forest scene, typically the ground surface and the structure of the vegetation with specific regard to the position, size and shape of the trees.

The expression data type refers to the storage form of the geodata set that can be either regular or irregular. The spatial information content is stored as vector coordinates in case of irregular storage format. Point coordinates have no extent thus the distance between the neighbours can be arbitrary allowing representation of irregular patterns. The regular spatial structure resulted in well-defined neighbourhood relations as the data stored as an array of small cells with identical size and shape. Both data type can have spatial extent in two or three dimensions.

Most of the laser scans are stored with rectangular coordinates in irregular pattern so the primary storage structure of the point cloud is a type of 3D vector. It is convenient to reduce the number of dimensions from three to two by creating a thin horizontal subset where the
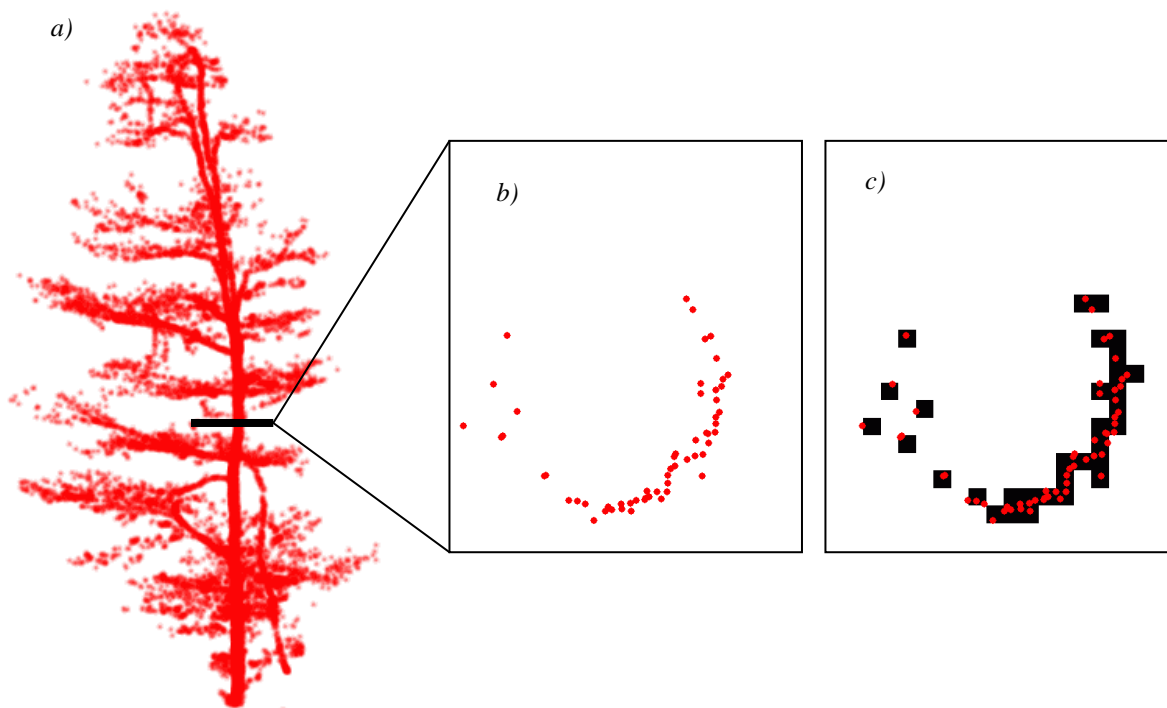
height difference of the points is not significant (*Figure 2-9*). In this case, the height coordinates can be neglected in the course of processing that simplifies the algorithm and saves computational time.

The regular variant of the 2D vector data type is called raster. It is composed by uniform cells of equal spacing with neither overlap nor gap between the adjacent elements. The shape of the cells is squared in far the most cases, however rectangular or hexagonal structures are also possible.

Extending horizontal squared cells in the height domain, the shape of the elements turns to be cubic called voxels (volumetric pixel), while the corresponding 3D grid structure is referred to as voxel space (*Figure 2-10*). Voxel space can be interpreted as a stack of horizontal rasters of unit height. The inverse of the statement is also apprehensive: Raster is a voxel space of unit height. Regular data composed of squared cells are also named as grid structure in general including rasters and voxel spaces. Grid data can be displayed as digital images (Czimber, 1997).

Grid data are arranged in columns, rows and planes indexed by (i, j, k) non-negative integers. Each cell is located in this grid coordinate system and represented by a digital number. The spatial resolution of the grid is expressed by the cell size d. A point cloud given with vectors of (x, y, z) coordinates can be stored as a grid composed of n_i, n_j, n_k cells, where the symbol $\lceil \; \rceil$ refers to the *ceil* function:

$$n_i = \left\lceil \frac{x_{max} - x_{min}}{d} \right\rceil, \; n_j = \left\lceil \frac{y_{max} - y_{min}}{d} \right\rceil, \; n_k = \left\lceil \frac{z_{max} - z_{min}}{d} \right\rceil \tag{2-4}$$

Figure 2-9. Representation of laser scanned data a) 3D point cloud, b) horizontal subset of stem surface points and c) their representation in a binary raster. (Source data: Hidegvíz-völgy Forest Reserve, Hungary, 2006. Figure compiled by the author)
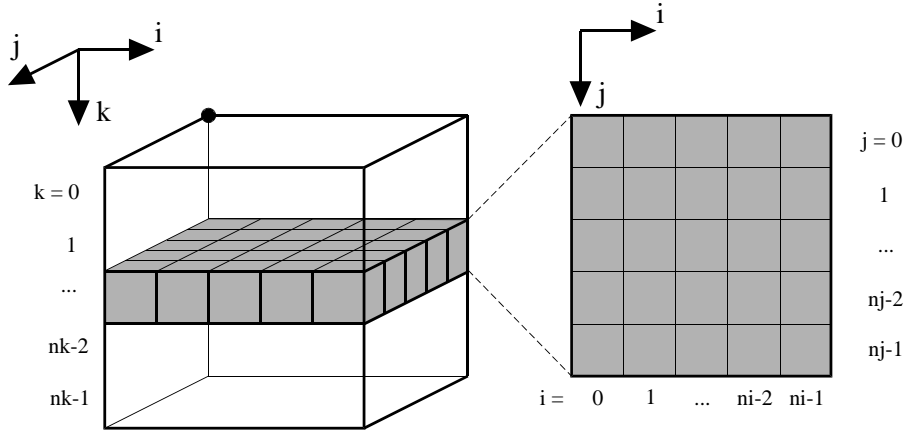
Figure 2-10. The 3D voxel space is composed of a set of 2D rasters. The cells are identified by the indices of columns (i), rows (j) and planes (k).

In a grid structure, the location of any point measurement is represented by the midpoint of the corresponding cell. If the top back left corner of the grid is georeferenced by (x_{min}, y_{max}, z_{max}) coordinates and the rows have the same orientation as the axis X, the cell indices of an arbitrary point with (x, y, z) coordinates can be calculated by the following formula, where the symbol $\lfloor \;\; \rfloor$ refers to the *floor* function:

$$i = \left\lfloor \frac{x - x_{min}}{d} \right\rfloor, \; j = \left\lfloor \frac{y_{max} - y}{d} \right\rfloor, \; k = \left\lfloor \frac{z_{max} - z}{d} \right\rfloor \qquad (2\text{-}5)$$

The corresponding relations for calculating the (x, y, z) coordinates from the midpoint of the cell (i, j, k) are as follows:

$$x = x_{min} + (i + 0{,}5) \cdot d, \; y = y_{max} - (j + 0{,}5) \cdot d, \; z = z_{max} - (k + 0{,}5) \cdot d \qquad (2\text{-}6)$$

Midpoints of the grid cells retain the original (x, y, z) coordinates with an error of $\frac{d}{2}$ at the worst case. The absolute error raised as the resultant of coordinate errors is up to $\frac{\sqrt{3}}{2} d$ that is reduced to $\frac{\sqrt{2}}{2} d$ at raster data with the omission of the height component.

Points within the area of a given raster cell (i, j, k) can be queried from the original point cloud, as the corresponding points fulfil the following system:

$$i \cdot d + x_{min} \leq x < (i+1) \cdot d + x_{min}$$

$$y_{max} - (j+1) \cdot d \leq y < y_{max} - j \cdot d \qquad (2\text{-}7)$$

$$z_{max} - (k+1) \cdot d \leq z < z_{max} - k \cdot d$$

The term 'distance' of cells (*A,B*) is generally referred to the Euclidian norm of the cells' midpoint that is computed by (2-8):

$$d_E = \sqrt{(X_B - X_A)^2 + (Y_B - Y_A)^2 + (Z_B - Z_A)^2} \;. \qquad (2\text{-}8)$$

The use of the Euclidian norm in a grid has the disadvantage that the neighbours of a cell sharing common vertex, edge or face are at different distances. Calculating the distance in Manhattan norm is often more convenient, as in this case, all the connected neighbours of a

given cell are at the same distance irrespective to their relative position (Jain et al., 1995). The Manhattan norm (or city-block distance) of two voxels is computed as (2-9):

$$d_M = |x_B - x_A| + |y_B - y_A| + |z_B - z_A| \qquad (2\text{-}9)$$

The use of Manhattan norm has the further advantage that its computation is less complicate because the Manhattan norm of two cells with integer grid coordinates yields always integer result. The set of points that are equidistant in Euclidian norm from a given point are located on a circle, while in Manhattan-norm the points are on a square.

The digital number assigned to a grid cell is interpreted as a specific attribute of the represented space or volumetric element. In the simplest case, the attribute is a binary code expressing the existence or the absence of a laser scanned point measurement within the cell by the constants 1 and 0 respectively. This kind of grid representation considers the location and neighbourhood relations of the point measurements. Extending the domain of binary codes allows for the storage of graduated data. For example, storing the counts of point measurements for each cell resulted in a point density raster, or computing the average of the intensity values per cells resulted in an intensity image. The term range image refers to raster that contain the distances of the scanner position and the closest point measurement within the corresponding grid cells (*Figure 2-11*) It may be confusing that the term range image was used as synonym expression for the point cloud in earlier studies. The colour of the reflecting surfaces is recorded by digital camera and it can be displayed using RGB code.

Figure 2-11. Range image: range data stored in a raster. Rows and columns represent constant scanner angle values. (Source data: Hidegvíz-völgy Forest Reserve, Hungary, 2006. Image compiled by the author)
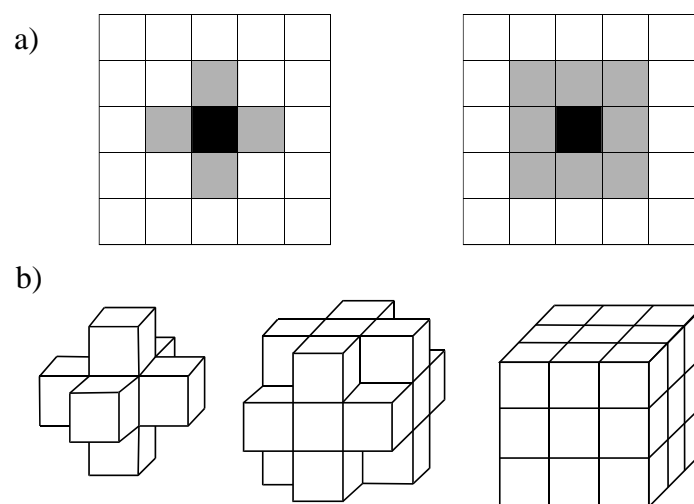
2.4.2. Image objects

The main goal of tree mapping algorithms is to detect point measurements of tree stems in the laser scanned point cloud. This can be achieved based on general geometric features such as shape and size of the point patterns. However, a single vector or a cell is only a primary element in the data set of the reflecting object and alone reveals nothing about its geometric features. To retrieve information on the shape of the objects an extended subgroup of the primary data has to be analysed with special regard to the spatial relations of its elements.

Neighbourhood relations can be defined in straightforward way at grid data structure. A raster cell has four neighbours with common cell side additionally four others at the corners. A voxel has six neighbours sharing common face; twelve sharing common edge and eight at the corners (*Figure 2-12*). A set of connected cells with similar values compose region. Delineation of regions is done according to a homogeneity criterion of cell values. A plenty of homogeneity criterion has been defined in algorithms for segmentation of remotely sensed images (e.g. Benz et al., 2004, Czimber, 2009).

The algorithms introduced in the present thesis process one-bit ('black and white') binary grids. Cells containing at least one laser point measurement are coded '1' and called signed (foreground), while the complement set of cells are coded '0' and called empty (background). A set of signed cells in connection to each other is called region in binary image processing. Delineation of regions is achieved through Connected Component Labelling algorithms (CCL) that find all regions in an image and assign a unique label to all cells in the same region (Jain et al, 1995). Image objects are regions organized in data structure that ensures unique identification for each region and enables linking attributes. The size of the smallest image object is one cell. Attributes of image objects relate to size, position, shape, and neighbourhood relations that contribute to their thematic classification.

While connected image objects cover one contiguous region of a scene, disconnected image objects can consist of several isolated parts (*Figure 2-13*). In case of disconnected image objects, the aggregation of single regions contains reasonable meaning; the coherent objects represent one physical object. Image objects can be organized into hierarchic levels, where the totality of all image objects in each level covers the entire scene. This means that all image objects on a lower level are completely contained in exactly one image object of a higher level (Baatz et al, 2004). Objects on higher levels are called aggregations (super objects). Disconnected image objects should be treated as aggregations as they contain multiple continuous regions.

Figure 2-12. Neighbourhood relations of a raster cell (a, b), and of a voxel (d–f).
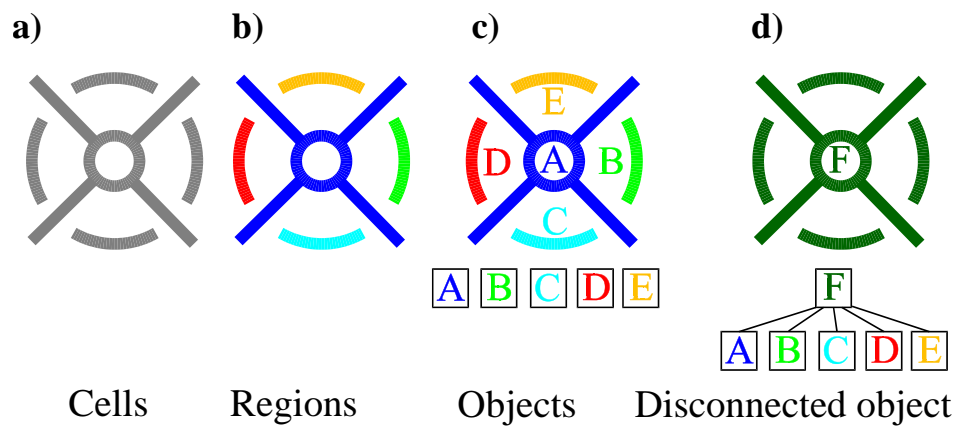
Figure 2-13. Group of binary cells (a), regions (b) and objects with unique labels A,B,C,D and E (c) composing one disconnected image object labelled with F (d).

Regions of connected image objects are the fundamental elements of binary image processing, however connected image objects can further be split to components (sub objects). Soille and Vogt (2008) presented a morphologic segmentation method that can be used for characterising binary patterns with emphasis on connections between their parts. The resulted components are classified to one of the seven categories (core region, islet, loop, bridge, perforation, edge, and branch). All the terms and idioms in relation to object-based image analysis can be extended to 3D grid data.

2.5. Processing concepts

Three main concepts have been outlined in the literature focusing on the topic of modelling trees from terrestrial laser scanner data. The concepts differ in objective (what to be modelled or estimated), scale (number of target trees), and modelling principle (physical or stochastic approach). The border between the concepts is blurred as they overlap some times to each other and there are some transient methods exist.

1. Tree mapping and estimation of attributes on individual level. The main motivations are (1) to find solutions for using TLS as an alternative technique for the automatic retrieval of classic forest inventory parameters and (2) to widen the range of descriptive data that can be used for forest management applications and ecological investigations. The data capture is typically involves several trees e.g. those that are within a forest inventory sample plot. Due to economical reasons, the surveying is often completed from a single vantage point so the algorithm should be able to manage point clouds from single and multiple scanning positions as well. Specific challenges are the filtering of vegetation points and their classification according to the individuals. The biophysical attributes are estimated through relatively simple structural models.

2. Reconstruction of tree structure. Tree models of this kind reveal the architecture of a single tree including the crown structure with high level of details. Tree models have to provide information on (1) the start point and end point of each branch and (2) radii at these points. In addition, topological models account for the branch hierarchy. To ensure complete model, the sample tree is measured from multiple scanning positions. The field of potential applications involves the reconstruction of especially valuable trees and assessment of tree volume for the improvement of local volume tables. Time series of tree models are non-destructive means for monitoring tree growth thus they suit for the purpose of ecological researches. Other studies have focused on tree models to explain the impacts of the canopy structure on gas and water exchange and

to improve the existing radiation transfer models (Cote et al., 2009). Due to the realistic structure and high level of details, these models can be utilized in software packages developed for visualization and design.

3. Retrieval of forest stand attributes on plot level. Studies of this approach are addressing the issue of parameter estimation from terrestrial laser scanner data without distinguishing individual trees in the dataset. The models rather describe the spatial distribution of the aggregated mass of wood and leaves throughout the sample space. The methods used are dominated by stochastic models and aimed at estimation of leaf area index (Henning and Radtke 2006b, Strahler et al. 2008), gap fraction (Danson et al., 2007), and biomass (Ku et al., 2012).

Present dissertation is intended to deal with tree mapping and estimation of tree metrics on individual level. Accordingly, the overview presented in the following subsections is primarily focusing on concept 1. Furthermore, it implies some studies from the field of tree reconstruction (concept 2) that deemed prospective in forestry-related parameter retrieval.

The review is organized according to the main processing steps of the workflow aiming at tree mapping and parameter estimates:
1. Generation of digital terrain model
2. Filtering of irrelevant data
3. Tree detection
4. Derivation of tree models and attributes
    a. Diameter and basal area (area of stem cross-section)
    b. Stem models
    c. Tree height
    d. Crown structure

The input data for tree mapping is practically the registered point cloud without thematic classes. If the map is required to be located in a projection system, the point cloud should be georeferenced. The digital terrain model (DTM) is necessary to make difference of point measurements from the ground and the vegetation, and to transform height coordinates into relative heights above the ground. Commercial software packages are available for the calculation of high quality DTMs that simplifies to filter vegetation points in indirect way as a complement set of terrain points. Point measurements reflected from the low vegetation or resulting from measurement errors are irrelevant from the viewpoint of tree detection, so they should be eliminated through filtering. The filtering can be regarded as a simple classification of points into 'tree' and 'non-tree' thematic classes. Detection of trees means that all the remaining vegetation points are classified so that only of those reflected from a given tree are assigned in the same class. The classification is primarily based on the spatial arrangement of data points thus the detection is closely related to the creation of a structural model, which is used for locating the position and quantifying the size and shape of the tree. The possibility for the classification of point measurements according to tree species or even species groups is strongly limited. Although Haala (2004) found differences in the point cloud with regard to tree species using fusion of laser scan and digital imagery data, the potential of the technique is hardly enough for practical use. The increasingly spread of full-waveform technique in terrestrial laser scanning is expected to be a step towards the tree species classification. Using the descriptive full-waveform information in relation to the reflectance properties and roughness of the target surface, the automatic retrieval of taxonomic groups or even health conditions seems prospective but needs experimental support. The quantitative description of the target trees is based on the creation of their structural model. The simplest models are

devoted to the estimation of stem diameter or basal area at a given height. If the domain of the models is extended in vertical range, stem models and stem metrics are revealed. Tree height can be yielded by finding the tree tops and matching them with the corresponding tree positions. Crown models generally account for the horizontal and vertical extent of the crowns as well as the hierarchic arrangement of branches.

2.6. Generation of digital terrain models

The first step of the workflow is the creation of the digital terrain model (DTM) and the related classification of points according to the reflecting surface as terrain and off-terrain measurements. Many different concepts for filtering terrain points have been proposed so far, and some of them are available in commercial software packages. For convenience, the terrain elevation is regarded as reference surface to normalize the heights of the point cloud. Hereby the heights of the objects located at distinct elevation above the ground become comparative throughout the scene. The DTM quality has primary influence on the subsequent estimation of stem diameters and tree heights. Filtering of terrain points has another aspect namely that off-terrain points are measurements from the vegetation in forested area. In fact, the complement set of terrain points will be used as input data for the detection of trees.

Filtering concepts rely on the hypothesis that points with locally low elevation relative to their neighbours are reflected from the ground because the laser light is unable to penetrate below the terrain surface. The methods used in wide range of practice have been developed for processing airborne laser scanner data; however, with some modification of their parameters they are appropriate for TLS data as well.

The most frequently used filtering concepts for DTM generation over forested areas from TLS data can be divided into three groups:

1. Filtering based on adaptive threshold
2. Progressive TIN densification
3. Surface interpolation of weighted points.

The earlier filtering methods calculate a threshold on the height coordinates upon which the actual point is either accepted or rejected as a terrain point. Basic variants of these procedures can be implemented through short scripts written in mathematical program packages. The efficiency of the adaptive thresholding is restricted by sharp edges and discontinuity of terrain points. Block minimum filters use a moving horizontal plane with a corresponding upper buffer zone that defines a region in 3D space where terrain points are expected to reside. The plane is located at points with locally the lowest elevation. Points above the buffer zone are deemed off-terrain points. The thickness of the buffer zone is needed as input data, but some more sophisticated routines consider the histogram of elevations and calculate it automatically. A structure element, describing admissible height differences depending on horizontal distance is used at morphologic filtering. The smaller the distance between a ground point and its neighbouring points, the less height difference is accepted between them. This structure element is placed at each point so off-terrain points are identified as those above the admissible height difference. The structure element itself could be determined from terrain training data. For steeper areas, higher admissible height differences are allowed (Vosselman, 2000).

The second group of filters works progressively, where more and more points are classified as ground points. The classical routine of progressive TIN densification starts by selecting some local low points as sure hits on the ground. The algorithm assumes that any areas bigger than the expected largest building have at least one hit on the ground and that the

lowest point is a ground hit. An initial model from selected low points is created. Triangles in this initial model are mostly below the ground with only the vertices touching ground. The routine then starts refining the model upwards by iteratively adding new laser points to it. Each added point makes the model follow the ground surface more closely. Iteration parameters determine how close a point must be to a triangle plane so that the point can be accepted to the model. Iteration angle is the maximum angle between point, its projection on triangle plane and closest triangle vertex (*Figure 2-14*). Iteration distance parameter makes sure that the iteration does not make big jumps upwards when triangles are large. This helps to keep low buildings out of the model (Axelson, 2000, Soininen, 2005).
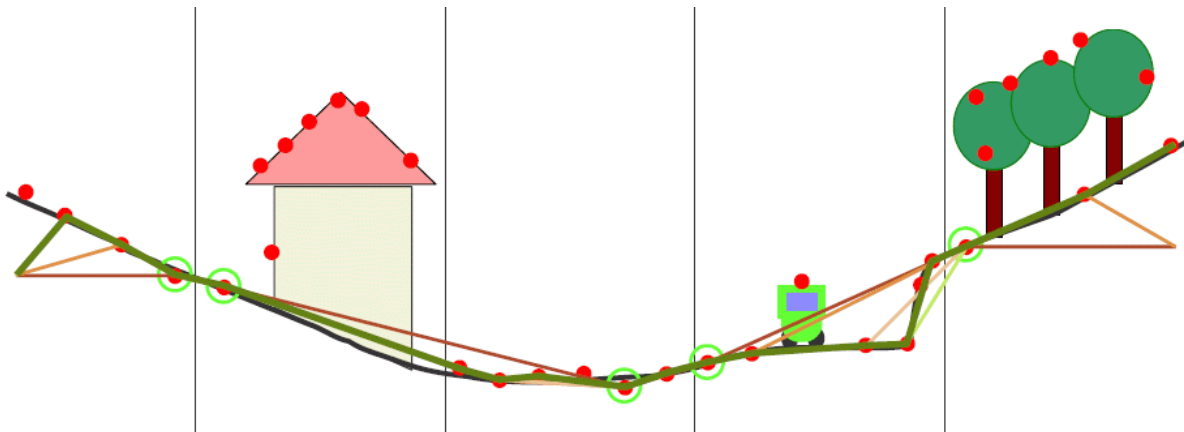

Figure 2-14. Progressive TIN densification (Mandelburger, 2005).

The third group of algorithms is based on a surface model that iteratively approaches the ground surface through the recalculation of weights for each point according to its height difference relative to the model. The algorithm Robust Filtering computes the surface with equal weights for all points (for all z-measurements) in the first step (Kraus and Pfeifer, 1998). This surface runs in an averaging way between terrain points and vegetation points. The terrain points are more likely to have negative residuals, whereas the vegetation points are more likely to have small negative or positive residuals. These residuals are used to compute weights for each measurement (*Figure 2-15*). Now, the weights can be used for the next computation (iteration) of the surface. Points with large negative residuals have maximum weights and they attract the computed surface, whereas points with medium residuals have smaller weights and less influence on the computed surface. This algorithm has been implemented within the program package SCOP++. In SCOP++, the surface is computed by subdividing it into several patches. By doing so, parameters of the weight function are set in an adaptive way for each patch. The method has been embedded in a hierarchical approach to handle extended gaps in terrain data resulted from dense vegetation or large buildings (*Figure 2-16*).
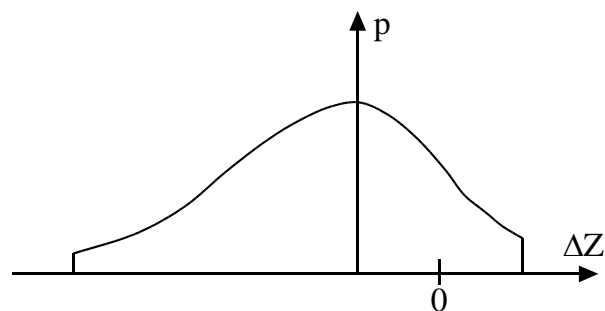

Figure 2-15. Weight function for filtering terrain points.(Kraus and Pfeifer, 1998)
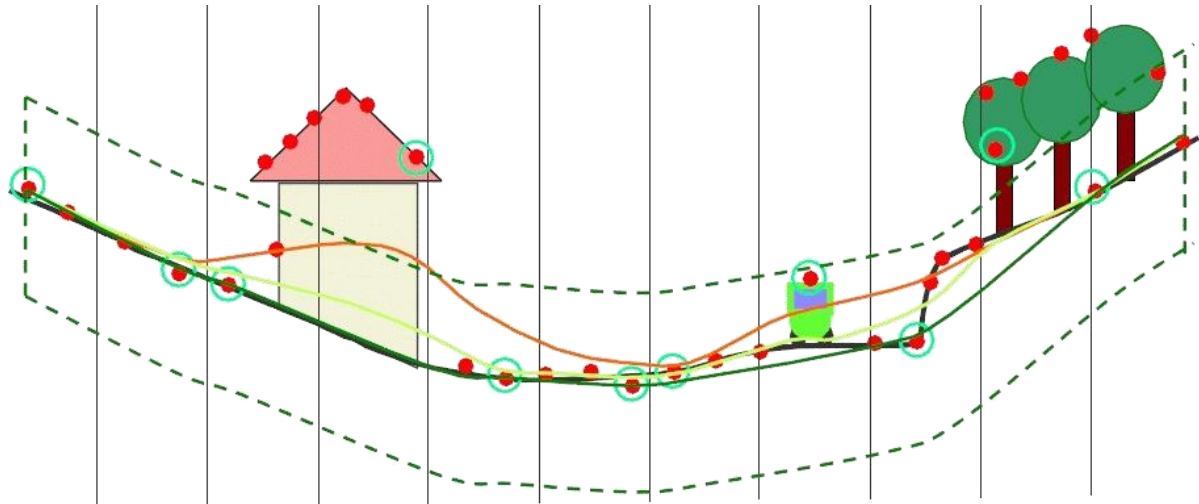
Figure 2-16. Iterative refinement of the ground surface by weighted points (Mandelburger, 2005).

The concept of Active Contours (Snakes) has its roots in the digital image processing. In general, the shape of an active contour is the solution of parameterization that minimizes an energy function that includes internal energy and a potential field. The internal energy is described using physical characteristics associated with the contour, usually material properties like elasticity and rigidity. The potential field is given by the height data. The contour used in this case acts like a sticky rubber cloth or a rubber band net that is being pulled upwards from underneath. The net is attracted by the height data points and sticks to points that are assumed to represent the true ground. The elasticity forces in the rubber band stops the net from reaching points not representing the true ground. The solution is a net that forms a continuous model of the ground surface (Elmqvist et al. 2001). Weinacker et al. (2004) modified the concept to work in hierarchic manner and implemented in software TreesVis.

2.7. Filtering of irrelevant data

The shape of the trees can be visually identified in the point cloud, although the stem surface points are surrounded by measurements of irregular pattern (*Figure 2-17*). Some of the scattered data are caused by range finding errors e.g. phase ambiguity or multiple echoes generated by partial interception. The remaining points around the trees are reflected from small or thin components of vegetation for example leaves and twigs. Due to the sparse point density relative to their extent, these reflecting objects can be interpreted neither visual nor automatic manner. Measurements from unidentifiable objects are regarded as irrelevant from the viewpoint of tree detection. Considering the irregular pattern and sparse arrangement, these measurements appear isolated especially as they are usually single points or small group of points relative afar from the stem surface points. Isolated data come into view as speckles in regular data structure. In the presence of thick undergrowth, the ratio of isolated points can exceed the ratio of stem surface measurements that may cause the failure of standard object detection techniques. Their filtering is necessary for automatic tree detection but it facilitates the visual interpretation of forest stands as well.

Points reflected from beyond the efficient ranging distance of phase-shift-based instruments appear as if they were within the ambiguity interval. Actually, these ghost points are reflected from afar so their intensity values are lower than those are of the surface points within the effective range. Ghost points from multiple echoes have alike lower intensity because of the smaller area of reflection.

Figure 2-17. Stem surface points with significant amount of data reflected from other vegetation components.
(Source data: Pro Silva demonstration site, Pilis, Hungary, 2006. Figure compiled by the author.)

Filtering ghost points can be achieved by thresholding the minimum intensity value. Schilling et al. (2011) found this technique effective, as it reduced the point number by 15–29% in advance a tree modelling procedure. According to the experience of Simonse et al (2003), natural objects never have high intensity values. This means that a very high intensity also indicates data noise when measuring in forest stands. Twigs and leaves reflect only a few laser measurements resulted in isolated points or small group of points being relative afar from their neighbours. A single point can be removed if it does not have enough neighbour within a given search radius. Due to the viewing geometry, the search radius should be increased with respect to the distance from the sensor. A commonly used gridding technique for the elimination of isolated points is to fill only the cells of those that contain point counts exceeding a given minimum value. Aschoff and Spiecker (2004) mapped the horizontal section of the point cloud into a point count raster and removed isolated points by adaptive thresholding of the minimum cell values. The routine considered the number of surveying points and summarized the potential point counts for each cell. Gorte and Pfeifer (2004) defined neighbourhood operations and filtering rules on object size (i.e. minimum cell counts) to remove isolated cells from the voxel space. Simonse et al. (2003) proposed filtering for range images assuming that neighbouring cells contain point measurements with similar distances. If a cell value extremely deviates from the value of its neighbours, it represents isolated data.

Specific filtering is needed to remove point measurements reflected from branches for the estimation of stem diameter. This holds high importance especially at conifers where dead branches remain on the lower part of the bole. As branch points are often arranged into sparse groups of linear or amorphous pattern, their local context has to be also considered. Bienert et al. (2007) developed a filtering routine for point count rasters to separate point measurements from the bole and from the branches. It can be used for single scan data knowing the nominal scan resolution and scanning position. Assuming regular scanning pattern, the theoretical maximum of point measurements can be calculated for each cell by summing up the laser beams passing through the region of the cell. Comparing the maximum and the actual point counts, cells below a distinct value were assumed to contain smaller objects then the cell size and were treated as irrelevant speckles (*Figure 2-18*).
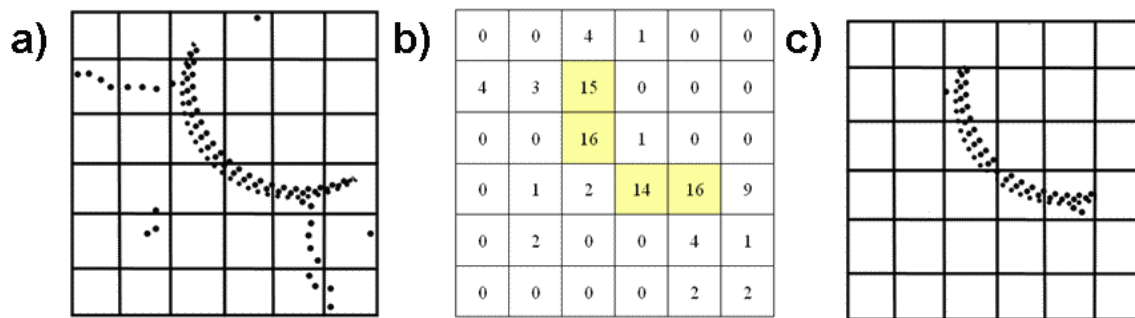
Figure 2-18. Filtering for single scans by elimination of cells with few measurements (Bienert et al, 2007). The threshold of minimum point counts is 13 per cells in this example, which was computed upon the scanning resolution and the target distance.

Litkey et al. (2008) introduced a filtering technique following the detection of tree points for conifers with vertical boles. A line was fitted to tree points along each vertical scan line using a robust approximation technique. Points that deviated from the linear trend were filtered out to remove branch points.

Although the removal of isolated points is a prerequisite for stem detection especially in the presence of undergrowth, intensive filtering might cause the elimination of tree data. Data gaps degrade the level of details and so, they result in inaccurate models. Special attention should be paid at detecting young trees with small diameter or at the removal of isolated points in the canopy; because the filtering tends to reduce the data from thin stems or twigs.

2.8. Tree detection

Detection of trees is the process of delineating point measurements of stem surfaces and assigning them to classes according to the reflecting trees. Based on the classified data, individual tree models can be created as a basis for subsequent assessment of biophysical attributes. The detection can be carried out in vector or grid data structure of either two- or three dimensions.

The goal of the tree detection in 2D is the estimation of tree position and stem diameter at the height of the horizontal data subset. Tree position is defined as the stem centre coordinates at a reference height being the same as the height of the diameter estimation. Practically, this height is 1.30 meter above the ground level in the standardized forest inventories of European countries. The object detection is carried out in the thin subset of data located at the reference height thus the difference in the vertical (z) coordinates can be omitted. Please notice, that the value of the vertical coordinates are defined in terms of elevation above the ground. Point measurements from stem surfaces form approximately circular arcs or closed circle in the horizontal subset of data depending on the number and constellation of scanning positions (*Figure 2-19*). The shadow effect from low vegetation and neighbouring trees causes data gaps or even occlusion of the trees (*Figure 2-20*). Visual interpretation on horizontal point cloud sections was used for the identification of trees and isolation of the stem surface points in early studies on forestry-related processing of terrestrial laser scans (Hopkinson et al, 2004; Watt and Donoghue, 2005). Thies and Spiecker (2004) as well as Henning and Radtke (2006a) fixed reflective tapes prior the data acquisition at the reference heights of tree stems to be mapped. The intensity values of stem surface points were significantly higher than of those reflected from other components of vegetation that allowed using a simple threshold for filtering stem points.
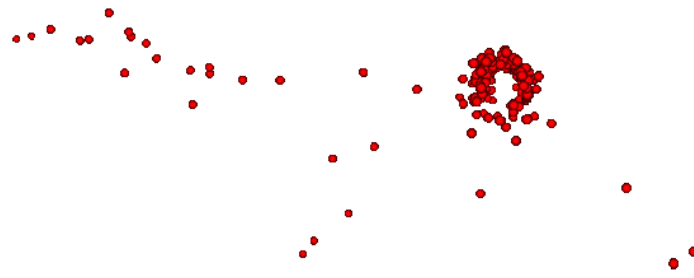
Figure 2-19. Stem surface points from multiple scanning positions in a 10 cm thick horizontal point cloud section. Isolated points have been reflected from probably branches. (Source data: Hidegvíz-völgy Forest Reserve, Hungary, 2006. Figure compiled by the author.)
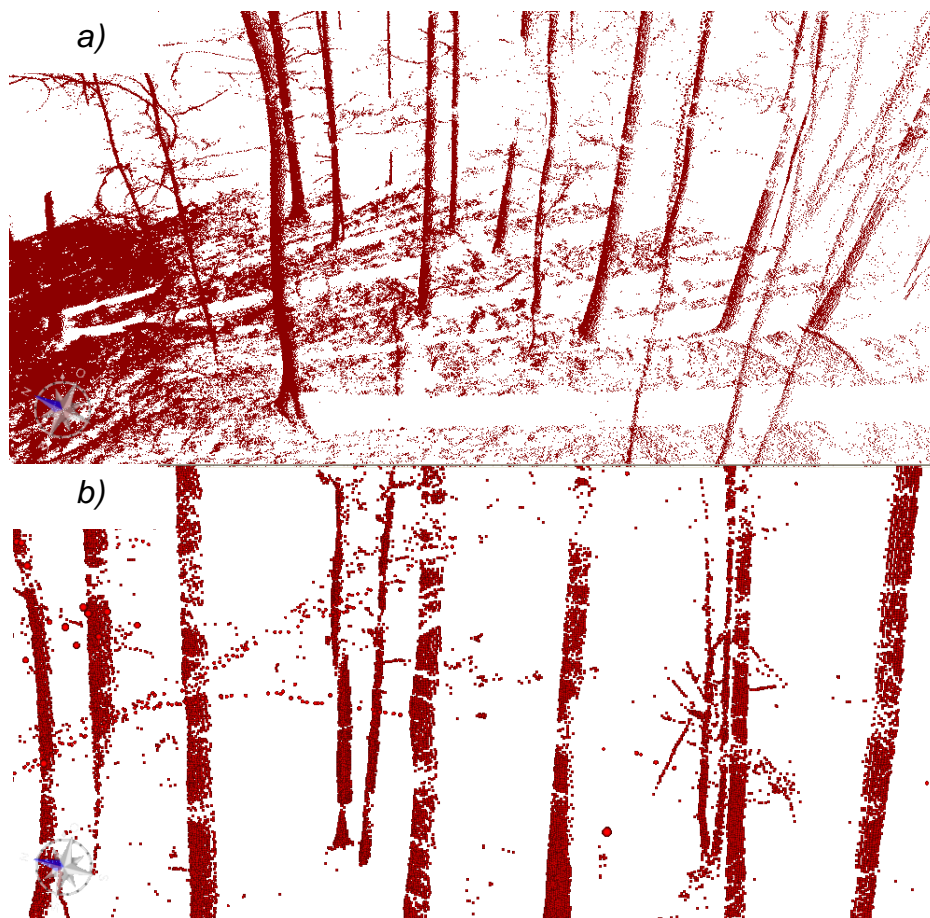

Figure 2-20. Shadow effects resulted from a) stems and b) branches. (Source data: Hidegvíz-völgy Forest Reserve, Hungary, 2006. Figure compiled by the author.)

Simonse et al. (2003) searched for the positions and diameters of horizontal stem slices mapped into binary raster image as the parameters of circular arcs using Hough-transform. The Hough-transform is a standard tool in digital image processing which uses a parametric description of simple geometrical shapes in order to reduce the computational complexity of their search in a binary image. This is achieved by transforming each cell of the original binary image into a feature space ('Hough image') defined by the parameters of the shape to be detected. The resulting coordinates of the transformation are binned in an accumulator grid with as many dimensions as the number of unknown parameters. The parameters of the shapes are obtained as local maximum values in the accumulator (*Figure 2-21*).
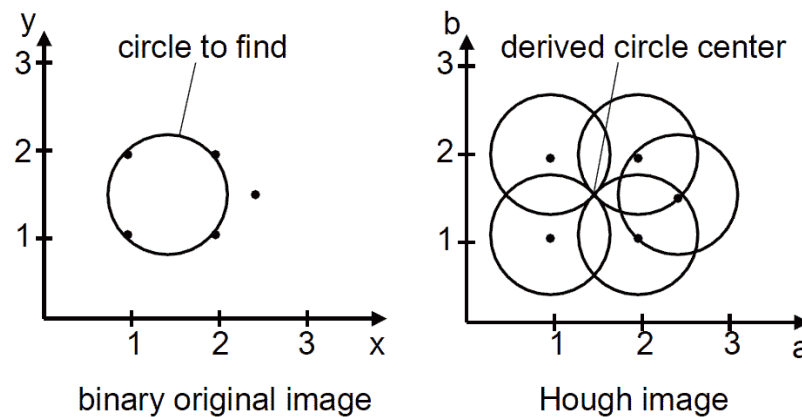
Figure 2-21. Concept of Hough-transformation for circle detection (Simonse et al., 2003).

Simonse et al. (2003) used modified Hough-transform where only the positions of circle centres corresponding to tree locations were searched. Because the circle diameter i.e. stem diameter was not known before applying the algorithm they started with a value of 100 cm and reduced it in small increments. Schilling et al. (2011) made additional modifications on Hough-transform so that the algorithm uses point count raster of horizontal point cloud sections as input data and favours to the cells containing multiple points. Extraction of circles by Hough-transform and its variants have become widespread techniques for the detection of stem slice sections, however they require numerous and fine-tuned parameters as input data.

Aschoff and Spiecker (2004) created image objects from the cells of the rasterized horizontal point cloud section and calculated their inner and outer circles. Objects with inner and outer circles with nearby centres and similar diameters were declared as stem slice sections. They experienced that the reliability of the stem recognition can be improved using horizontal point cloud sections at multiple heights as the centres of overlaying stem cross-sections are aligned roughly along a vertical line and the diameters decrease in ascending height. Bienert et al. (2007) developed a stem detecting algorithm that uses rectangular moving window technique on point count raster. Cells with local measurement densities exceeding a given threshold were considered as stem components. Stem components within the moving window were labelled with a unique ID resulting in disconnected image objects. The position and diameter of the trees were obtained through a robust circle fit algorithm. The main disadvantage of this method is that the stems of those being closer than the size of the moving window cannot be separated. The algorithm 'Crescent moon' (Király and Brolly, 2008) assumes point data from single scan and circular shape for stem cross-sections. The routine searches for the point measurements that represent the tangential point on the horizontal stem slice sections viewing from the direction of the sensor position. Knowing the two tangential points, the circle's parameters can be calculated by selecting a third point along the angular bisector. The three point positions can be further improved by averaging the point coordinates in their close neighbourhood. Wezyk et al. (2007) generated TIN model from the point measurements. Following the elimination of long edges, the point groups of stems and low vegetation patches were represented as subnets. To select those representing tree cross-sections, polar coordinates for the vertices were determined with respect to the subnet centroid. In case of circular shapes, the standard deviation of the radial distances is relative small and the distribution of polar angles is uniform so subnets meeting these criteria are classified as tree stems.

Haala et al. (2004) determined the fundamental surface type for each cell of a range image by the calculation of mean and Gaussian curvature signs. The corresponding cells were combined to image objects, from which the ones having cylindrical shape were classified as

tree trunks. The range images created by Litkey et al. (2008) contained horizontal distances thus the cell values of the stems with approximate vertical attitude were in close arrangement. Image objects were created based on the similarity of neighbouring cells. Stems are identified as image objects with elongated shape in vertical direction. Range images contain one distance value per cells, which limits the fields of application to processing single-scans. Huang et al (2011) mapped the point cloud into a voxel space up to the 20% of total height to reduce the influence of branches. The individual stem detection process is based on the 3D voxel histogram techniques. Vertical columns composed by exclusively filled cells were projected to a horizontal raster with identical resolution. The value of the raster cells depicted the extent of the corresponding vertical column expressed in voxel counts. A clustering algorithm based on Euclidian distance was used to classify the cells of individual trees followed by circle fitting to locate the position.

Methods for automatic tree detection are evaluated in terms of reliability and accuracy. Reliability is quantified concerning correct detections, omissions, and misclassifications. The output of a stem detection algorithm contains correct detections and misclassifications. Misclassifications are detection errors: findings without reference data in the previously specified proximity. The ratio of misclassification is the proportion of misclassifications regarding all the output set. Omitted trees are those reference samples that have not been recognized in the laser scan. The overall detection rates reported by the cited authors vary in the range of 22–94% using single scans and between 52–100% at multiple scans. These intervals are wide however, there is high difference between study sites and stand conditions. Care should be taken at the direct comparison of the reported reliability of different methods, as the detection rate is strongly influenced by several external factors. Those with the highest relevance are as follows:

1. Number and constellation of scans (scan mode). The use of combined point clouds originated from multiple scanning positions enhances the detection rate, as trees are measured from multiple directions. Thies and Spiecker (2004) reported 30% increase in detection ratio by raising the number of scanning positions from one to five.
2. Stem density. High stem density induces occlusions, which reduces the detection rate. Watt and Donoghue (2005) found reduction in the effective range of their tree mapping method from 30 to 8 meters at the increase of stem density from 600 to 2800 trees·ha^{-1}.
3. Density of low vegetation and branching. Clusters of point measurements reflected from the undergrowth or branches have pattern similar to tree stems that may cause misclassifications. Bienert et al. (2007) pointed out the negative effect of branching in conifer stands, where the rate of misclassification was reduced by 40–100% through the integration of a branch filtering routine in the stem detection procedure.

Furthermore, the reliability is affected by the radius of sample plots that varies in the range of 10 to 50 meter among the cited studies. Each algorithm has been optimized to more or less specific test site conditions so these should be considered at the evaluation of the performance. Accuracy is the degree of conformity of the estimated stem coordinates to its actual (reference) position expressed in terms of Euclidian distance. Several studies have proved that accuracy of detected stem positions is in the magnitude of some centimetres irrespectively of the detection method (Hopkinson et al, 2004, Watt and Donoghue 2005, Thies and Spiecker 2004). This level of accuracy meets the requirements of the forestry practice to identify the individual trees in the field.

2.9. Tree models and attributes

### 2.9.1. Stem diameter and basal area

Stem diameter is the most important quantitative parameter with respect to the calculation of tree volume by allometric equations. The diameter can be estimated in the same height section as it was used for the 2D stem detection, while 3D models allow estimating the diameter at arbitrary height of the stem. The height of the diameter is determined relative to the ground level, which implies the importance of the DTM quality. The so-called breast height (1.30 m above the ground) has specific role as a standard height for the measurement of stem diameters referred to as DBH, i.e. diameter at breast height. The cross-sectional area of the plane cutting the stem at breast height normal to its longitudinal axis is called basal area (Husch et al., 2003). The basal area can be computed from the DBH and vice versa. The reliability of the diameter estimates refers to the robustness of the estimation method against the effects of point measurements reflected from branches or other objects apart from the stem. Accuracy means the conformity of the estimated diameter to the reference measurements. DBH is classically determined using calliper or tape measure.

Watt and Donoghue (2005) aligned circles manually to the point measurements of stem slice sections. They found strong linear relationship ($R^2 = 0.92–0.98$) among the diameters of aligned circles and diameters from field measurements. This study emphasized that high stem density and intensive branching have negative influence on the reliability of DBH estimation. Hopkinson et al. (2004) delineated stem points manually to exclude the influence of branches and estimated tree parameters by fitting a circle with least squares adjustment. Automatic circle fitting is objective, reproducible and less labour intensive approach than manual circle alignment although the latter is less sensible to gross errors. Henning and Radtke (2006a) proposed the iterative refinement of fitted circles by removing the point measurement with the largest residual in each step. The circle fitting procedure was being repeated until the root mean squared error (RMSE) exceeded the limit of ±5 mm. Compared to the reference data set, the bias was –0.2 cm with standard deviation (SD) of 2.1 cm. Bienert et al (2007) fitted circles into stem slice sections at multiple heights. They developed a formula for ranking the reliability of circle fit by considering the RMSE, the central angle of the directly measured arc, the point density and the coherence in diameter with the overlaying circles. The DBH was estimated using linear regression on the diameters against their corresponding heights, which enhanced the reliability. The bias was –0.6 cm, with SD of 2.5 cm. Huang et al. (2011) refined the parameters of circles combining Hough-transform and circle fit algorithm in iterative manner. Hough circle has the advantage of being robust against outlying points while the circle fit provides more accurate diameter. In this way, the Hough circle had a role in the selection of reliable data points as input for the subsequent circle fit. Pueschel et al (2012) implemented two algebraic circle fit approaches in addition to the classic, geometric one and investigated the effect of using multiple scans. They found that the number of scanning positions had higher impact on the DBH accuracy than the adjustment method used for circle fitting.

Modelling of stem cross-sections by circle is typically a 2D approach. By filtering the stem surface points in a thickness of $0.5 − 1$ m, the stem modelling through cylinders becomes possible that allows for the reduction of the influence of stem leaning on the diameter estimation. However, the derivation of DBH from circles fitted at multiple height sections was found more accurate than fitting one cylinder to all data in the same height interval (Brolly and Király, 2009a). The parameters of circle or cylinder can be estimated upon the point measurements of a single scan, so the use of either to model the stem cross-section is convenient and cost effective.

Stem cross-sections surveyed from multiple scan positions can be modelled more accurately by shapes with higher degree of freedom. Aschoff and Spiecker (2004) used ellipse-fitting algorithm, Pfeifer et al. (2004) applied free form (B-spline) curves for accurate approximation of stem cross-sections. Király and Brolly (2010) introduced a method for the creation of concave polygons that reduces the effect of measurement errors by averaging the point coordinates for the calculation of the vertices. Wezyk et al. (2007) used inner and outer hulls of stem surface points for the direct estimation of basal area and achieved estimation accuracy of $0.3 - 2.1\%$. Examples on cross-sectional models are given in *Figure 2-22*.

Bias values were reported in the range of $-2.3 - 1.9$ cm that indicates the presence of systematic errors in the cross-sectional models. The overestimation of diameter can be traced back probably to the outlying points in the surrounding of the stem slice section that cause distortion in the fitted shapes. Brolly and Király (2009a) found relationship between the degree of underestimation and roughness of the bark. The systematic error can be eliminated by calibration based on sample trees. Király and Brolly (2010) calculated the total basal area of a stand of 118 trees using circular, cylindrical and polygonal models and found that the maximum difference was 1.2%. The DBH estimation accuracy (RMSE) achieved by using laser scan is in the range of $0.7 - 3.4$ cm and is deemed to be competitive in most cases to classic field measurement tools used in the forestry practice (e.g. Hopkinson et al., 2004, Thies and Spiecker, 2004). It has to be emphasised that the result of diameter estimation strongly depend on the stem detection method as it provides the data pool for the calculation.
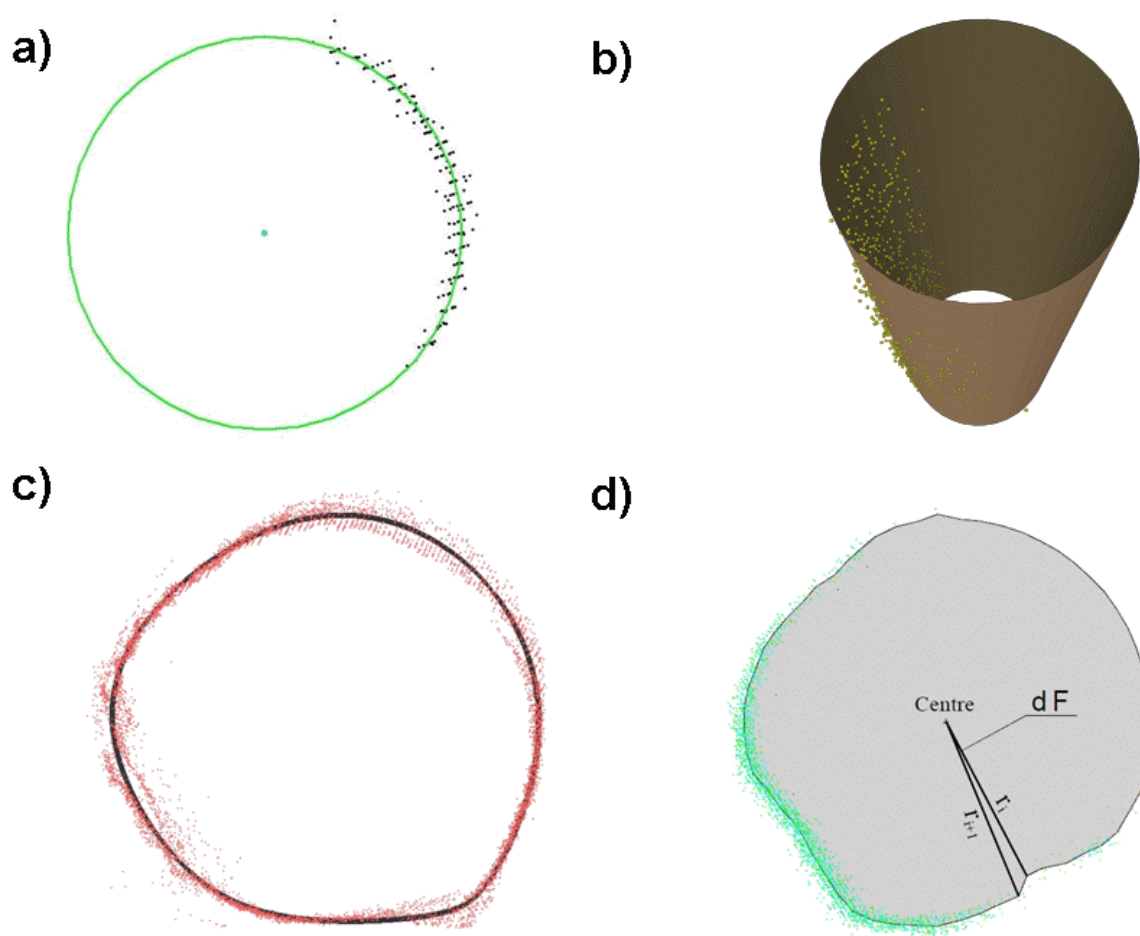

Figure 2-22. Models of stem cross-sections as a) circle, b) cylinder, c) free-form curve (Pfeifer et al., 2004), d) concave polygon (Király and Brolly, 2010).

2.9.2. Stem models

Laser scanner data enables evaluating the stem form and volume of standing trees. The retrieval of exact quantitative stem attributes can be hardly achieved on standing trees above some meter height using classical measurement tools. In this context, terrestrial laser scanning allows for widening the range of traditional forest inventory parameters with additional stem-related attributes, such as stem profile, lean, sweep, and stem height. Stem profile is a graphed diameter up the stem versus the corresponding height. Taper of the log is defined as the difference in diameter between the butt end and the upper end of the log, divided by the distance between these two elements (Husch et al., 2003). Taper of arbitrary part of the log can be estimated considering the stem diameter profile. The preparation of particular timber products requires logs with limited taper, thus the stem profile provides essential information for the wood quality assessment. Sweep is also a substantial quality index, which is defined as the maximum pitch per meter of the log (Thies et al., 2004).

Aschoff et al. (2004) described the stem profile up to 20 meter height using regression of circle diameters that were fitted to stem slice sections in the point cloud at 0.5 m intervals up the stem. Bienert et al. (2007) used similar method to determine stem profiles of 22 standing conifer trees. The estimated stem profiles were validated against detailed diameter measurements after falling. They found –0.6 cm bias with RMSE of ±2.5 cm up to a height of 8 meter. The accuracy was decreased above this height due to the reduction in stem point density in combination with the occlusion effect of heavy branching. Thies et al. (2004) reconstructed the branch-free stem of deciduous trees by means of successive cylinders in telescopic arrangement. Cylinder parameters were estimated by least squares adjustment of the consecutive stem slice sections in the point cloud with a thickness of 0.5 meter. The five initial values (positions and orientations of the axis, cylinder radius) for the parameter estimation were taken from the previous cylinder, which ensured smooth connection. The sweep was estimated by calculating the chord lengths along the connected cylinder axes and the corresponding pitches (*Figure 2-23*). To yield the leaning of the stem, the centre coordinates of the first fitted cylinder were taken as the origin of a polar coordinate system in which the horizontal distance of the cylinders' centre point was plotted.

Thies and Spiecker (2004) considered the length of the stem equivalent to the height of the crown base, which was defined as the height of the first branch. They used data from multiple scans and applied cylinder-fitting procedure up to the crown. The stem length was estimated at the height where the RMSE, i.e. the indicator of the goodness of fit, exceeded the predefined threshold of ±3 cm. The authors found their results unsatisfactory and explained the fail of the method by crown overlap. Nevertheless, tree models with more detailed description of the crown structure perform better in estimating the stem length. Schilling et al. (2012) created tree models in the voxel space and represented the generalized crown structure as graph. Based on 37 samples, the estimation error of the stem length was 1.3 m with RMSE of ±1.0 m.
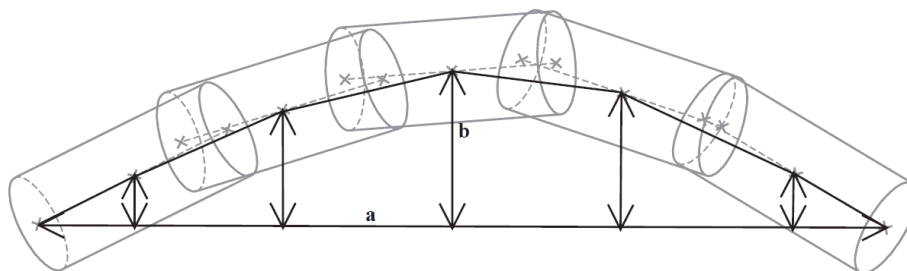
Figure 2-23. Fitted cylinders in telescopic arrangement, the approximated tree axis as the connections of cylinder axis centres, a chord (a) and the corresponding pitch (b). (Thies et al., 2004)

Thies et al (2004) estimated the stem volume by summing the volume of the fitted cylinders. Pueschel et al. (2012) used similar concept but approximated the stem shape within horizontal sections with conic frustums up to 10 metre height. The relative accuracy of the volume estimates was 1–6% for multiple scans and 18–25% for single scans. Aschoff et al. (2004) proposed generation of triangulated irregular network (TIN) model over the height interval of the automatically extracted cross-sectional circles to interpolate the stem surface and to derive its volume. Király and Brolly (2010) compared results of volumetric calculations based on different body of revolutions and prisms. In addition, the stems were classified based on the form-numbers and the appropriate body of revolution for each partition was assigned. Stem models are adequate for visualization purposes and attract the attention of the public for the opportunities of terrestrial laser scanning (*Figure 2-24*).

Figure 2-24. Stem models as a series of cross-sectional circles (Király and Brolly, 2007).
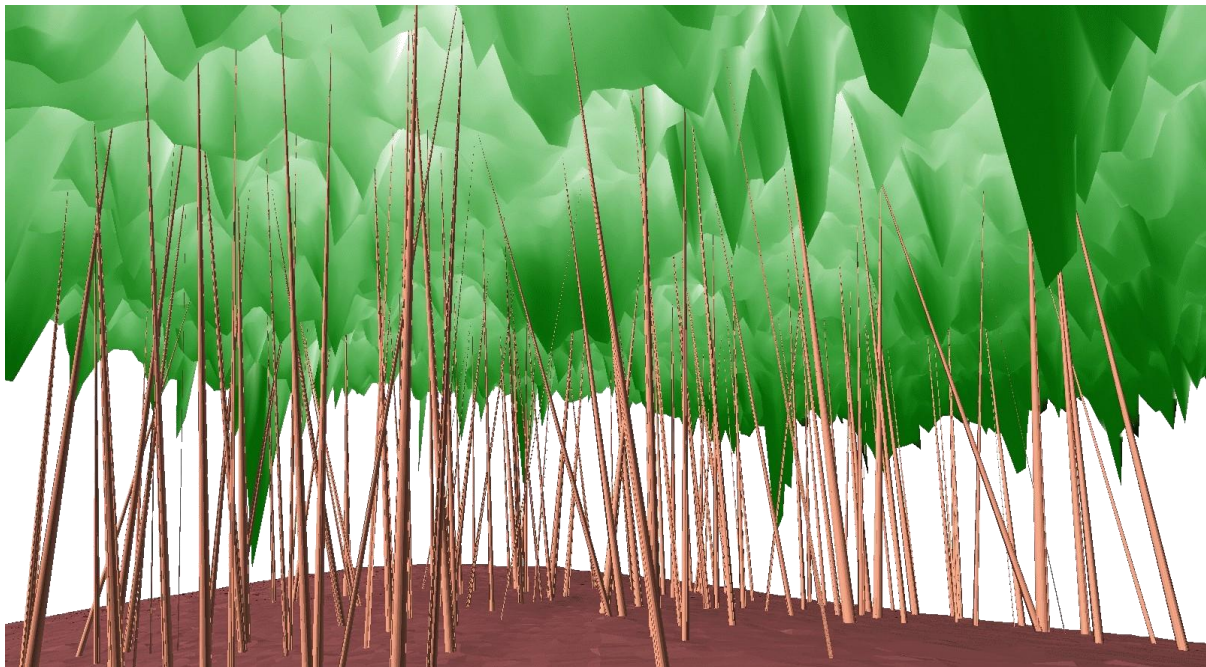
2.9.3. Tree height

Total tree height is the distance along the axis of the tree stem between the ground and the tip of the tree. In case of leaning trees, the total height is approximated by the vertical component of the axis. Tree height is one of the most important attribute of individual trees as it is a necessary parameter of the allometric equations for volume estimation and it is a reliable indicator of the site conditions. Height measurements of trees are taken indirectly with hypsometers, which are based on trigonometric principles although using this technique is time consuming and labour intensive. Estimation of tree height using terrestrial laser scans is still challenging as the identification of tree tips is restricted by the specific viewing geometry, which resulted in reduced point density and occlusion of the neighbouring tree crowns.

The simplest methods search for the highest point measurement within a given radius around the tree position and consider that as tree tip. This early technique has been extensively used up to nowadays (Hopkinson et al. 2004, Bienert et al. 2006, Huang et al. 2011). The authors reported systematic bias in the range of −1.5–0.4 meter with random error

of 0.8–1.1 meter. The estimation accuracy is comparable to that of hypsometers. The main disadvantage of this sampling-based height estimation method is that the search radius strongly affects the result; furthermore vertical stem axes and radial symmetry of the crowns are assumed. Brolly and Király (2009a) created raster-based digital crown surface model with cell size of 0.2 m by assigning the highest point measurement to each cell (*Figure 2-25*). Tree tips were identified as local maxima using inverse watershed algorithm (blob detection) followed by low pass filtering of the surface. The lower parts of the tree stems were modelled by fitted cylinders that indicated the main direction of tree leaning. The axes of the cylinders were extended up to the crown surface and each stem was linked to the nearest tree tip. Considering the main leaning direction the accuracy of the tree height estimation was improved by 19% resulted in a bias of –0.3 m and RMSE of ±1.8 m.

The above-mentioned techniques are not suitable for multi-layered forests. Thies, Spiecker (2004) used the laser-derived diameter profile and approximated the tree height by a common taper function. Input variables to the taper function are DBH, tree height and a set of tree-species specific parameters. As tree height is the parameter to be calculated and at the same time part of the input variables, a direct fit cannot be realised. For this reason, they iterated the tree height from 5 m to 50 m with a step size of 10 cm and calculated the deviation of the resulting function versus the profile in each iteration step. The height with the minimum RMSE was assumed as the tree height. This method yielded results with relative accuracy of 7%, although the tree species should be known in advance to select the appropriate species-specific parameters. To avoid using these parameters, the lower part of the stem diameter profile was created based on the diameter estimates from laser scanner data and the upper part was extrapolated. It was assumed that the diameter decrement is strictly monotonic up the stem and the tree height can be assessed as the intercept of the taper function (*Figure 2-26,* Király and Brolly, 2008). The method was validated on larch samples and resulted in relative accuracy of 16%.

Figure 2-25. Tree height estimation by means of cylindrical stem models and crown surface model (Brolly and Király, 2009a).
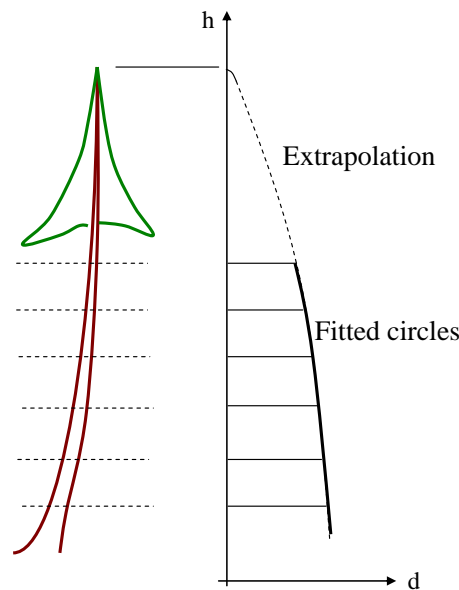
Figure 2-26. Tree height estimation through extrapolation of the taper function. (Király and Brolly, 2008)

Schilling et al. (2012) created tree models in the voxel space and estimated the tree height with the highest voxel within the object. The resulted bias was 1.75 meter with RMSE of ±1.49 meter. The reason of the significant underestimation is that the complete tree models consisted of one connected image object. As the point measurement density is reduced in the upper region of the crown, the occlusion effect of the twigs causes the isolation of voxels. Consequently, these voxels should be integrated into the model to avoid underestimation of tree height.

2.9.4. Crown structure

The size and the structure of the tree crowns show strong correlation with stem volume, vitality, growth and the competitive ability of the tree. Furthermore, the potential of the canopy as ecologic niche for animals and epiphyta is also related to the crown structure. The crown is the main part of the tree that can be viewed by remote sensing techniques from ground-based and airborne platforms. This fact accounts for the key role of the crown structure in the integration of data from different platforms because the crowns are identical objects that were recorded in both data sets. The architecture of crowns is more complex than that of the tree stem as it has hierarchic structure composed of multiple branches with various orientation and size. As a result, modelling of crown structure needs data on higher resolution than tree mapping applications, which requires data capture from multiple scanning positions. Tree models of Pfeifer et al. (2004) intended to provide information on the start point and the end point of each branch, and the radii at these points. The stem and the main branches were modelled by sequence of fitted cylinders. The base cylinder was described by the known radius and an axis segment (i.e. the two axis end points). Shifting this cylinder forward (or backward) in the axis direction, an approximate position for the next cylinder was found. Points being close to this approximate cylinder were selected for the refinement of its parameters. If the new parameters were in accordance with the predefined quality criteria, the cylinder was accepted and the tracking continued. Following the assignment of the unclassified points to the closest reconstructed branch, the outer hull of the crown was yielded in the form of polygons in different heights. The study presents a demonstrative example on the performance of the algorithm, but provides no validation on crown size parameters. Gorte and Pfeifer (2004) segmented the point cloud according to branches. The point measurements

were converted into the voxel space and a skeletonization routine was applied which reduced the stem and branches to single voxel thickness. Voxels of the skeleton were organized into a graph using Dijkstra's minimum spanning tree algorithm. The stem and the branches were labelled with unique IDs followed by the establishment of the topologic database (*Figure 2-27*). Bienert et al (2010) presented tree-wise segmentation procedure in the voxel space with the goal of deriving structural models for meteorological simulations. They computed various attributes for individual voxels. For instance, the main direction of the branches within a voxel was specified as the eigenvector with the largest eigenvalue of the covariance matrix calculated from the 3D point coordinates. The crown structure was modelled by means of disconnected image objects where the linking of corresponding objects was based on the distance of object centroids. Data from thin twigs were eliminated in the course of the segmentation by deleting the voxels with few point measurements in order to reduce the degree of overlapping between the crowns. Presumably, this filtering lead to systematic underestimation of the crown size, although quantitative evaluation of the tree crown metrics was not reported.

Bucksh and Fleck (2011) detected branch dimensions of fruit tree canopies in leaf-off state using their 'SKELTRE' algorithm. The point cloud was subdivided by adaptive octree algorithm. Octree is a data structure based on the recursive subdivisions of the model space into volumetric elements. The algorithm requires only one input parameter, which is the minimum allowable cell size to terminate the subdivision process. The octree data structure was converted to a graph, followed by the skeletonization procedure. The skeleton was geometrically embedded into the point cloud. The median distance of point measurements from the skeleton graph was taken as the branch radius allowing even the estimation of fine branches with correlation coefficient of 0.92. The methodology proposed by Cote et al (2011) used terrestrial laser scans in combination with allometric relationships to define the total amount of foliage in the crown and to build the tree branching structure. Intensity information of laser measurement was also involved to extract the stem and to separate the main branches and foliage. Assuming correlation between the availability of light and the mass of foliage together with branching frequency, the fine branching structure was reconstructed by a 'branch colonization routine' at the crown regions where the point density was too sparse for the direct modelling. The validity of the proposed model was evaluated on five conifer trees. The error of leaf area estimation for individual trees was ranged from 17 to 67 percent relative to the reference leaf areas.
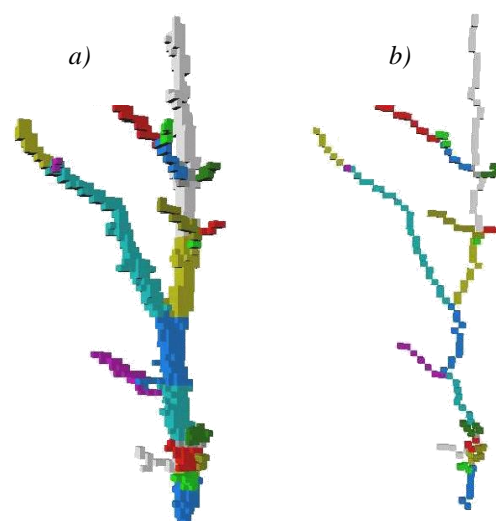
Figure 2-27. 3D crown structure represented by a) contiguous voxel objects and b) generalized skeleton (Gorte & Pfeifer, 2004).

3. Aims and scope

The main objective of this thesis is to introduce novel algorithms for the automatic processing of terrestrial laser scanner data recorded in temperate forests with special regard to the challenges of diverse stand structure. The algorithms address the following issues:

1. Filtering of irrelevant data
2. Locating of tree stems (tree mapping)
3. Retrieval of individual tree metrics, such as
   a. Diameter at breast height
   b. Total tree height
   c. Horizontal crown projection area

The primary data source of the algorithms is the registered point cloud with elevation coordinates relative to the ground surface. The algorithms contain procedures for the identification of data from individual trees by geometric feature detection techniques. Following the extraction of tree data, models of the stem cross-sections or models of the complete tree structure are created, upon which the stem centre position and the biophysical attributes (diameter at breast height, tree height and crown projection area) are estimated. The algorithms make use of different data structures and dimensions of model spaces. The objectives of the algorithms are specified in detail as follows:

1. Reduction of irrelevant data for processing of laser scans in 2D and 3D feature space. The interference of the laser beam with the low vegetation and twigs results in isolated data that adversely affects the performance of the tree mapping applications. The filtering must highlight tree data and eliminate data of other thematic classes.

2. Extraction of trees from the point cloud. The algorithm should have the capacity to process point cloud data captured from single and multiple scanning positions. In addition to the location of tree centres, the algorithm must provide accurate estimates of stem diameters.

3. Stem mapping in the raster domain. The algorithm must enable the mapping of trees using the merged laser scans over the complete area of forest compartments with close-to-nature stand structures. Special attention should be paid to counteracting the negative effects of low vegetation. In order to yield reliable stem diameter estimates, a special routine should be included to sort out the data from branches apart from the stem surface.

4. Detection of juvenile trees. As most of the classic tree detection algorithms are scale-dependent, i.e. they do not support the detection of small trees, a specific solution is needed to take the advantage of the high scanning resolution by extracting the location of juvenile trees composing the regrowth patches with DBH below 10 cm.

5. Extraction of tree data and creation of complete tree models in the 3D domain. The algorithm should have the ability to classify the laser scanner data according to individual trees and to create 3D models including the individual tree crowns for conifers and deciduous trees.

6. Retrieval of quantitative tree metrics. Estimates on forestry-related parameters (stem diameter, tree height, and crown projection area) should be provided based on the physical models as outcomes of the above described tree detection (modelling) techniques. The parameter retrieval routines should be applicable under diverse site conditions such as uneven-aged, multi-layered and mixed stands with considerable coverage of low vegetation in the shrub storey.

4. Materials and methods

The outline of this chapter is the following: The first sections characterize the materials and the pre-processing stages resulting in the data source used for the development and validation of the new methods. The next sections is the essential part of the dissertation: the detailed description of the algorithms. Methods for removal of irrelevant point measurements are presented at first, as the filtered data is used as input for the subsequent mapping and modelling applications. The introduction of the other algorithms takes place according to the data structure used, beginning with 2D stem mapping algorithms, which is followed by 3D tree detection and modelling techniques.

4.1. Study sites

4.1.1. Hidegvíz-völgy Forest Reserve

The Hidegvíz-völgy Forest Reserve (N46.671, E16.445) is located in the Sopron hill, 10 km west from the town of Sopron at altitude of 450 – 520 m (*Figure 4-1*). The core area is 19.7 ha, including the compartments of Sopron 185 B, C and 186 A, D. The climate of the area is classified as 'beech'. The characteristic soil types are acidic, non-podzolic brown forest soils with surface water gley, and colluvial soils, formed on gneiss and mica bedrock (Horváth et al., 2012).

The double-layered, abandoned old beech stand was in the age of 83 years at the time of the data acquisition according to the forest plan (ÁESZ 2004). The main species of the upper canopy are beech (*Fagus sylvatica*, 21%) and sessile oak (*Quercus petraea*, 19%) with a mixture of larch (*Larix decidua*, 12%) and spruce (*Picea abies*, 10%). The height of the upper layer varies in the range of 24–27 meter. The lower canopy layer is composed of evenly distributed 10–22 meter high hornbeam (*Carpinus betulus*) and birch (*Betula pendula*) individuals.
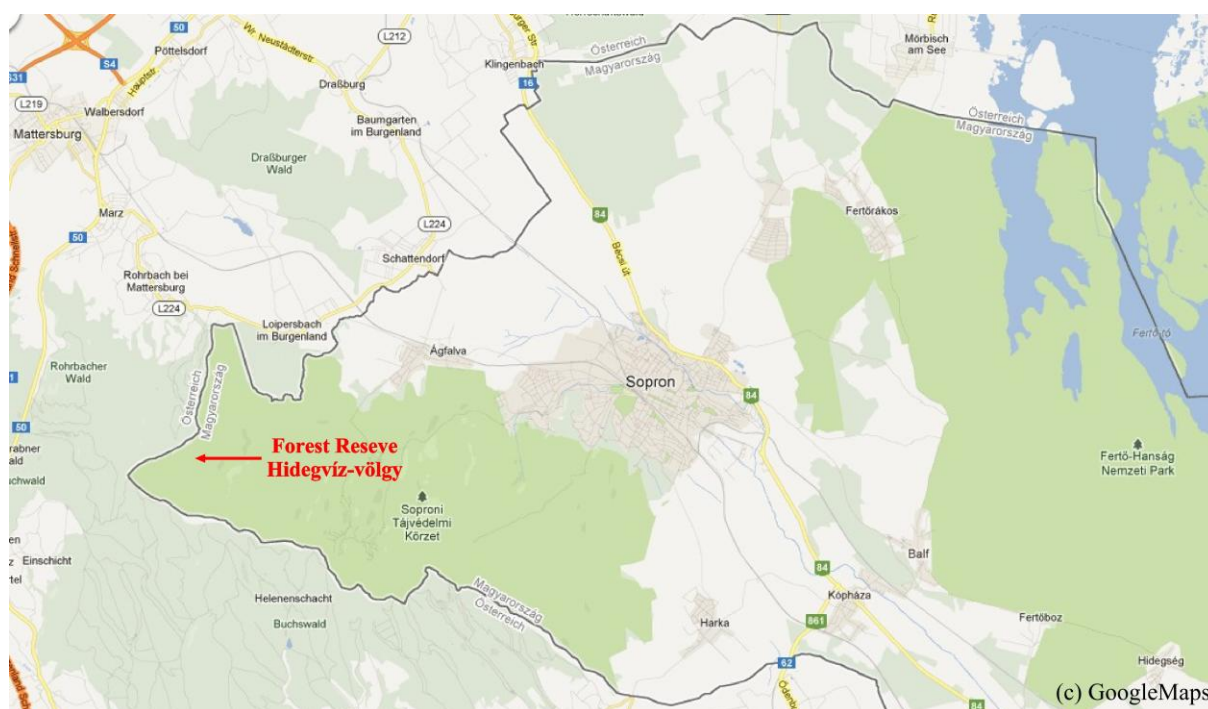

Figure 4-1. Location of the Hidegvíz-völgy Forest Reserve. (Shaded relief)

The core area has been withdrawn from management by law being left for natural development and free of any direct human intervention since the year of 2000. This resulted in intensive gap dynamics, involving the ruination of suppressed birch individuals and the perishing of spruces destructed by bark beetle. The abundance of the regrowth and shrubs was negligible at the time of the data capture, but considerable amount of lying deadwood was presented in varying spatial distribution (Vitális, Zakariás, 2005).

A grid network of permanent sampling points ('Forest n+e+t') was set up in order to retrieve information about the pattern and dynamics of the tree populations and stand structure (Király, 2006). The density of permanent sampling points is four per hectare, which was set as a regular grid of 50×50 m. The network was established with the contribution of the NYME EMK Department of Surveying and Remote Sensing in 2005–2007. The diverse stand structure and the geodetic level accuracy of the sampling network supported this forested site to be the first one in Hungary that is surveyed by terrestrial laser scanning (Király et al., 2007).

4.1.2. Pro Silva demonstration site, Pilisszentlélek

The compartment Pilisszentlélek 25 A (N47.722, E18.860) is located 20 km in south-east direction from the town of Esztergom (*Figure 4-2*). The total area of the compartment is 9.5 ha. A forestry road splits the compartment into two distinct parts. The altitude of the site varies in the range of 430–500 meter above the Baltic Sea level. The valley of stream Szentlélek structured the geomorphology in east-west direction with slopes of south-north aspects and inclination of 5–10 degrees.

Figure 4-2. Location of the Pro Silva demonstration site. (Shaded relief)

41

The forest has been managed by the Pilisi Parkerdő PLC according to the Pro Silva directives since 1999, which resulted in the enforcement of natural processes in the forest dynamics. One of the main objectives in the demonstration site is the switchover to a selection system that ensures spontaneous forest renewal and forest development, through moderate, single tree selection harvesting and the use of natural regeneration (Pro Silva, 2012). According to this objective, the stand is uneven aged with multi-layered canopy structure. The main species in the dominant layer are beech (*Fagus sylvatica*) and sessile oak (*Quercus petraea*) with a mixture rate of 55% and 23%, respectively. The mean age of the dominant trees was 97 years at the time of data acquisition, while the age of hornbeams (*Carpinus betulus*) composing the lower canopy is varied in the interval of 40–50 years (ÁESZ, 2002). The regeneration layer contained beech regrowth with patch-wise distribution and 2–5 meter height.

4.2. Data acquisition

4.2.1. Laser scanning in the Hidegvíz-völgy Forest Reserve

The terrestrial laser scans were recorded in the surroundings of the permanent sample point No. 05-11 on April 7 2006 (in leafless state) using Riegl LMS-Z420i instrument. The survey was carried out from the sample point and three additional scanning positions (*Figure 4-3*). In addition to the normal panoramic view, scans with tilted scanner head angle of +50° were recorded from each scanning position. Furthermore, an axis tilt angle of −60° was set in the central scanning position in order to acquire point measurements from the complete upper hemisphere around the sample point. This constellation ensured detailed survey of the ground, stems and canopy within a radius of 30 meter. The scanning frequency was 24.1 KHz with angular step of 0.06° and 0.12° in azimuthal direction at the normal and tilted scanner attitudes, respectively. The sum of the point measurements is 11.7 million.
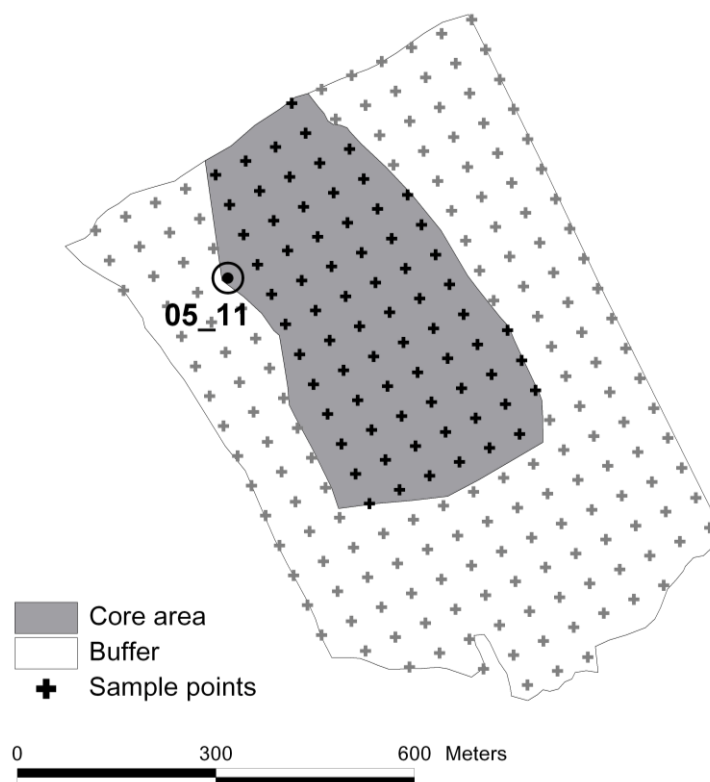

Figure 4-3. The Hidegvíz-völgy Forest Reserve with the 'Forest n+e+t' sample points. Sample point No. 05-11 was a TLS surveying point at the same time.

The georeferencing was carried out using control targets along with the known coordinates of the neighbouring permanent sample points of the Forest n+e+t. The mean linear error of the georeferencing is 0.01 meter, with a maximum error of 0.03 meter (piLine, 2006). The surveying and the georeferencing were completed by the piLine Ltd.
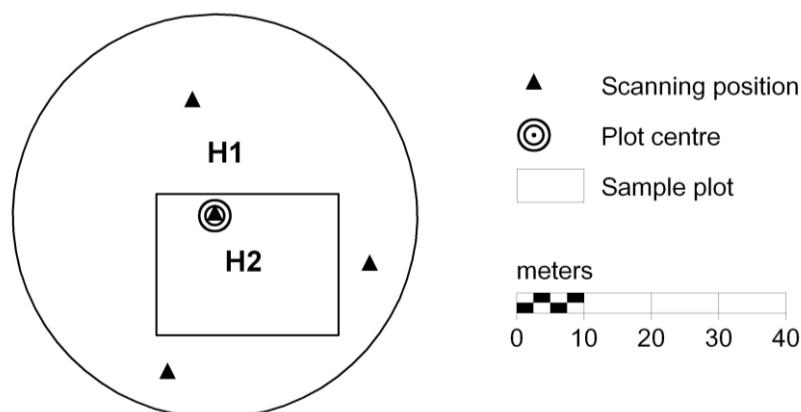
4.2.2. Laser scanning in the Pro Silva demonstration site

The laser scanner survey was carried out in April 2009 with Riegl LMS-Z420i instrument in the leafless state of the forest. Two scans were recorded from each of the 38 scanning positions using azimuthal angular resolution of 0.06° and scanner head tilt angle of +50° and −30°. The survey covering the area of the entire demonstration site was completed in four days. The total number of recorded point measurements was 3.6 billion. The geodetic reference network used for the georeferencing was surveyed by means of Leica 1200 GPS receivers. Three base points were established using GNSS technique outside of the forest. The network was surveyed by traversing across these base points by a total station Sokkia Powerset 3000 (Kiss 2009). Reflectors were used to mark the control points and tie points at the ground level. The automatic registration of scans failed at higher elevation above the ground as artificial targets were missing furthermore the bark surfaces and branches were not feasible for feature extraction. This required more time consuming visual interpretation of the point clouds and manual assignment of tie points (piLine, 2009). The laser scanning and the orientation were accomplished by the piLine Ltd. The mean linear 3D error of the georeferencing is 0.05 m, with a maximum of 0.10 m.

4.3. Sample plots

4.3.1. Sample plots in the Hidegvíz-völgy Forest Reserve

Two sample plots, denoted by H1 and H2, were established in the Hidegvíz-völgy Forest Reserve (*Figure 4-4*). H1 is a circular sample plot with 30-meter radius around the permanent sample point No. 05-11. The radius of 30 meter corresponds to the approximated height of a dominant tree that is the proposed scale in the investigations on the pattern of forest stand dynamics. H1 is used as sample plot for locating individual tree positions and stem diameter estimation using the data merely from the central scan position. Sample site H2 has rectangular shape of 21 × 27 meters. This smaller sample plot is devoted to the analysis of individual tree structures including crown metrics from the combined data of the four scanning positions. All the trees, whose crown is completely within the sample plot, were viewed from multiple surveying points. Tree crowns outside of the sample plot were cropped. Both sample plots are located on gentle slopes of 5°–10°.

Figure 4-4. Sample plots H1 and H2 with scanning positions.

4.3.2. Sample plots in the Pro Silva demonstration site

The area of the entire demonstration site is denoted as P0. It is for the validation of the comprehensive stem map created with the combination of data from all the 38 scanning positions. The minimum diameter of stems to be mapped is 10 cm. The detection of individual trees in regeneration phase was carried out in three smaller sample quadrates of 10 × 10 meters with label of P1, P2, and P3 (*Figure 4-5*). These quadratic sample plots were distinguished according to the regeneration density and branching intensity (*Table 4-1*). Both factors were assumed to have potential impact on the performance of tree detection as tree density determines the degree of occlusion and branches generate isolated points. The three quadrates are located on slopes of 10°–15° steepness.

Figure 4-5. Sample site P0 including the sample plots P1, P2 and P3 with the scanning positions.

Table 4-1. Stem density and branching frequency in sample plots P1, P2 and P3.

Sample quadrate	Sample trees	Branching intensity
P1	41	medium
P2	212	medium
P3	58	high

4.4. Reference measurements

The performance of the new algorithms introduced in this thesis is regarded as the result of this study. The ground-truth tree locations and substantive tree parameters are represented by the reference database containing measurements from field surveys and visual interpretations. Visual interpretation does not imply the errors and fails of the data acquisition. Therefore, the validation against the visually interpreted reference data is only applicable for the evaluation of the automatic algorithms, but care should be taken in extending the findings generally to the whole technology.

4.4.1. Reference measurements in the Hidegvíz-völgy Forest Reserve

Individual tree positions were surveyed by a Leica 1200 total station in the year of the laser scanning (Bazsó 2008, Mokos 2008) for each tree exceeding the minimal DBH of 5 cm. The resulting database contained the species, the stem centre coordinates and DBH for 211 individuals. The DBH was measured using tape. The input for the automatic stem mapping at sample plot H1 was limited to the laser scanner data obtained from the central scanning position. This restriction represented the test conditions at minimum costs of data acquisition. Trees whose stem was occluded at breast height were excluded from the reference database. As a result, the sum of trees used as reference in the course of the validation procedure was 173. The histogram of DBH is illustrated in *Figure 4-6*.
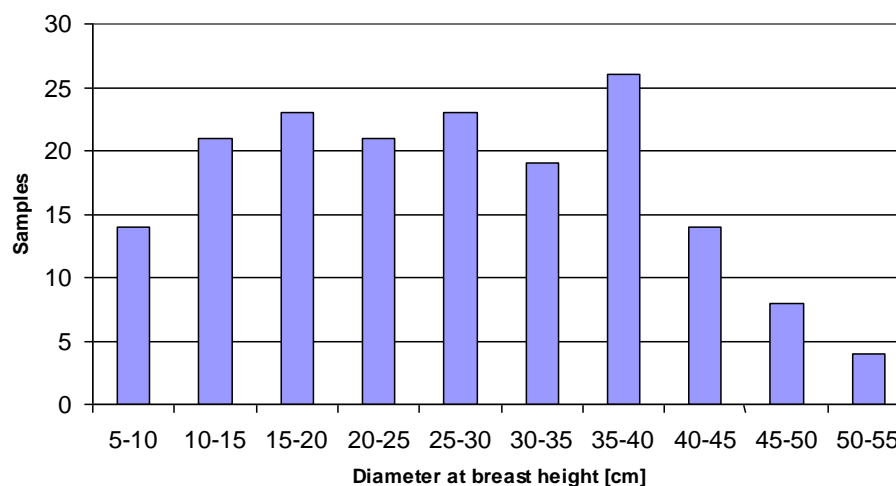
Figure 4-6. Histogram of DBH values in sample plot H1.

Reference data of tree height and crown projection area within the sample plot H2 was measured by computer aided visual interpretation of the laser scanner point cloud. The point cloud used for the interpretation was composed of the scans from all the four scanning positions. The interpretation and measurements were carried out using the software package Fusion v. 2.9, which has been developed by the US Forest Service especially for laser scanning based forest inventory purposes (McGaughey 2010). All together 41 trees were identified at breast height within the sample plot. Of these trees, the total height was measured for only 25 individuals being completely within the borders. The interpretation had to consider at the location of the tree top measurements whether an isolated point above the upper region of the crown had been reflected from a branch or being ghost point (data noise). As the branches are thin at the top of the canopy, partial reflection of the laser beam might encounter in the upper region. To avoid the estimation errors caused by these ghost points, the operator marked the top point measurement in accordance to the crown shape (*Figure 4-7*). Individual tree crowns were delineated using the specific measurement tool of the Fusion software, which is a semi-transparent vertical cylinder with elliptical base. The horizontal position of the ellipse, the length of the axes and the direction of the main axis is set by the operator iteratively viewing the model space from multiple directions. The delineation is complete, when all the crown points are completely within the possible smallest cylinder. Using this measurement tool, the crowns for that of 15 trees reaching up the dominant canopy layer were delineated. The shape of the horizontal crown projection was assumed elliptical and its area was calculated from the measured axes. The trees in the lower canopy layer have few branches resulting in amorphous crown shape so they were ignored. Stem centre coordinates were taken over from the reference database of sample plot H1. Descriptive statistics of tree heights and projected crown areas are listed in *Table 4-2* and *Table 4-3*.
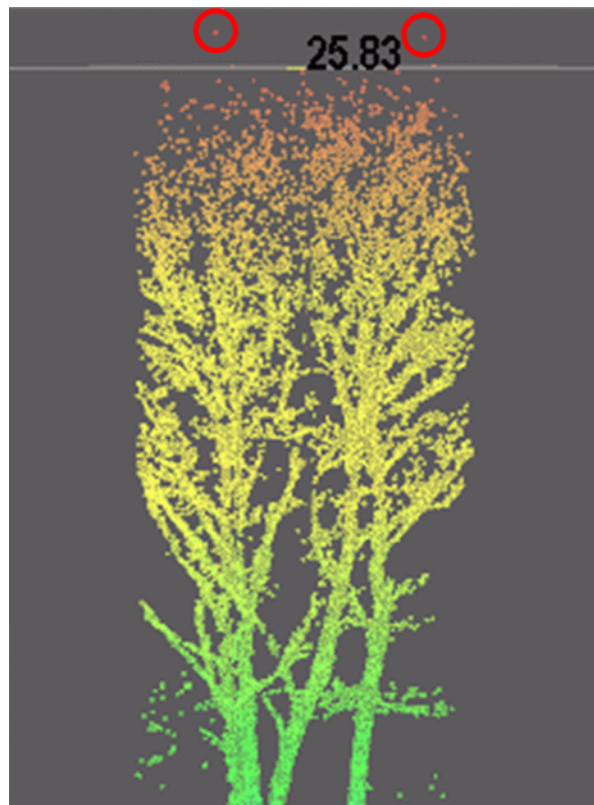
Figure 4-7. Example for tree height measurement in the point cloud using the software package Fusion. Marked points were considered as ghost points. (Data from sample plot H2)

Table 4-2. Statistics of tree heights[m] in sample plot H2.

Class	Canopy layer	Samples	Mean	SD	Min	Max
Conifer	Upper	9	26.2	0.9	24.7	27.2
Deciduous	Upper	6	23.5	1.8	22.9	25.6
Deciduous	Lower	10	16.0	4.4	8.8	20.7
Total		25	21.5	5.5	8.8	27.2

Table 4-3. Statistics of crown projection areas [m^2] in sample plot H2.

Class	Canopy layer	Samples	Mean	SD	Min	Max
Conifer	Upper	9	13.6	5.8	5.2	20.8
Deciduous		6	33.6	28.1	11.4	75.9
Total		15	21.6	20.1	5.2	75.9

4.4.2. Reference measurements in the Pro Silva demonstration site

Individual tree locations accepted as reference for the validation of the automatic stem detection technique within the study site P0 were obtained from the laser scanner point clouds through a semi-automatic detection technique. The semi-automatic manner refers to the visual identification and manual estimation of stem positions prior to using the method of Király and Brolly (2007) for the filtering of stem point measurements. The tree map used as reference depicts the location of the individuals with minimum DBH of 10 cm. Tree positions were validated and completed in the course of in-situ revision with Thales MobileMapper[TM] CE GNSS receiver. In addition, the tree species were specified at the field revision. The revised

reference map contains the position and species of 1561 trees. All the stems are assumed visible from at least one of the scanning positions, so no further analysis concerning the visibility was performed. The DBH was yielded as the average of two calliper measurements made from perpendicular directions in 2011 (Léber, 2012). Due to the time span between the laser scanning and the field survey, the measured DBH of each tree was decremented by its diameter growth approximated for 3 years. Knowing the site class, the species and the actual DBH, the age of the tree and the corresponding increment in diameter can be estimated using the yield tables published in Sopp (1974). The histogram of DBH classes at the epoch of 2009 is presented in *Figure 4-8*. Tree locations within the sample quadrates P1, P2 and P3 were estimated by visual interpretation of the point cloud. The DBH of the object trees was found in the range of 3 – 7 cm by manual point cloud measurements. Following the manual selection of stem surface points, each stem was approximated by a fitted 3D line segment. The tree position was calculated as the point coordinate on the line segment at height of 1.30 meter aboveground.

Table 4-4 provides a summary on the sample plots and reference data along with the corresponding experimental objectives.
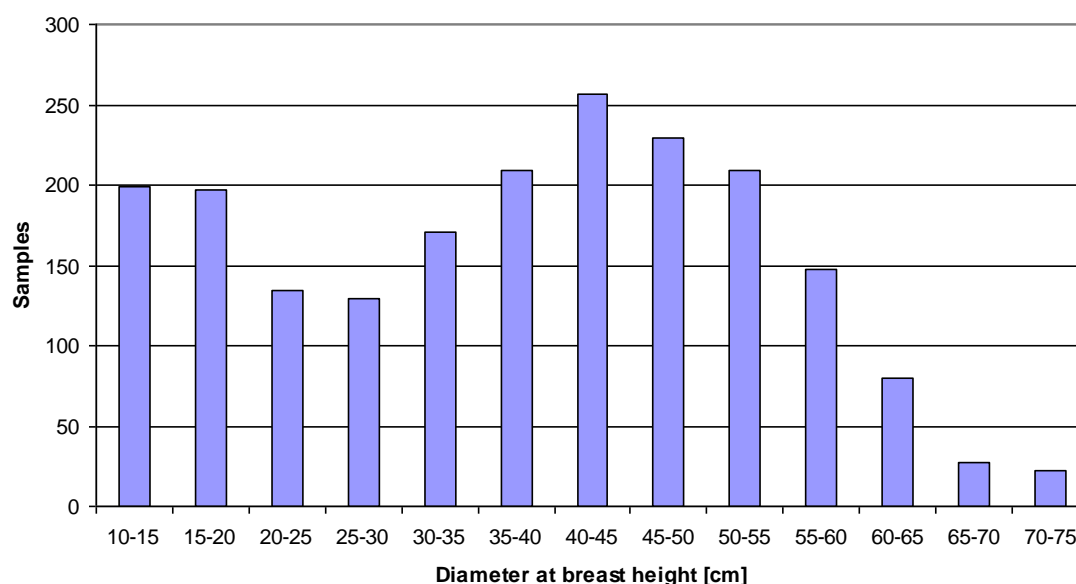
Figure 4-8. Histogram of DBH values in sample site P0.

Table 4-4. Summary of the reference data and experimental objectives in the corresponding sample plots. (At sample plots P1, P2 and P3 the number of scans refers to the number of scanning positions within 40 meters, as the further ones provide negligible amount of data.)

Plot ID	Area (m2)	Trees	Scans	Reference	Objective
H1	2 827	173	1	Field survey	Tree mapping DBH
H2	567	25	4	Field survey and Interpretation	Tree mapping Tree height Crown projection area
P0	95 724	1561	38	Field survey and Interpretation	Filtering Tree mapping DBH
P1	100	41	1		
P2	100	212	2	Interpretation	Filtering Detection of juvenile trees
P3	100	58	1		

4.5. Methodological concepts

The developed algorithms contribute to the forestry-related processing of terrestrial laser scanner data in the fields of (1) filtering of irrelevant measurements, (2) automatic tree detection and (3) tree parameter retrieval. The latter two were encapsulated into a common shell as the model having created at the detection phase was used for the parameter estimation. The main features of the filtering methods are listed in *Table 4-5*. The algorithms aiming at stem detection and tree parameter retrieval make use of vector and grid data structures with two as well as three dimensions. The presentation of the algorithms is practically subdivided according to the dimension of the data structure. Specification of the data structures, age of the target trees, biophysical attributes to be estimated and the respective sample plots for the validation are summarized in *Table 4-6*. Filtering has important contribution in increasing the reliability of tree detection at the sample plots covered with low vegetation in the Pro Silva demonstration site.

Table 4-5. Filtering concepts

Dimension	Structure	Sample area	Section
2	Raster	P0	4.7.1
3	Voxel space	P1, P2, P3	4.7.2

Table 4-6. Concepts of tree mapping and tree parameter retrieval.

Dimension	Structure	Age class	Sample area	Attributes	Section
2	Vector	Mature	H1	DBH	4.8.1
	Raster		P0	DBH	4.8.2
3	Voxel space	Mature	H2	h, a	4.9.1
		Juvenile	P1, P2, P3	-	4.9.2

h: total height

a: crown projection area

4.6. Pre-processing

4.6.1. Generation of digital terrain models

The DTM of the Hidegvíz-völgy Forest Reserve was created upon the merged scans from all the instrument set-ups using a coarse-to-fine iterative method (Király and Brolly, 2007). The initial surface was generated by TIN calculation where only the points with the lowest elevation within a grid of 10×10 meters were taken into account. Points within a predefined vertical difference to the surface were classified as terrain points and were used as data pool in the next iteration. Dividing the grid cells to half size and repeating the point selection at smaller resolution were resulted in a finer TIN model with closer approximation of the ground surface. Filtering of terrain points with cell size of 0.5 meter considered sufficient for the representation of geomorphologic details. Point measurements with gross errors were eliminated manually followed by visual inspection at the end of each iteration cycle.

The DTM of the Pro Silva demonstration site was generated using the concept of active contours implemented in the commercial software TreesVis (Weinacker et al. 2004). The data set contained high number of gross errors that seemingly reflected from below the ground level (low points). Point measurements with the lowest elevation within a grid of 1 meter were removed, which proved to be efficient in large area of the compartment. The remaining gross errors occurred typically near the scanning positions, which were delineated manually.

Changing the sign of the elevation coordinates (i.e. multiplication by –1) within the delineated subsets, low points appeared as if they had been reflected from high objects and could be removed by the standard filtering routine of TreesVis (Brolly and Király, 2009b). The sign of the elevation coordinates were set back to positive following the filtering. The shaded model of the terrain is depicted in *Figure 4-9*.

Elevation coordinates of both dataset were converted to relative height above the ground using the DTMs. The ground surface is considered as the reference for *z* coordinates.
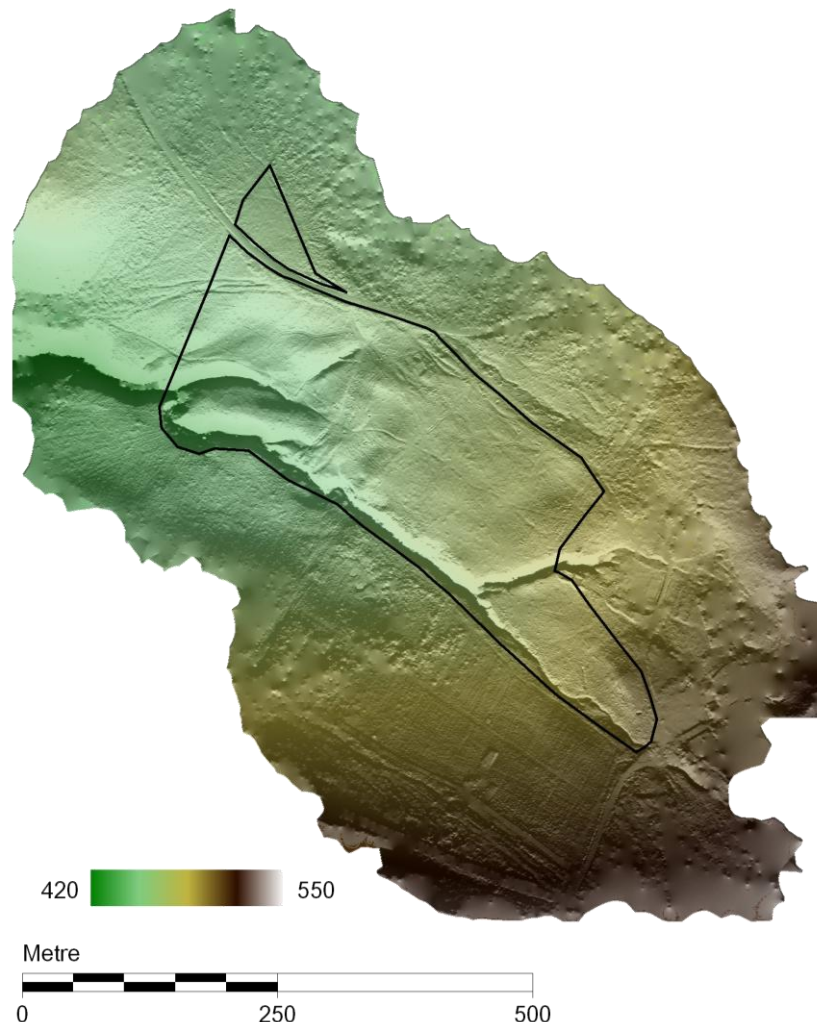
Figure 4-9. Shaded relief display of the DTM at the Pro Silva demonstration site. (Illumination from south. Colour bar represents altitude in meter above the Baltic level).

4.6.2. Conversion of the point cloud into grid data structure

Most of the algorithms presented in this thesis operate over raster or voxel space that requires the point cloud to be mapped into a regular grid structure. The spatial resolution of a grid data structure used for stem mapping should be specified with regard to the spatial extent of the desired model space, the required accuracy of the tree locations and the structural characteristics of the stand. There is a trade-off at choosing the spatial resolution between the performance of object detection and the accuracy of the resulted models. The coordinates of the original point measurements are preserved with higher accuracy using higher spatial resolution, although the smaller cell size is resulted in the fragmentation of the image regions, which reduce the efficiency of the object-based shape detection. Grid structures of low resolution require less memory but the large cell size causes the loss of the fine details of the

object structure and results in coarse models. The spatial resolution of the grids used in this study was optimized following visual comparison of data samples. The point clouds were converted into binary grid storage format. Cell values indicated the presence or the absence of point measurements with binary codes of '1' or '0' respectively. Cells with value '1' are referred to as 'filled' or 'foreground', while the complement set is called 'empty' or 'background'. Description of data structures used at the certain sample sites is given in *Table 4-7.*

Table 4-7. Data structures and model space parameters.

Sample area	Structure	Vertical extent [m]	Resolution [cm]
H1	Vector	1 - 2	0.1
H2	Voxel space	0.5 - 30	$10 \times 10 \times 10$
P0	Grid	1.3 - 1.5	2.5×2.5
P1 P2 P3	Voxel space	0.5 - 3.5	$5 \times 5 \times 5$

4.7. Filtering of irrelevant data

The goal of the filtering is to remove irrelevant data such as ghost points and measurements from low vegetation or twigs to support the tree detection. Irrelevant data of these kinds usually appear as isolated points or small group of points with irregular pattern. Isolated points are primarily caused by the interference from twigs of low vegetation and sometimes they represent the outstanding data amount. Although the clustered arrangement of irrelevant points is less common, it is more challenging to distinguish them from the clusters of stem surface measurements. Clusters of irrelevant points are introduced by dense regrowth patches, thick branches, or twigs with withered leaves. Low vegetation and branches are analogue source of misclassification at stem mapping as trees and buildings are at DTM generation. Ghost points are usually single measurements; however, the omission of regular sensor calibration may cause clustered data noise. Two techniques have been developed for filtering irrelevant measurements in binary grid data structures: one for raster and another for the voxel space. As isolated measurements appear as speckles in regular data structures, the term 'speckle filtering' is also accepted in the terminology of digital image processing.

4.7.1. Filtering of irrelevant data in 2D grid structure

The input for the filtering is two overlaying horizontal sections of the point cloud converted into raster format. One of them should be at the height of mapping reference. The supposed height difference of the sections is $20 - 50$ cm, while the optimal thickness is $5 - 10$ cm. It is assumed that the overlaying stem slice sections are close in position and similar in pattern if the vertical difference is sufficiently small. Contrarily, most of the irrelevant data are arranged in random pattern without spatial correlation between the overlaying rasters.

The point cloud sections are mapped into distinct binary rasters with identical georeference and spatial resolution. The complete filtering routine has two steps; however, conducting only the first one often provides reasonable result. The first step is accomplished by a cell-wise AND logical operation between the cells. Let denote c_{ij}^I and c_{ij}^{II} the cell values $\{0, 1\}$ at the location (i, j) in the height sections *I* and *II*. The resulting new raster contains the intersection of the foreground cells i.e. cells in the resulting rasters are filled only if both the source cells are filled:

$$\{ c_{ij}^I = 1 \ \text{AND} \ c_{ij}^{II} = 1 \}. \tag{4-1}$$

This operation eliminates the isolated cells but unfeasible when the irrelevant data are arranged into small clusters. In the second step, the input for the logical operation is extended to the local surrounding of each cell using a kernel with size of 5×5 cells. The return value of the filtering is the sum of corresponding filled cells within the kernel that are in the same position regarding both of the height sections. Let denote (i_0, j_0) the grid coordinates of the filled central cell. The filter value is computed by the following formula:

$$F(i_0, j_0) = \sum_{j=j0-2}^{j0+2} \sum_{i=i0-2}^{i0+2} c_{ij}^I \cdot c_{ij}^{II} \tag{4-2}$$

The filter value F is a positive integer in the interval $[1,25]$, and it has higher value when the samples are matching (*Figure 4-10*). Using a minimum threshold on the filter value eliminates the clusters with irregular patterns. The optimal threshold can be specified on a subset of sample data by visual comparison of the filtered results. Excessive filtering threshold induce the reduction of stem measurements, which result in data loss mainly at the endpoints of the cross-sectional arcs.

The filtering algorithm is demonstrated on the data at sample site P0. The mean heights of the horizontal sections are 1.30 and 1.50 meter aboveground. The thickness of the point cloud sections is 0.1 meter. The minimum threshold for the filter value was set to 6.
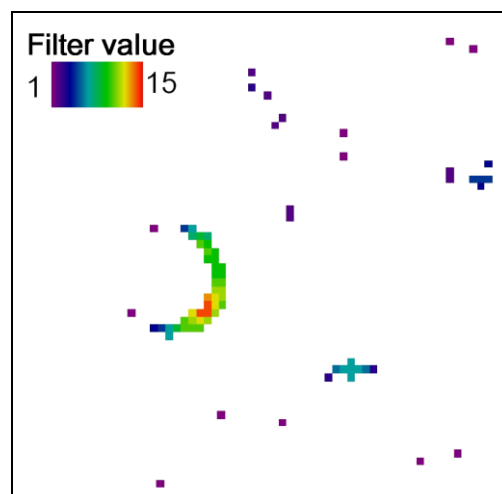
Figure 4-10. Filtering values in a height section. Cells with warm colours indicate higher spatial correlations between the overlapping height sections. (Data from sample plot P0)

4.7.2. Filtering of irrelevant data in 3D grid structure

The reduction of 3D irrelevant data is also based on local filtering, however, the cells of the structuring element are composed of voxels resulted in 3-dimensional shape. The filtering value indicates the sum of voxels within the volume of space defined by the structuring element in the surrounding locality of the central voxel. Stems have shape of solid body of revolution elongated in vertical direction. In contrast to stems, the arrangement of voxels from low vegetation and branches introduces no directional preference. The structuring element should be constructed in a way that the filter returns high value for group of voxels for vertically elongated patterns. In order to meet this requirement the following issues should be concerned:

51

1. The filter has vertically anisotropic effect, thus the structuring element has to be elongated along the vertical axis.
2. The filtering has no preferred azimuthal direction, so the structuring element should be radially symmetric around the vertical axis.
3. With regard to leaning stems, the structuring element considers the deviation from vertical direction resulted in incremental filter radius away from the centre.

These theoretical findings lead to a structuring element with the design depicted in *Figure 4-11*. The filtering has three parameters: (1) height of the structuring element (2) maximum radius and (3) threshold on the minimal filter value i.e. the sum of filled voxels within the structuring element. Filled voxels with filtering value below the threshold are classified irrelevant (*Figure 4-12*).

It has to be mentioned that this filtering operation can be also used alternatively to highlight the voxels composing stems with high probability. Using the structuring element in highlighting mode the minimum threshold should be set to higher value to allow the selection of voxels that surely belong to stems.

The filtering over the voxel space was conducted at the sample quadrates P1, P2 and P3. Results from various parameter set were evaluated from which the optimal one was selected through visual assessment. These parameters are as follows: Height: 11, Diameter: 5, Threshold: 5.
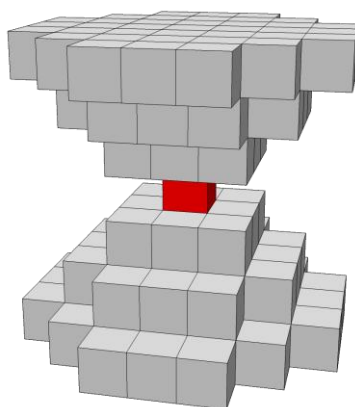
Figure 4-11. Structuring element designed for 3D filtering.(Parameters: height: 7, diameter: 7)
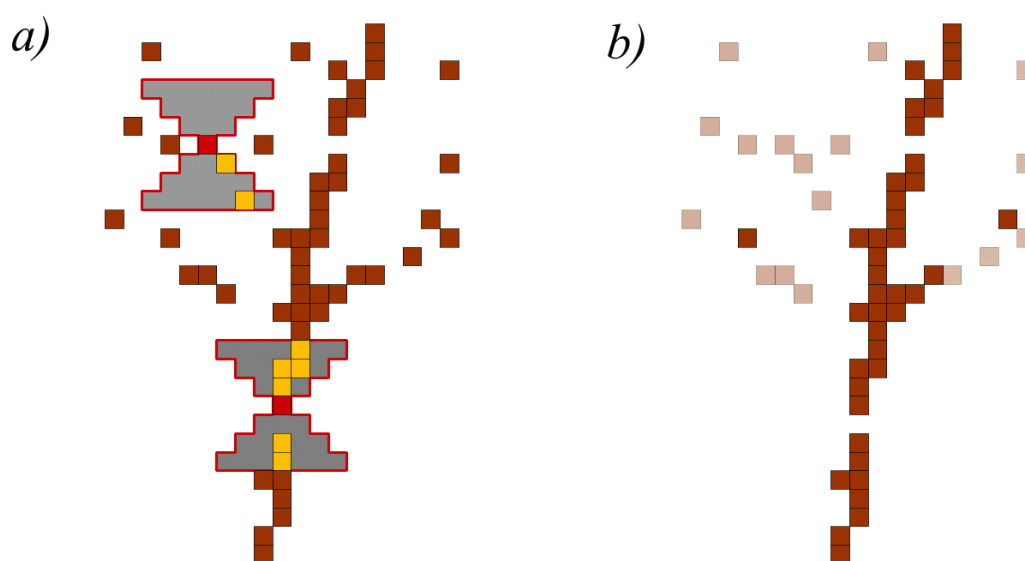
Figure 4-12. Operating scheme of anisotropic filtering (a), and its effect (b). (Parameters: height: 3, diameter: 3, threshold: 4).

4.8. Stem detection in 2D data structure

Two stem detection algorithms are presented in this section resulting in the coordinates of stem centre positions and stem diameter. The reference height of the stem mapping is 1.30 m above the ground. The shape of the stem cross-sections is assumed to be circles in both of the methods so the diameter of the circles represents the stem diameter at breast height (DBH). The first method, introduced in section 4.8.1 detects the stems by delineating the clusters of point measurements directly in the point cloud. The algorithm presented in section 4.8.2 converts the point measurements into a raster and creates image objects from the regions of stem cross-sections.

4.8.1. Detecting stems as point clusters

Stem slice sections can be distinguished from point groups of low vegetation because the stem surface points are arranged in groups with characteristic form and size. The distinctions in size and shape are captured by two theoretical concepts resulting in two routines. The first one is the partitioning of the point cloud into clusters with an iterative method. The second step is the classification of each cluster as either stem slice section or low vegetation. This step includes a proposal for geometric circle fitting by means of an iterative least-squares adjustment that in contrast to the classic Newton numerical scheme requires less accurate initial values for the parameters to be computed.

4.8.1.1. Partitioning the point cloud

Clustering is tool for data mining in statistics that assigns data into separate groups, i.e. clusters, according to a defined similarity criterion (Fogaras and Lukács 2005). In case of point coordinates, the clusters should be delineated so that the sum of squared radial distance of points within the clusters is minimal and, at the same time, the sum of distance across cluster centres is maximal. This method has been adapted assuming each stem cross-section is represented by a cluster, thus the clusters describe the locations of the stems. The clustering expected to assign the coherent stem surface points to identical clusters. There are various clustering methods applied in the fields of digital image processing for unsupervised image classification and segmentation (Czimber, 1997). The algorithm presented in this study is a kind of partitioning technique because any given point is assigned to only one cluster and each cluster has to contain at least one point.

Clusters are described by their centre and radius. The centre is located in the centroid of the member points; the radius is the Euclidean distance between the centre and the farthest member point. The distance between two clusters is identical to the Euclidean distance between the corresponding cluster centres. Clusters are the geometric representations of the stem cross-sections, so the radius of the largest cluster (R) must be identical to the radius of the largest stem. The algorithm needs a rough estimation on the radius of the expected largest stem in the study area, which is a limitation to the maximum cluster size (*Figure 4-13*). The algorithm is unable to separate multiple stems within the same cluster. It follows that (1) Two trees can be separated only if the distance between their centre exceeds R, otherwise the centres are assigned to the same cluster. (2) The minimum distance among the clusters is limited; therefore, the maximum number of clusters is also limited. As a result, there is no need for the number of clusters as input.
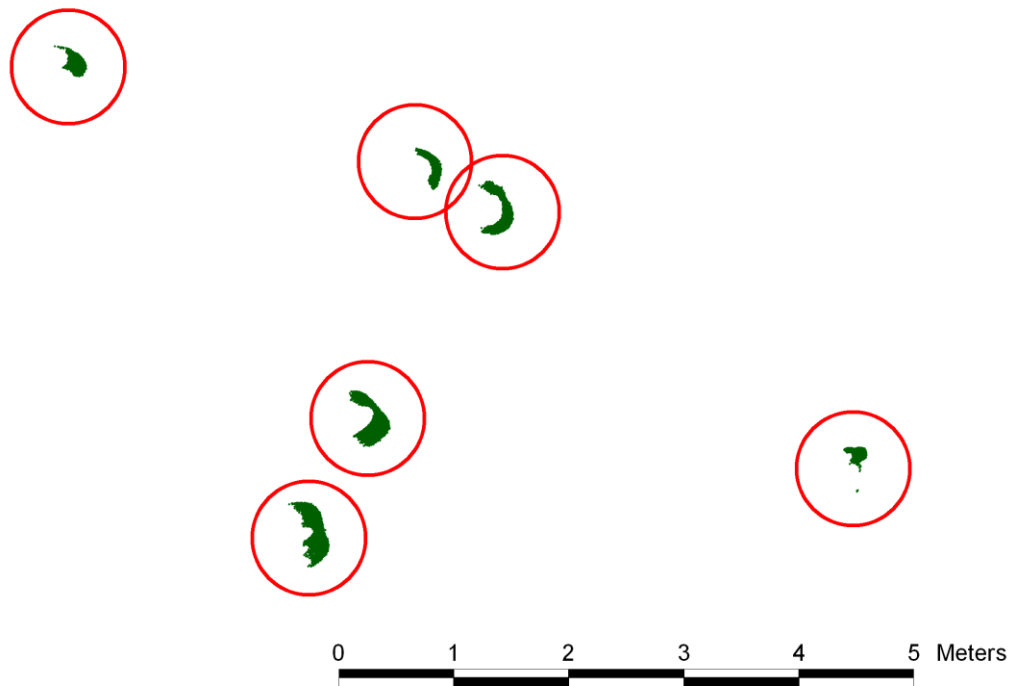
Figure 4-13. Stem point measurements within the maximum cluster radius are assumed to belong to the same tree. The vertical thickness of the subset is 1 meter. (Data from sample plot H1)

The partitioning algorithm is iterative, where the initial number of clusters is zero. An iteration cycle contains the following steps: The point measurements are taken out sequentially from a list. The cluster centres are queried around each point within the distance of *R*. If the query was successful, the point is assigned to the closest cluster; else, a new cluster is created whose centre is identical to the location of the point. Finally, all the points are assigned into a cluster and the list is empty. The cluster centres are recalculated as the centroid of the member points. If any pairs of the recalculated centres are closer to each other than *R*, the corresponding clusters are merged and the new centre will be the centroid of the member points. The points are took out from the clusters and reloaded into the sequential list.

The cycle is repeated iteratively, until the average change of cluster centres exceeds the threshold of 1.0 mm. In the last step, the points are queried within a distance of *R* around each cluster centres and the unique label of the corresponding cluster is assigned to each of the member point. The clusters are considered as stem candidates, although some of them are composed of point measurements from low vegetation and branches. The algorithm of clustering was implemented using quad-tree structure (Czimber, 1997) as spatial index to speed up the searching procedure of the closest cluster centroids.

4.8.1.2.   Classification of clusters

The filtering of stem clusters is achieved by analysing the point pattern. Stem point measurements are arranged along cylindrical stem surfaces, which resulted in circles with approximately identical radius at horizontal cross-sections. In order to check the cylindrical feature of the clusters, horizontal circles are fit to the points located at the bottom, middle and top height of each cluster (*Figure 4-14*).

If the number of data points exceeds three, the parameters of the circle are calculated through geometric fit where the sum of squared Euclidian distance of the data points to the circular arc is to be minimised. The calculation concept is referred to as least squares adjustment or minimization in L2-norm. In addition, if the measurement errors have normal

distribution, the solution of least squares adjustment corresponds to the maximum likelihood estimates (Závoti, 2001). The data points are of uniform weight. The parameters to be estimated are the (x,y) centre position and R radius being analogue to the tree centre position and stem radius (*Figure 4-15*). The goodness of fit is indicated by the root-mean-square error (RMSE) with three degrees of freedom. A major concern in geometric circle fit is that the respective minimization algorithms include non-linear equations without explicit formula. Thus, they usually require linearization and iterative numeric schemes such as the general Gauss-Newton method. The Gauss-Newton method needs 'sufficiently accurate' initial values otherwise the routine converge to a local minimum (Henrici, 1985). The accurate estimation of initial values cannot be guaranteed in our case as the pattern of stem surface points is often asymmetric and covers merely a partial sector of the circle. The proposed routine requires no linearization of the equations used hence it is less sensible to the initial values. The procedure refines the parameters of radius and position in separate steps resulting in convergent solution but the calculation procedure is computationally more demanding than the classic Gauss-Newton method. Running the routine with input of some thousand points has no influence on computation time from practical point of view.

A point pattern in a height section is accepted as circular if the RMSE of the circle fitting is below a given tolerance otherwise the fitting is imprecise. A given cluster is classified as stem if minimum two of its cross-sections are circular and the standard deviation of the circle radii is below the predefined thresholds.

The results of the clustering-based stem detection method were validated on the sample plot H1 with the following user-defined parameters. The subset of points used as input for the clustering was in the elevation interval from 1.0 to 2.0 meter. The maximum cluster radius (namely the largest tree radius to be expected) was 0.5 m. Clusters with less than 50 points were omitted. The horizontal point cloud sections were cut from the point clusters at the levels of 1.0, 1.5 and 2.0 meter, with thickness of 10 cm. A horizontal point cluster section was considered circular if the RMSE of the circle fit was below ±3.0 cm. A cluster was accepted as stem if at least two circle fits were reasonable and the maximum absolute difference in radius was below 5 cm.

Clustering   Checking circularity
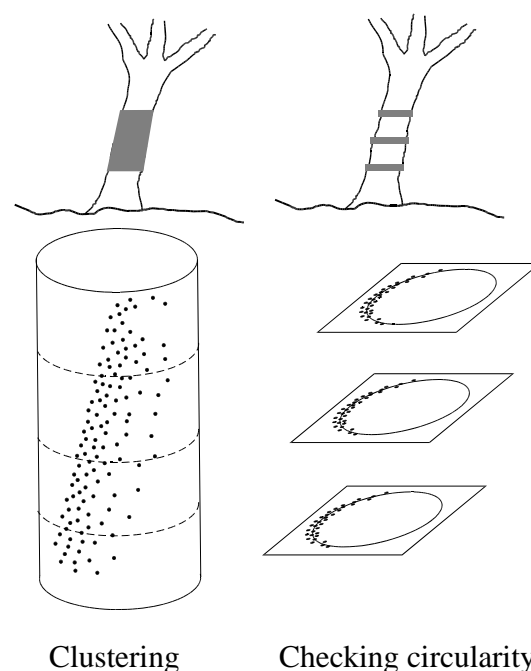
Figure 4-14. Point slice used for the clustering and its sub-sections for checking the circularity of the clusters.
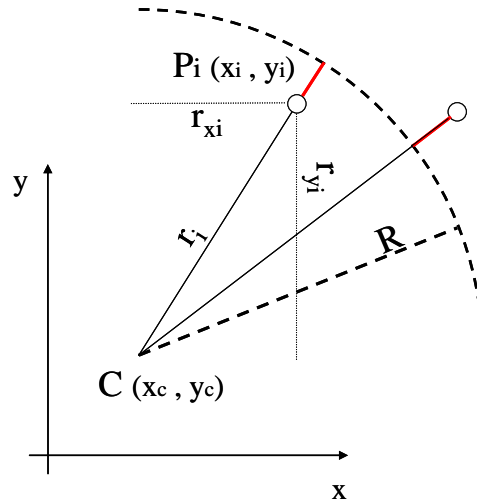
Figure 4-15. Notations for the geometric circle fit.

4.8.1.3.   Routine for geometric circle fitting

Let denote n ($n{\geq}3$) the number of input points, R ($R{>}0$) the circle radius, $\mathbf{c}$ the vector pointing into the circle centre, and $\mathbf{p_i}$ ($i = 1\ldots n$) the vector of the i-th data point. The objective function:

$$f(R, x_c, y_c) = \sum_{i=1}^{n}\left(\left\|\mathbf{c} - \mathbf{p}_i\right\| - R\right)^2 = MIN \tag{4-3}$$

The initial values of the circle centre coordinates (x_c, y_c) can be obtained as the average of the point coordinates representing the centroid of the data points. Introducing the notation r_i for the Euclidean distance of the i-th data point and the circle yields the following formula:

$$r_i = \left\|\mathbf{c} - \mathbf{p}_i\right\| = \sqrt{(x_i - x_c)^2 + (y_i - y_c)^2} \tag{4-4}$$

In the first step, R is considered as variable resulting in the following object function:

$$f(R) = \sum_{i=1}^{n}(r_i - R)^2 = MIN \tag{4-5}$$

This function may have its extreme where its first derivative is set to zero:

$$\frac{\partial \sum_{i=1}^{n}(r_i - R)^2}{\partial R} = 0 \tag{4-6}$$

As (4-6) is summing up squared expressions, the extreme exists, and it is the minimum. The value of R can be yielded as the average of r_i:

$$R = \frac{\sum_{i=1}^{n} r_i}{n} \tag{4-7}$$

The goal of the second step is the estimation of the coordinates of the corresponding circle centre. This requires the orientation of the vector $\mathbf{c} - \mathbf{p}_i$ expressed by the sine and cosine functions of its azimuth:

$$\cos \alpha_i = \frac{x_i - x_c}{r_i} \qquad (4\text{-}8)$$

$$\sin \alpha_i = \frac{y_i - y_c}{r_i} \qquad (4\text{-}9)$$

The objective function in the second step is:

$$f(x_c, y_c) = \sum_{i=1}^{n} \left[\sqrt{(x_i - x_c - R \cdot \cos \alpha_i)^2 + (y_i - y_c - R \cdot \sin \alpha_i)^2} \right]^2 = MIN \qquad (4\text{-}10)$$

As the rooted expression is a sum of two non-negative items, it can be simplified:

$$f(x_c, y_c) = \sum_{i=1}^{n} \left[(x_i - x_c - R \cdot \cos \alpha_i)^2 + (y_i - y_c - R \cdot \sin \alpha_i)^2 \right] = MIN \qquad (4\text{-}11)$$

The variables are separate so the function can be rewritten as:

$$f(x_c, y_c) = \sum_{i=1}^{n} (x_i - x_c - R \cdot \cos \alpha_i)^2 + \sum_{i=1}^{n} (y_i - y_c - R \cdot \sin \alpha_i)^2 = MIN \qquad (4\text{-}12)$$

The global minimum is achieved when both the sums of squared expressions are set to zero:

$$\sum_{i=1}^{n} (x_i - x_c - R \cdot \cos \alpha_i) = 0 \qquad (4\text{-}13)$$

$$\sum_{i=1}^{n} (y_i - y_c - R \cdot \sin \alpha_i) = 0 \qquad (4\text{-}14)$$

Solving the equations yields the refined centre coordinates:

$$x_c = \frac{\sum_{i=1}^{n} (x_i - R \cdot \cos \alpha_i)}{n} \qquad (4\text{-}15)$$

$$y_c = \frac{\sum_{i=1}^{n} (y_i - R \cdot \sin \alpha_i)}{n} \qquad (4\text{-}16)$$

Step 1 and 2 are iterated until the change in any of the parameters exceeds 0.1 mm.

4.8.2. Stem detection by image objects

This technique was developed to detect trees in stands with high branching density and significant coverage of low vegetation. As the amount of isolated data might be dominant, the stem data cannot be delineated from the point cloud using constant cluster radius. In order to filter irrelevant vegetation components in the proximity of stems, analysis of neighbourhood relations is necessary. Grid data structure is especially appropriate for such purposes as the systematic spacing of grid cells directly implies neighbourhood relations. Stem slice sections have the following appearance in grid structure:

1. Stems located far from the scanner positions are sampled with relative low data density. The resulting data gaps fragment the cross-section of stems into multiple image regions. Trees captured from two diametric positions are often feature similar discontinuity at the edges of the point patterns.
2. Some of the contiguous regions involve additional cells from branches or low vegetation in addition to those representing the stem surface. The following algorithm was developed with respect to some specific issues that come to the front especially in case of stands with close-to-nature structure and surveying of trees from multiple scans.

4.8.2.1.   Filtering of stems as disconnected image objects

Data gaps in stem slices cause that the contiguous image regions represent only a fragment of the stem. These fragments are not appropriate input for object detection, as they have no characteristic form. Therefore, it is desirable to use disconnected image objects for the representation of each stem slice section. Disconnected image objects are defined in this study as group of cells that are located within a given Manhattan-distance and represent the same physical object (Brolly and Király, 2010). This rule can be regarded as an extension of the classic connectivity concept where the Manhattan-distance for the aggregation of two cells is one.

The creation of disconnected image objects is implemented using a buffer zone with radius equal to the desired aggregation distance (*Figure 4-16*). The set of cells within the same buffer zones are combined into a disconnected image object. The buffer zone can be removed following the arrangement of component cells into a data structure. As the buffer radius should be limited to a few cells to prevent combining data from stems and from the surrounding low vegetation, many of the resulting disconnected image objects represent incomplete parts of stem slice sections. The laser measurements are reflected from the tree surface thus the wood is represented as a data gap in the image of stem cross-section. Theoretically, data noise might introduce outlying measurements inside the wood but actually, this kind of gross error is rare. As a result, the objects representing the stem surface contain an approximately circular arc even in the presence of branches. In case of multiple scans, the arc may be enclosed to a circle. The following algorithm is aimed at selecting disconnected image objects that feature curved (approximately circular) shape.

(a)   *(b)*   *(c)*
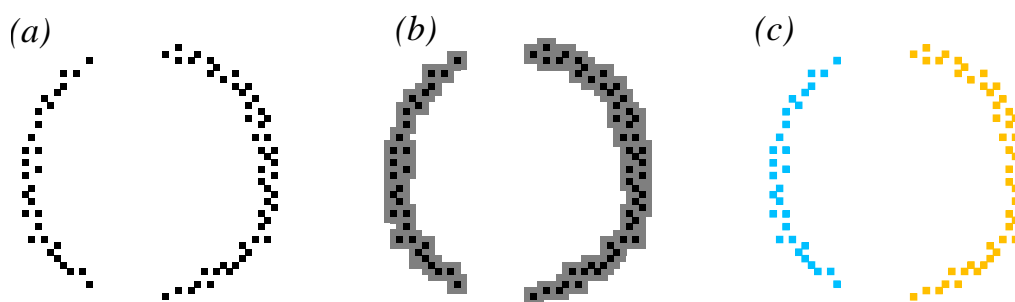
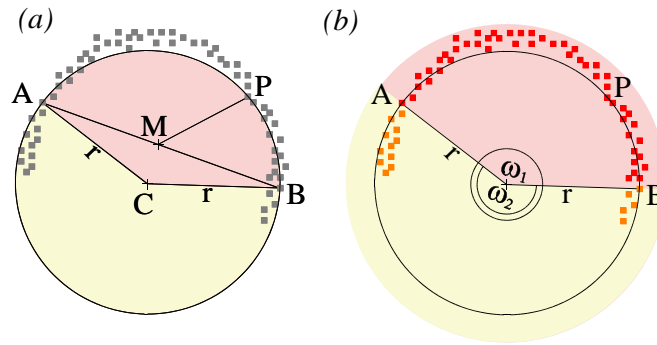*Figure 4-16. Illustration on the aggregation of cells into disconnected image objects using a 1-cell buffer.*

Figure 4-17. Calculation of the filter value for the selection of circular objects.

Endpoint cells (*A, B*) of the longest line segment composed of solely background cells are searched in each disconnected image object (*Figure 4-17*). The midpoint of the line segment is denoted by *M* and *P* is the closest cell to it. If the cell triplet *A, P, B* is not collinear, it determines a circle with centre point *C* and radius *r*. The line segment *AB* represents a chord in the circle that specifies two sectors with central angles ω_1 and ω_2. The circular arc length of the corresponding central angles can be calculated as

$$i_k = r \cdot \omega_k \quad k = \{1,2\} \tag{4-17}$$

Filled cells of those are selected that lie in the neighbourhood of *C* at a distance of *r* with a tolerance of ±25%. The counts of the selected cells are N_1 and N_2 according to the corresponding circular sector. The filter value *F* is to be calculated for both sectors using the following ratio:

$$F_k = \frac{i_k}{N_k} \quad k = \{1,2\} \tag{4-18}$$

The decision rule of the filtering is based on the conformity in arc length AB (or BA) estimated independently by (4-17) and by the sum of cells composing the circumference. As the measure of arc length i_k is calculated in the unit of cell, the ratio *F* with value close to 1 indicates circular shape. Circular image objects have higher probability to represent a region from the cross-section of a stem surface. The higher one is chosen from the two filtering values to represent the significance of the investigated disconnected image object. If the value F exceeds a minimal threshold, the image object is deemed to represent a complete or considerable part of a stem and classified as stem object. The threshold is constant for the entire scene. Its optimal value can be set in a smaller sample area by visual assessment of the results with different thresholds.

Stems of mature trees are composed of multiple disconnected image objects from which the one having measured from the closest scanner position is the largest with significant curvature while the others that are located on the opposing side of the stem, are small fragments without characteristic shape. Many studies (e.g. Thies and Spicker 2004, Király et al. 2007) support that the integration of measurements from multiple scanner positions facilitates the quality of the cross-sectional stem models even if the point density is different at the certain parts of the tree. As only the largest disconnected image object is classified as stem object in most cases, the smaller ones have to be assigned to them to create a complete model of the stem cross-section and to improve the accuracy of diameter estimation. The assignment is accomplished by selecting all the cells around the centre point *C* of each stem object with the corresponding radius *r*. Objects with selected cells are encapsulated on a higher object level into an aggregation (super object) that yields the complete image-object-based representation of the stem (*Figure 4-18*).
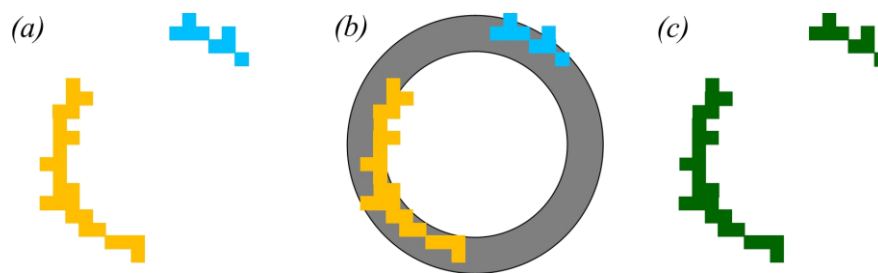
Figure 4-18. Merging of image objects using a ring buffer into a higher object level to represent complete stem slice sections.

4.8.2.2.   Modelling the stem cross-sections

The following objective is to estimate the stem centre position and stem diameter through a parametric circle fit. As the objects often include measurements from the interference of branches apart from the stem, stem surface cells within each object have to be distinguished. In this way, the outlying points can be discarded that enhances the robustness of the circle fit. The approximate location of the stem centre C, defines the direction of the concave surface of the stem. The laser beam does not penetrate into the wood, therefore point measurements are not expected on the inner side of the stem surface. The point measurements along the cells of the concave surface of the stem are considered more reliable for the circle fit. These stem surface cells were selected by a query being similar to that is used at the ray tracing algorithm (Czimber, 1997). Using this analogy, the viewpoint is located at the stem centre and a ray is drawn to each cell. Cells of those are selected that can be viewed from the viewpoint along the ray without being occluded by any other cell (*Figure 4-19*). The centre and the selected cell are considered neighbours in this context, as no other foreground cells are located along the shortest way between their midpoints. The accuracy of the DBH estimation can be enhanced by considering two aspects:

1. The utilization of original point measurements is preferred for the cross-sectional circle fit as they provide higher accuracy and higher sampling density in comparison to the midpoints of the stem surface cells.

2. It was found in our previous study that the underestimation of 0.2–2.4 cm in DBH calculation through circle fit relates to the bark roughness (Brolly and Király, 2009a). The beam divergence was 0.25 mrad corresponding to 25 mm increase in footprint size per 100 m range. It is assumed that significant proportion of the laser points represent the rifts leading to DBH underestimations relative to the results of the calliper measurements. The stem surface cells resemble the bottom of the rifts, thus they represent the inner bark surface. This inherent bias relative to the calliper measurements can be moderated by taking account the data reflected from the outer bark surface.

A two-stage iterative procedure is proposed to comply with these considerations. First, a circle is fitted to the midpoints of the stem surface cells, whose diameter is assumed to represent the inner bark stem diameter. This circle is refined in the second step. The circle diameter is extended by a distance of a few centimetres in accordance with the magnitude of the representative bark roughness. The original point measurements are queried within the extended radius that ensures the sampling of the outer bark surface. As the extension is limited to a few centimetres, the effect of isolated measurements reflected from branches or low vegetation is restricted. The final model of the stem cross-section is created as a circle fitted by the least squares adjustment of the selected raw point measurements as proposed in 4.8.1.3. Parameters of the fitted circle deliver the exact stem centre position and stem diameter.
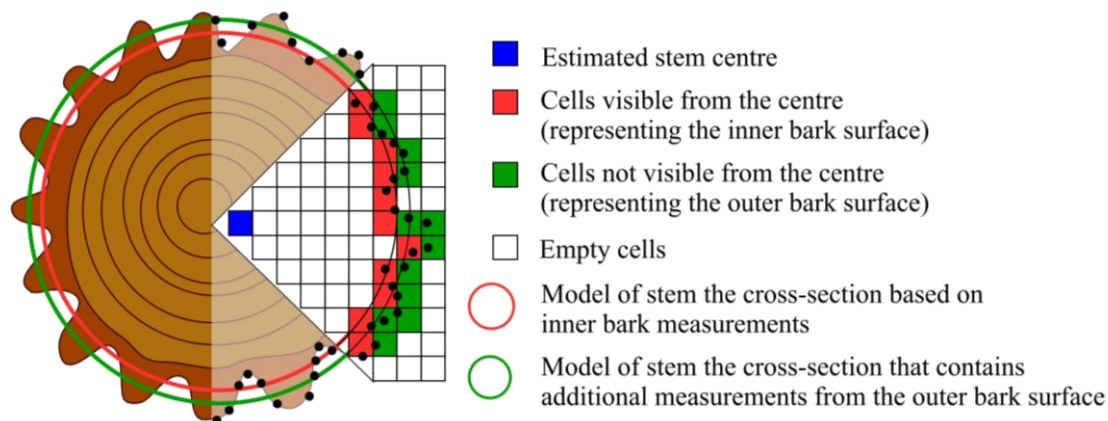
Figure 4-19. Modelling of stem cross-section to estimate DBH. Measurements that are visible viewing from the centre have been reflected from the inner bark surface. These points are considered reliable as they do not contain data from branches. In order to avoid the underestimation of DBH, additional points from the outer bark surface should be involved to the model.

Special attention was paid for the memory allocation issues at the implementation of this algorithm. It was required to process data from multiple scanning positions in one session considering the limitation on the memory access under the 32-bit Windows® operation systems. To do so, the raster of the point cloud section was tiled during the file reading and only the one under processing was loaded into a memory buffer. The processing of image objects was ordered so that the amount of time-consuming read-from-file operations and floating-point routines were minimized.

The performance of the algorithm was tested on the data of sample site P0. The height of the horizontal point cloud section was 1.30 m, with thickness of 10 cm. Grid resolution was chosen to 2.5 cm. Preliminary filtering of irrelevant data was accomplished using the algorithm introduced in 4.7.1. The radius of the buffer zone was 3 cells. The minimal threshold for the classification of stem objects was 0.6, which was specified on a test quadrate of 100×100 meters. The search radius for the query of the stem points was equal to the inner bark stem radius extended by 3 cm.

4.9. Detection and modelling of trees in 3D grid structure

Tree detection and modelling techniques utilizing the 3D spatial data content of the point cloud have the potential to deliver the most thorough structural attributes of the target trees. In addition to the estimation of stem location, structural models open the door to retrieve tree height, crown projection area and other crown-related features. The scope of 2D stem detection methods is limited to trees with diameter exceeding 5–10 cm, as below this size the data pattern does not resemble the characteristic shape of the horizontal stem cross-section. Algorithms based on 3D data have higher capacity to detect young trees as the model space is extended in the vertical direction of the vegetation. The following algorithms are operating in the voxel space that is especially appropriate data structure for the modelling of the complex spatial neighbourhood relations within the tree crowns.

4.9.1. Detection and modelling of mature trees

This algorithm contains two routines. The first one detects the tree stems and their larger branches as connected image objects. It is essential that the target trees are exceeding the size of the low vegetation so their DBH has to be at least approximately 10 cm. The connected image objects are appropriate to locate tree positions but they resulting in incomplete tree models as the smaller twigs are usually fragmented into multiple image regions. The second routine addresses the issue of assigning them to the detected stems and creates disconnected tree models for the accurate retrieval of tree height and crown projection area.

4.9.1.1.   Stem detection using anisotropic filtering

The most straightforward voxel model of a tree is composed of solely connected elements; consequently, the tree is represented as a single and contiguous voxel object. The main advantage of this concept is that each voxel object corresponds to a given tree. In fact, the trees are spatially not isolated in natural stands as the branches in the canopy (even in leaf-less state) might touch each other and multiple stems (shoots) have common root swelling. Vegetation parts closer together than the resolution of the model space cause undesired bridge of voxels between the distinct trees. When multiple individuals are merged in a common object, ambiguity arises in the number of objects and of trees, which has to be resolved in the course of stem detection. Bienert et al (2010) addressed this issue by the elimination of voxels that contained few laser points. Their algorithm assumes that the bridges are exclusively caused by thin twigs in the canopy represented by small number of measurements. This filtering has the drawback of reducing the crown size that would be necessary for the accurate estimation of crown-related metrics and it neither accounts for the common root swelling of shoots.

The stem detection technique proposed in this study extracts stem voxels in a horizontal subset of the voxel space. The vertical limits of the subset are specified so that the bridge effect from twigs and low vegetation is excluded (*Figure 4-20*). The top of the subset is aligned to the canopy base, while the bottom is above the layer of low vegetation. The stem voxels are arranged in vertically elongated regions. The structuring element introduced at the filtering of irrelevant data (4.7.2) is used to select the set of voxels composing such elongated features. Voxels with low filtering value are not removed but remained deselected. Connected objects were created from the selected voxels using the 3D variant of the classic CCL algorithm. Objects with cell counts exceeding a minimal threshold are considered to represent the seed regions (initials) of stems (*Figure 4-21*). As the seed regions are limited to the subset, the voxel objects are extended to the entire model space by a region-growing algorithm. In order to resolve the ambiguity caused by the bridges, the regions are growing simultaneously. Each image object expands one voxel into the directions of its neighbours within one growing cycle. The cycle is being repeated as long as there are unclassified voxels in the neighbourhood of either stem objects. In this way, the path length from the closest seed region determines the membership in case of the ambiguous voxels. The resulted contiguous voxel objects represent individual stems at the end of the routine.

The algorithm was validated in the study site H2. The resolution of the voxel space was 10 cm. The subset of seed regions was set in the elevation range of 2.0–7.0 meter. The height of the structuring element was 5 voxels with maximum radius of 1 voxel. Threshold on the minimal value for the selection of the central voxel was 5. Seed regions composed of minimum 50 voxels were accepted as representing a stem.
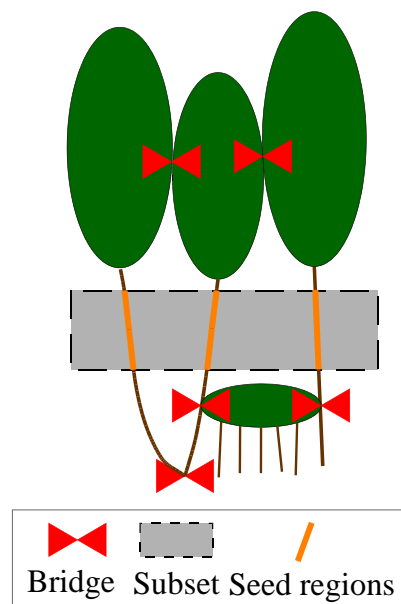
Figure 4-20. Potential bridges between voxel objects that should be eliminated for the delineation of trees.

Figure 4-21. Seed regions as initials for the region growing. (Data from sample plot H2, vertical range of the subset: 2.0–7.0 m. Perspective view)

4.9.1.2. Crown modelling by disconnected voxel objects

The viewing (polar) geometry of the TLS provides decreasing sampling density up the stem. The occlusion effect of branches further reduces the data density in the canopy. As a result, the branches in the upper parts of the tree crowns are represented as many separate voxel regions referred to as fragments. Voxel objects created in the tree detection routine are of connected type thus the model of the crown is incomplete, as the fragments have not been assigned to the identified trees (*Figure 4-22*). Following the integration of fragments into a disconnected voxel objects, the resulted structural model is expected to be appropriate for the estimation of tree height and crown projection area.

Figure 4-22. Separate objects (green) representing fragments of the branches and the upper stems. Contiguous stem objects are brown. (Data from sample plot H2. Perspective view)

Gorte and Pfeifer (2004) and Bienert et al (2010) assigned the fragments to the stem objects utilizing the nearest neighbour search algorithm. This may cause misclassification in multiple layer stands especially where the transition between the two canopy layer is continual and the objects in the lower canopy layer are fragmented, as the end of the branches are often closer to another tree than to the corresponding stem. This kind of misclassification concerns the upper part of the crowns leading to inaccurate height estimation especially at the subdominant trees. The proposed routine intend to improve nearest neighbour search by (1) systematic selection of representative voxels among which the distance of two objects should be specified (2) progressive implementation of the assignment procedure.

Each fragment is represented as continuous voxel object. Assignment of fragments being closer to the stem is considered more reliable than of those that are in the peripheral region of the crown. Fragments are assigned to the stems in the order of ascending distance: the closer fragments are processed earlier. As the branches of deciduous trees are usually connected to the stem at their endpoint of lowest elevation, the voxel with the minimum z value was selected in each fragment to represent the location of the object for the distance measurement. Soon after the closest fragment is being assigned to the stem, the fragment object is integrated into the stem object as its disconnected component. That means the model of each tree is being created progressively through the expansion of the stem objects. The maximum gap distance can be limited by the user to prevent assigning data to the stem objects apart from the tree (e.g. ghost points above the tree tops). This parameter has influence on the crown size so a calibration against crown reference measurements on a few samples is needed to set the optimal value. The calibration can be based upon either tree height estimates or crown metrics

such as crown diameter or projection. From practical viewpoint, the field measurement of tree height is more convenient than the estimation of crown diameter. The tree height and the crown projection area can be directly measured on the resulted disconnected tree models. The tree height is obtained as the highest elevation difference within the component voxels. The crown projection was delineated by the convex hull of the horizontal projection of the crown voxels. In this study, the convex hull algorithm of Andrew (1979) was implemented. The crown projection area was estimated by the area of the horizontal convex hull.

The stems detected by the anisotropic filtering in the sample area H2 (4.7.2) were completed by assigning the crown fragments. The maximum gap distance was specified through the calibration against height estimates of five sample trees (three deciduous and two conifers) as references. The maximum gap distance of four voxels (40 cm) resulted in the smallest bias at the calibration was set to the entire scene. The gap distance is defined as the Manhattan-norm of the voxels' midpoints.

4.9.2. Detection of trees in regeneration phase

The scope of the algorithm introduced in this section is to detect trees with DBH in the range of 2–10 cm automatically (*Figure 4-23*). Trees of this size can not be distinguished from irrelevant isolated data in a horizontal point cloud section thus solely the algorithms of those are capable to manage this issue that consider the vertical vegetation structure as well. Reduction of irrelevant data is of primary importance as thin branches and the high stem density generate significant amount of isolated data within the regeneration patches. The 3D filtering procedure (4.7.2) is suggested for reducing the irrelevant measurements through the anisotropic removal of isolated data.
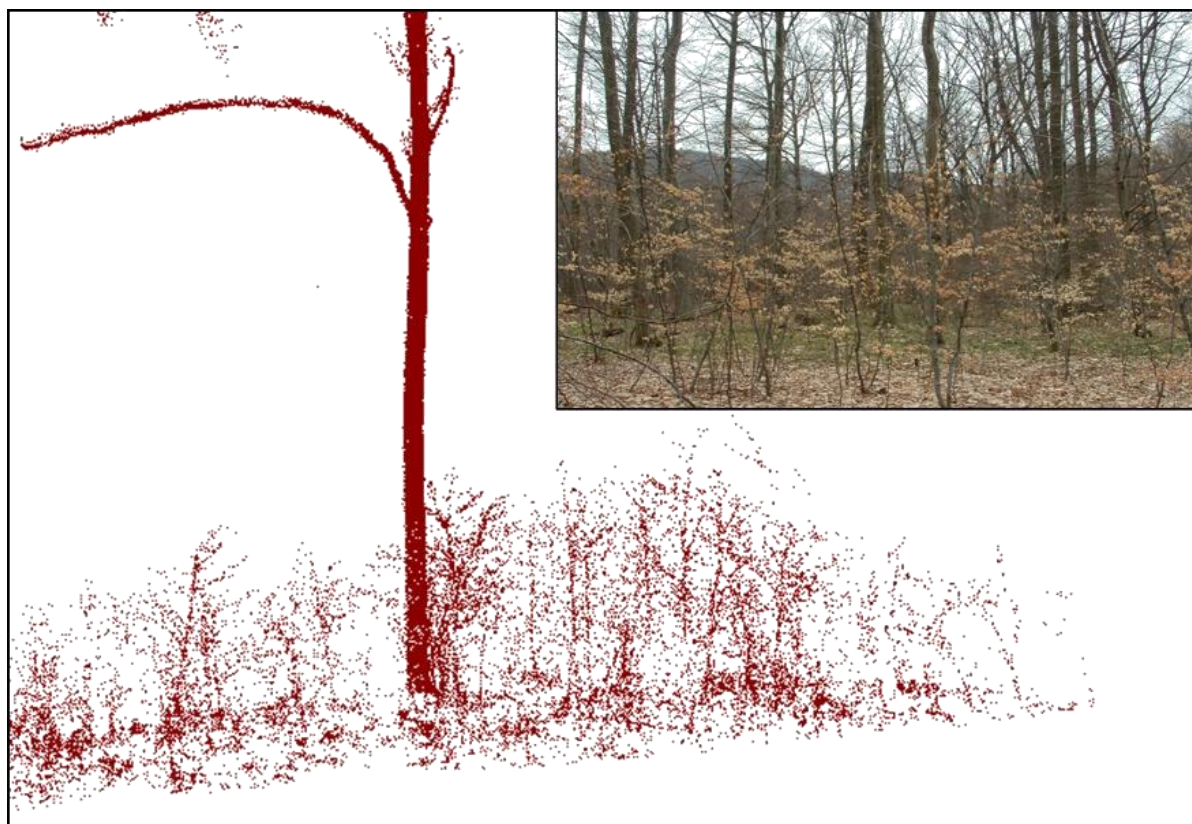
Figure 4-23. Regrowth as it appears in the photo and in the point cloud. (Data from sample plot P0)

4.9.2.1. Aggregation of voxel-objects

The tree detection is conducted in the binary voxel space. The detection procedure is object-based therefore; the voxels of contiguous regions are organized into 3D objects. The trees are usually composed of multiple objects as they are partly occluded by their neighbours. Hence, the single objects are representing tree fragments. In order to manage the discontinuity of trees and aggregate the fragments into a disconnected model, the objects are generalized to their vertical axis. The vertical axis is the shortest path between the highest and lowest voxels within the object that yields a one voxel thin representation of the vertical extent and orientation of the object (*Figure 4-24*). The generalization was implemented with the adaptation of 'Dijkstra' algorithm that is a graph search method for solving the single source shortest path problem (Cormen et al, 1990). Each object is represented as a graph whose vertices and edges were corresponded to voxel midpoints and connections in the directions of the neighbouring voxels respectively. The source node is the highest voxel and the traverse is directed towards the lowest voxel. The objects are represented solely by their vertical axis following the generalization. Objects of those whose vertical axis contained more than one voxel in the same height level were removed, as horizontal connections are deemed atypical for the axis of a tree stem.

Most of the voxel objects in the model space represent fragments of stems and of branches. The objective of the next step is to aggregate the voxel objects representing the fragments of the same tree into a disconnected voxel object and to eliminate the branches being irrelevant from the viewpoint of stem mapping. The hypothetical structure of a tree has three features in the voxel space:

1. It is extended to vertical direction
2. Its shape is approximately straight
3. The gap distances are short between its composing fragments.
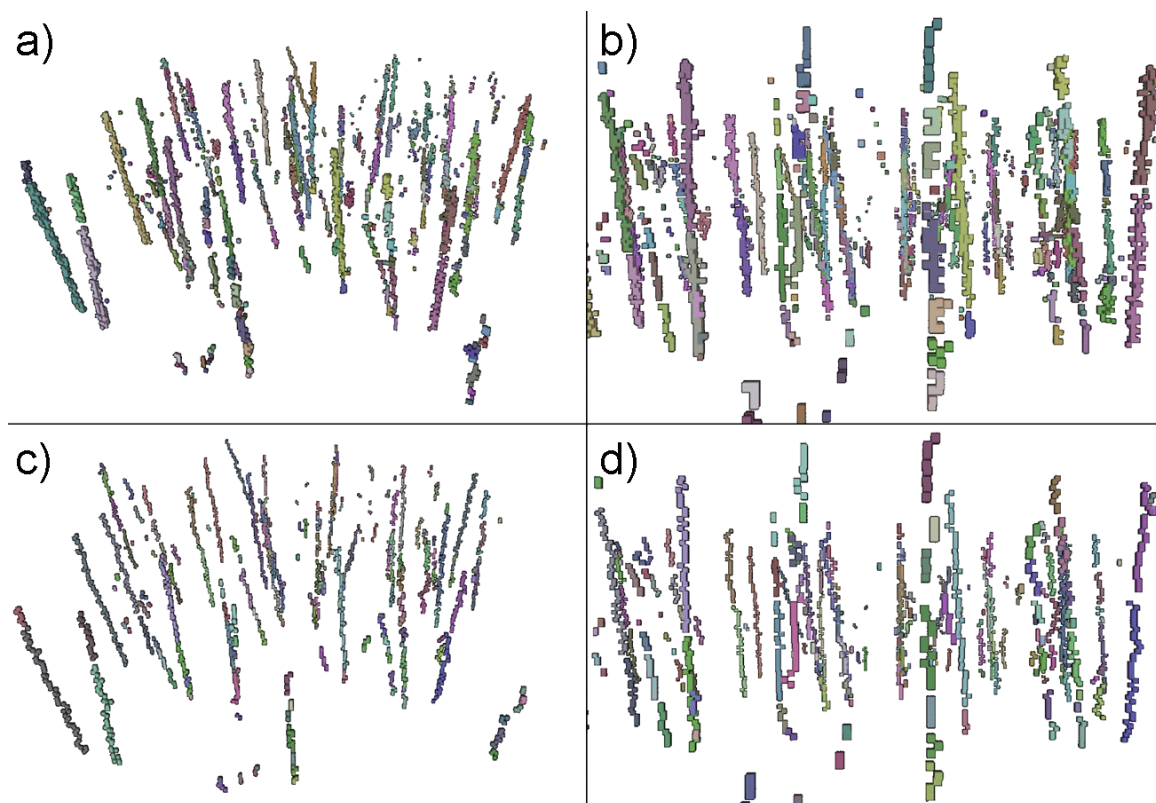
Figure 4-24. Detection of juvenile trees: a-b) contiguous voxel objects as tree components, c-d) generalized objects. (Data from sample plot P1. Perspective view)

The spatial alignment of arbitrary two fragments concerning to the above described three features is revealed using three parameters: P_E, P_S, and P_G for the extent, straightness, and gap distance respectively. All the parameters are normalized to $[0,1]$. The degree of conformity of the resulting disconnected voxel object to the hypothetical tree structure is quantified using the aggregation factor A yielded as the product of the three parameters:

$$A = P_E \cdot P_S \cdot P_G \quad [0,1] \tag{4-19}$$

The computation of A for disconnected image objects is achieved by substituting the data gaps with the shortest path between the corresponding end voxels. That is, the assignment routine treats objects regardless to their continuity.

The value of A is calculated in all the possible combinations of object pairs in the initiation phase. The aggregations are realized sequentially, in the order of descending A. Therefore, the objects of those are aggregated in each cycle, which results the maximum gain in the value of A (*Figure 4-25*). Following the aggregation, A is updated for the resulted disconnected voxel object and for its neighbours. As the vertical axis is definitely one voxel thick without horizontal connections, the maximum size of the aggregated objects is limited to the count of levels of the voxel space. The assignment procedure is being repeated until all the possible pairs have been aggregated or the maximum value of A exceeds a user defined threshold. This threshold puts limitation for distant objects to be aggregated thus it prevent assigning objects of distinct trees.

Some of the disconnected voxel objects represent irrelevant vegetation components, such as branch points arranged in linear pattern. It is assumed that the vertical extent of trees is in excess of branches and any other linear patterns. To extract those objects that are representing trees, a threshold is applied on the number of constituent voxels being proportional to the vertical extent. This feature is simple to visualize, so the optimal threshold can be set by real-time inspection on how the filtering results change according to the modification of the filtering value. Alternatively, the filtering value can be set by calibration at a smaller sample area.
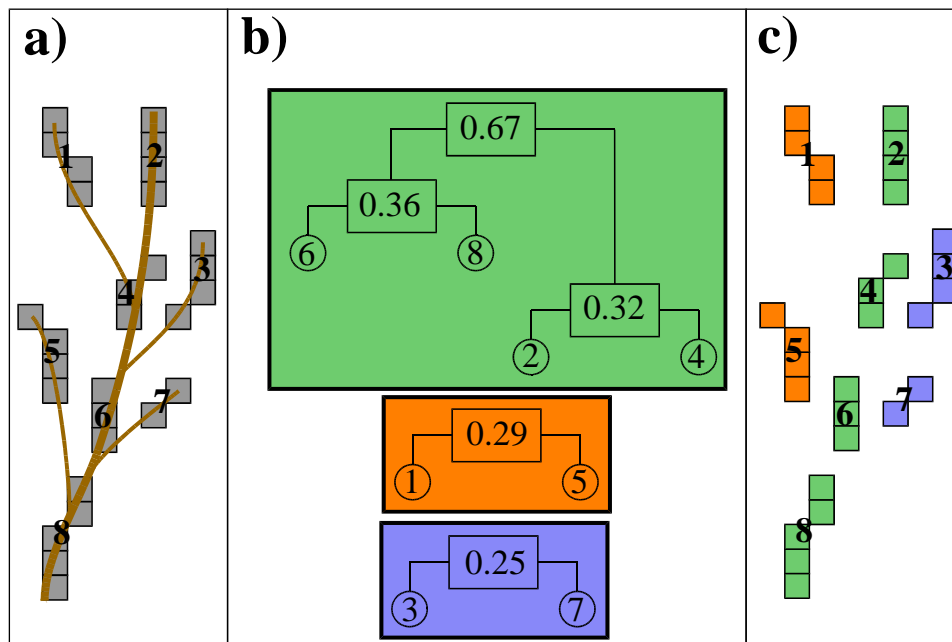
Figure 4-25. Aggregation of generalized objects representing a juvenile tree stem and branches (a). The procedure is accomplished in five steps where the objects of those are aggregated that resulted in the maximum value of A (b). The largest disconnected voxel object represents the stem being reconstructed from four fragments (c).

The algorithm is validated on the data of P1, P2 and P3 sample quadrates. The voxel space was generated from the point cloud at the elevation range of 0.5−3.5 meters with a resolution of 5 cm. The reduction of irrelevant data was achieved by the 3D anisotropic filtering, using the parameterization introduced at 4.7.2. The threshold of the aggregation factor was 0.01. The filtering value (i.e. the minimal number of voxels composing the vertical axis) was set to 20 by visual assessment on the resulted image objects.

4.9.2.2. Formula of the aggregation factor

Let denote $\{V_1, V_2 ... V_N\}$ the series of composing voxels in the vertical axis of a contiguous object and $d(V_i, V_j)$ the Euclidian distance between the voxels V_i and V_j. As the vertical axis is one voxel thick, there is only one path between V_i and V_j, which is defined as:

$$l(V_i, V_j) = \sum_{k=i}^{j-1} d(V_k, V_{k+1}) \tag{4-20}$$

The fragments A and B are composed of $\{A_1, A_2 ... A_N\}$ and $\{B_1, B_2 ... B_M\}$ series of voxels respectively as it is depicted in *Figure 4-26*. A and B can be aggregated only if A_N and B_1 can be connected by through a series of voxels that have neither horizontal neighbourhood, nor contain voxels from a third-party object.
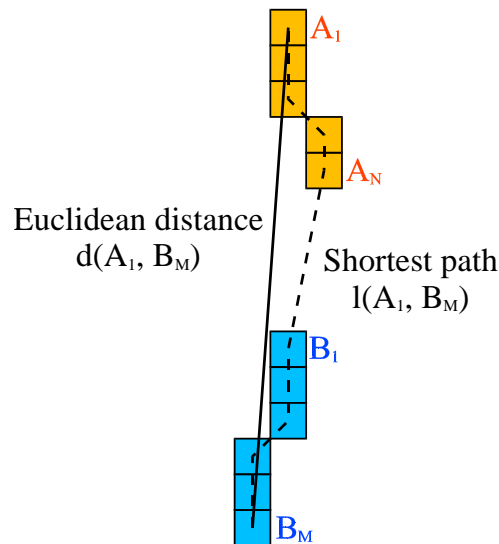
Figure 4-26. Euclidian distance of the farthest end voxels of two generalized voxel objects and the shortest path between them.

The straightness of the vertical axis resulted from the aggregation of A and B is quantified as the proportion of distance between its endpoints and the corresponding path length:

$$P_S^* = \frac{d(A_1, B_M)}{l(A_1, A_N) + d(A_N, B_1) + l(B_1, B_M)} \tag{4-21}$$

Two voxels belong to identical vertical axis only if it is possible to get from either to another through vertically and / or diagonally connected voxels. The Euclidian distance between two voxels that are in vertical neighbourhood is 1, while the distance is $\sqrt{2}$ or $\sqrt{3}$ for diagonal neighbours sharing common edge or corner respectively. The path between two voxels within a vertical axis never can be shorter than their Euclidian distance d and can be

never longer than $\sqrt{3} \cdot d$. Consequently, the codomain of P_S^* is in the interval of $\left[\dfrac{\sqrt{3}}{3}, 1\right]$ that is to be normalized into $[0,1]$ with the following formula:

$$P_S = \frac{1}{1 - \dfrac{\sqrt{3}}{3}} \cdot \left(P_S^* - \frac{\sqrt{3}}{3}\right) \tag{4-22}$$

The size of the vertical axis composed by aggregation is expressed by the extent parameter that concerns the number of voxels but disregards the gap between the objects:

$$P_E^* = N + M \tag{4-23}$$

The maximum extent of a vertical axis is limited to the *H* height of the voxel space. Thus the maximum extent of an axis resulted from the aggregation of two objects is *H*–1 as a gap of at least one voxel size is presented between them. The minimum extent is 2 voxels when both components are single voxels. The extent parameter is normalized to $[0,1]$ with the following formula:

$$P_E = \frac{P_E^* - 2}{H - 3} \tag{4-24}$$

Object pairs of those are favoured at the aggregations that are close to each other as it has higher probability that they represent the same tree. This preference is expressed by the gap parameter that is the inverse to the Euclidian distance of the end voxels:

$$P_G^* = \frac{1}{d(A_N, B_1)} \tag{4-25}$$

The distance of the voxels is defined as the distance of the voxel midpoints, thus the codomain of the gap parameter is in the interval of $[2, \sqrt{3} \cdot (H-1)]$. Following the normalization to the interval $[0,1]$ the formula below is yielded:

$$P_G = \frac{\sqrt{3} \cdot (H-1) - d(A_N, B_1)}{\sqrt{3} \cdot (H-1) - 2} \tag{4-26}$$

The aggregation factor is calculated as the product of the parameters for extent, straightness and gap distance with identical weights:

$$A = P_S \cdot P_E \cdot P_G \quad [0,1] \tag{4-27}$$

5. Results and discussion

The essential results of this thesis are the package of algorithms and their validation providing information on their applicability and limitations. The introduced algorithms were implemented as 32 bit console applications developed by the author using ANSI C programming language that enables fast processing speed and extensive control over the memory allocations. The applications are of modular structure that holds the possibility of subsequent integration. The point cloud data is read from and written to ASCII text files as coordinate triplets with relative heights. The exchange format of rasters is standard ERStorage data type supported by many GIS software packages including ERDAS ERMapper®, DigiTerra Map® and ESRI ArcView®. The display application for the rendering of the tree models in the voxel space was developed by Kornél Czimber using the Microsoft® DirectX application programming interfaces. (Figures in this study depicting perspective views of voxel models were captured as screenshots from this application.) The performance of the algorithms was validated through the results achieved by processing the laser scans captured from the sample sites.

5.1. Filtering of irrelevant data

The filtering procedure is considered efficient in case it removes most of the irrelevant point measurements (low vegetation, branches, and ghost points) without modifying the data of tree to be mapped. The ratio of the eliminated irrelevant data is referred to as filtering intensity. The preserved data of the target trees indicates the filtering reliability. There is an inverse relationship between the filtering intensity and reliability, where the priority of either feature is determined by the main purpose of the given application.

Data of sample sites located in Pilis (P0, P1, P2 and P3) were purified using the introduced filtering procedures. The results achieved by the automatic stem mapping algorithms at these sample sites refer to the efficiency of the filtering as well.

5.1.1. Filtering of irrelevant data in 2D grid structure

The sample site P0 was subject to the raster-based filtering, which reduced the number of data cells by 87%. The fact that only a slightly more than the one-tenth of all the grid data have been preserved for the forthcoming stem detection indicates the high intensity of filtering and, at the same time, it denotes the high coverage of low vegetation. The visual inspection of the results shows that the filtering retained most of the stem cells (*Figure 5-1*). The results of the first filtering phase (i.e. the AND operation among the overlaying single cells, designated by green) proved to be essential, which were improved slightly using the local structuring element (green cells). An important feature of the filtering is that it has the capacity to eliminate small regions of irrelevant data in addition to isolated cells. Most of the filtering errors were identified at leaning trees, where the patterns in the overlaying stem slice sections were misaligned. The misalignment resulted in lower spatial correlation that caused that the peripheral cells of the stems were classified as irrelevant data. This type of filtering error induced eventual loss of stem data in case of the small trees with diameter less than 4–5 cells or at larger stems when they were represented with very low data density.
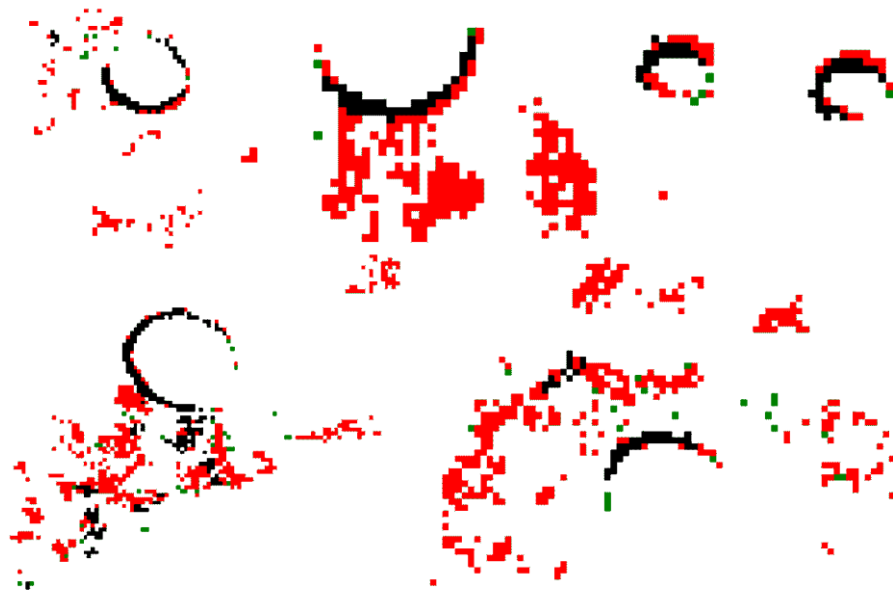
Figure 5-1. Examples on filtering of irrelevant data. Black cells were retained; red cells were eliminated by operation AND, while the green ones were eliminated by the structuring element. (Mosaic, assembled of the data from sample plot P0)

5.1.2. Filtering of irrelevant data in 3D grid structure

The quantitative results of the 3D anisotropic filtering achieved at the sample quadrates P1, P2 and P3 are listed in *Table 5-1*. The filtering routine removed voxels up to a proportion of 59%. This intensity seems lower than it was of the 2D filtering routine. It can be explained, as the objective of the raster-based stem mapping was to locate mature trees at the sample site P0, while the 3D filtering was aimed to prepare the mapping of juvenile trees in regrowth patches. As the low vegetation was irrelevant from the viewpoint of raster processing, the regrowth patches were eliminated. The 3D filtering routine performed high intensity in the elimination of single voxels in irregular patterns (*Figure 5-2*). The anisotropic feature ensured reliable filtering even in case of leaning stems. Using identical structuring element and filtering parameters, the lowest intensity was achieved at the sample quadrate P2, where the stem number was the highest thus most of the voxels represented tree stems. The high branching density at the sample quadrate P3 did not reflected as higher filtering intensity. This can be partially explained as the anisotropic filtering is optimized to preserve vertical structures so the voxels of branches with close to the zenith orientation were retained.

Table 5-1. Quantitative evaluation of 3D anisotropic filtering.

Quadrate	Sample trees	Point counts	Voxel counts		Voxel counts / tree	
			Original	Preserved [%]	Original	Preserved
P1	41	15619	11806	58.0	288	121
P2	212	55080	38371	36.8	181	114
P3	58	34787	22020	58.8	380	156
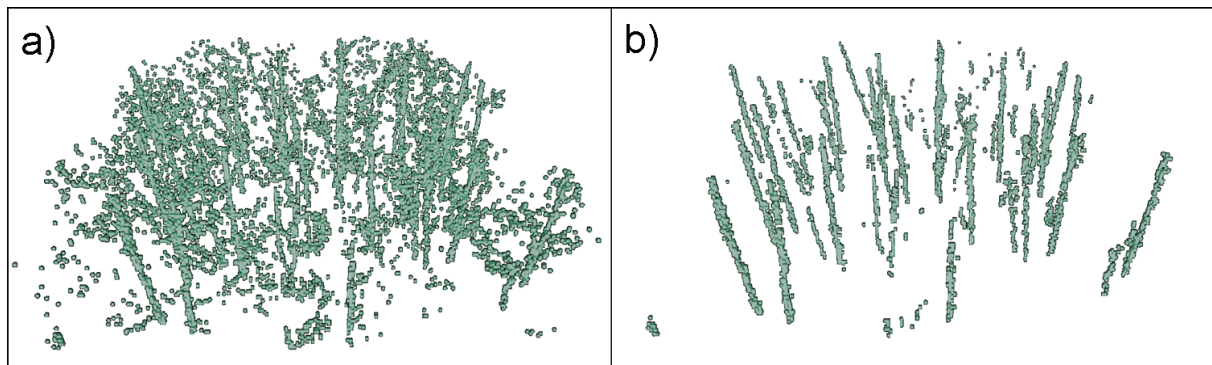
Figure 5-2. Voxel space generated from the original data of the sample quadrate P1 (a), and the result of the filtering (b). (Data from sample plot P1. Perspective view)

5.2. Tree detection

The result of tree mapping was evaluated by the comparison of stem centre coordinates of reference trees with those located by the detection algorithm. Stem models with matching reference position were considered correct detections if the distance of the two tree positions did not exceed a predefined tolerance. The tolerance in position was specified based on the magnitude of mean stem radius in the sample area. Tolerance of 30 cm was chosen for mature stands (H0, H1 and P0) and 10 cm for juvenile trees in regrowth patches. The matching had to be unambiguous i.e. exactly one model position could be assigned to each reference position and vice versa. Model positions without matching reference are referred to as misclassification. The number of omissions is equal to the number of reference trees without model positions within the tolerance; the algorithm failed to detect these trees (*Figure 5-3*). As the number of correct detections and of omissions is referred to the reference data, the sum of detection ratio and omission ratio is equal to 100%. The misclassification ratio is normalized to the number of correct detections.
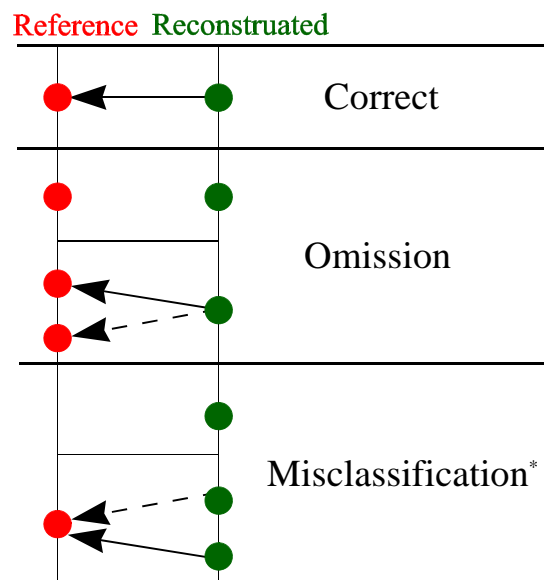
*Total correct = 100%

Figure 5-3. Graphical explanation of terms used for the evaluation of automatic tree detection. Acceptable assignments are marked with solid lines; dashed lines illustrate rejected assignments because of ambiguity.

5.2.1. Tree detection by means of clustering the point cloud

The algorithm detected 133 (76.9%) out of 173 visible trees at the sample plot H1 based on the single scan captured from the plot centre. The number of omissions and misclassifications are 40 (23.1%) and 8 (4.6%) respectively regarding the visible trees. If the occluded trees are accounted for, the detection rate falls to 63.0% and the omission raises to 37.0%. The low number of misclassifications relative to the number of correct detections is ascribed to the absence of low vegetation. The misclassified clusters mainly represent branches. A visual inspection supported that the omitted trees were indeed visible from the scanner position and they were represented in the point cloud.

The ratio of omitted trees is graphed versus the density of stem surface points in *Figure 5-4*. It can be stated that the omissions are especially frequent at point densities below 1 cm^{-2}. Following this tendency, the ratio of omissions exceeds the ratio of correct detections when the point density falls below 0.5 cm^{-2}. On the other hand, the ratio of correct detections is limited to about 80% throughout the upper range of data density. The visual interpretation of the stem slice sections yielded that the point pattern within the stem clusters often exhibits deviation from the hypothetic circular shape (*Figure 5-5*). The actual shape of stem cross-sections may introduce several types of distortion in the point cloud, especially when branches or stubs are arisen from them. In case of such irregularities, the RMSE of the circle fit indicates poor alignment, which resulted in the false rejection of the cluster. The evaluation of the RMSE with respect to the entire cluster has limitation in tree detection if point measurements from branches are included in the pattern.
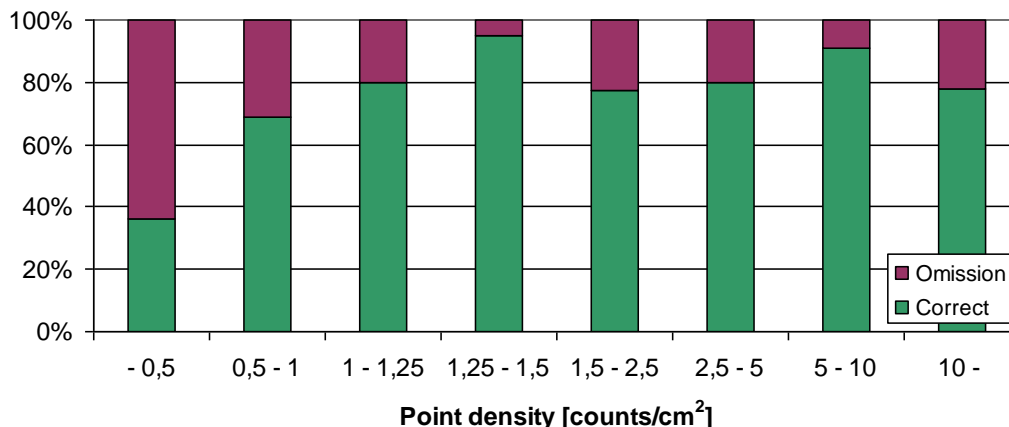
Figure 5-4. Proportion of correct detections and omissions according to the density of stem surface points.

Another issue is the recognition of stems close to each other as is the case at multiple stems from a common root swelling. The minimum cluster spacing is determined by the cluster radius indirectly as multiple cluster centres cannot coexist within the cluster radius. If the stems are closer to each other than the minimum spacing of cluster centres, the individual stems cannot be separated because they are merged in a common cluster. The shape of clusters including point measurements from multiple stems usually strongly differ from that of the circle. The rejection any of these clusters resulted in as many omissions as the number of stems within the cluster.

The smallest detected tree had a DBH of 5.4 cm, while the maximum DBH was 52.8 cm. This indicates that (1) The DBH of 1 meter for the expected largest tree was quiet inaccurate as it is almost twice as large as the actual maximum (2) The algorithm has capacity to detect trees in wide range of diameters. The performance of tree detection is correlated to the DBH (*Figure 5-6*).
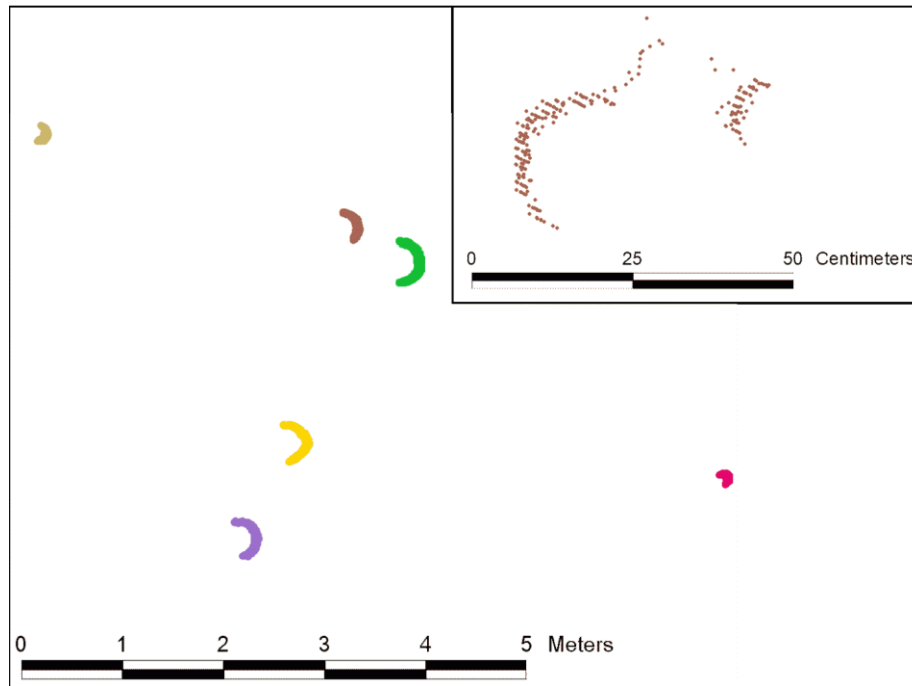
Figure 5-5. Clusters of point measurements with distinct colour depict individual stem slice sections. Inset: Clusters of multiple stems or branches have irregular shape. (Data from sample plot H1, vertical range: 10 cm)

The majority of trees with DBH below 10 cm were omitted and the rate of correct detections reaches its overall mean value starting around 20 cm. This is explained as the smaller trees were sampled with fewer measurements thus the corresponding clusters contain insufficient amount of data in the certain point cloud sections. In addition, the scattering of point measurements at the stem surface has the same magnitude as the stem radius at trees with DBH below 10 cm. The outline of these stem cross-sections are blurred and the pattern of point measurements tends to be stochastic or amorphous. This scale seems to be the limit of distinguishing stems and irrelevant isolated data through 2D point pattern analysis at the present scan settings.

To the author knowledge, this was the first application of clustering with the goal of partitioning a laser scanner point cloud for the extraction stem cross-sections (Brolly, Király 2009). The advantages of the technique brought the attention of other researchers who integrated the proposed algorithm with the corresponding parameter set into their own developments (e.g. Huang et al., 2011).
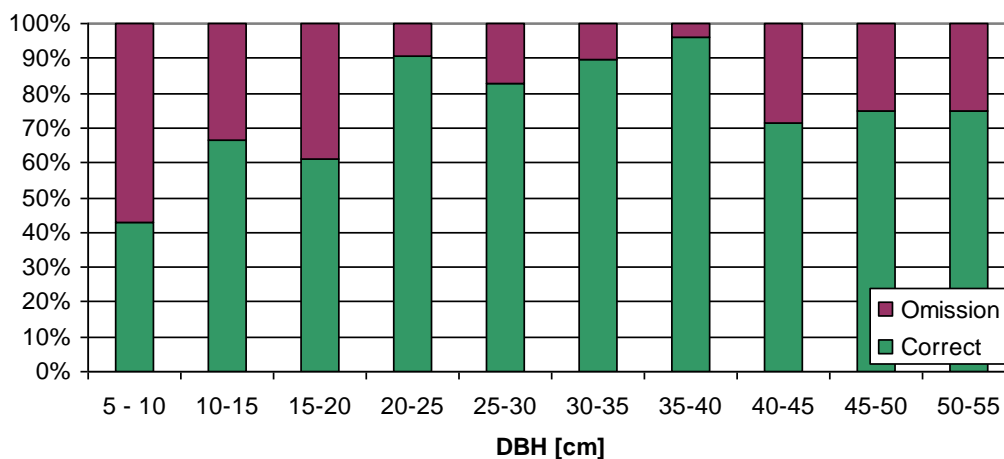
Figure 5-6. Performance of tree detection based on clustering in different DBH classes.

5.2.2. Tree detection by raster image objects

The algorithm yielded all together 1386 tree locations at the sample site P0 from the combined scans of 38 vantage points. 1100 trees were correctly detected (70.5%), 505 trees were omitted (29.5%) and 286 image objects were misclassified (20.6%).

The change of detection rates according to the DBH is depicted in *Figure 5-7*. It can be noticed that the ratio of misclassifications introduces stronger correlation to the stem size as those of omissions. The ratio of misclassifications is significantly higher (54%) at trees with DBH below 20 cm (8 cells) than at the larger ones. Most of the misclassified objects represent patches of low vegetation. The reliability of the detection is proportional to the number of cells characterizing the image object, as the redundancy consolidates the parametric description of the shape. The smaller the diameter of a tree, the fewer cells represent its surface at a constant viewing angle, which resulted in less reliable detection at the smaller range of DBH.

The number of omissions is less dependent on the stem size, although the algorithm skipped trees from the smallest DBH class with significantly higher rate (45%). The position of the reference trees were estimated based on the laser scan. Consequently, completely occluded trees have not been presented in the reference data set. The higher omission rate at the smaller DBH range can be explained by the unsatisfying definition of circularity. It is a general side effect of the filtering of isolated data that a few cells are deleted at the ends of the cross-sectional point patterns. In case of small trees, the removal of a few cells causes significant reduction in the represented arc length, which lowers the *F* filtering value considerably. Trees with diameter in excess of 15 cm (6 cells) are less prone to omission as the circularity of their stem cross-sections is better defined.
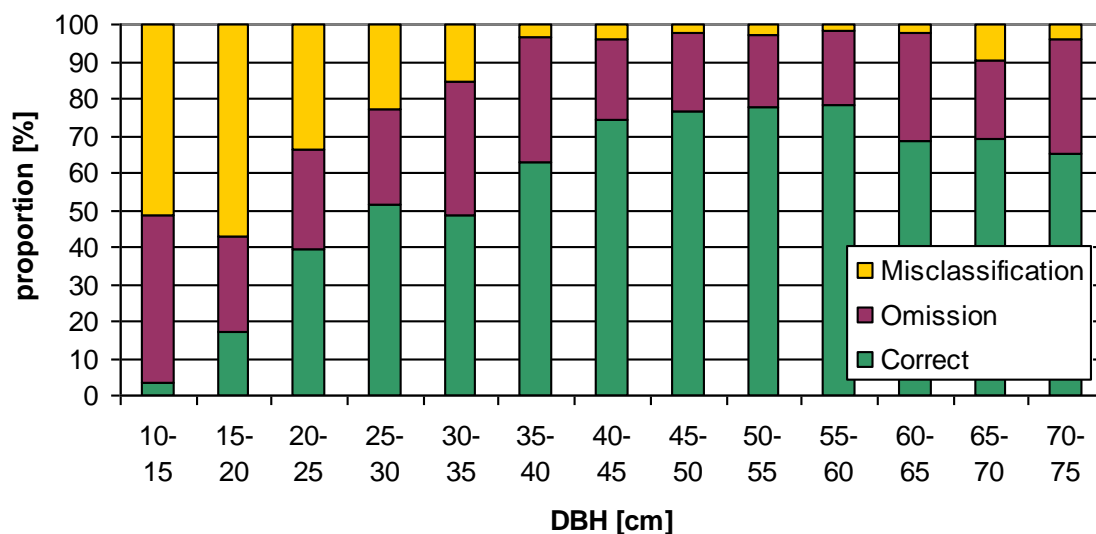
Figure 5-7. Performance of tree detection based on 2D image objects in different DBH classes.

Figure 5-8 illustrates image objects (along with the raw point measurements and the fitted circles) that were correctly recognized as stem slice sections. The stem slice sections surveyed from multiple scanning positions are composed of multiple image objects but in spite of the fragmentation, the fitted circle is aligned to all of them. This is ascribed to the precise registration of the point clouds and it implies to the efficiency of the aggregation procedure of image objects. As the circle is fitted to the selected cells of those representing the stem surface, the branches have no adverse effect on the diameter even these points are included in the image object. The main source of errors in terms of misclassification are the image regions composed of measurements from low vegetation, especially those having concave

boundary, because their appearance is very similar to that of stem cross-sections. If the viewing angle is narrow and the corresponding central angle is of small measure in the circle, the interpretation of stems becomes problematic even by visual inspection. A more restrictive filtering threshold decreases the rate of misclassifications; however, the ratio of omissions is expected to heighten especially in the range of smaller diameters. The issue of omissions is more common at the trees located along the boundary of the scene as they are usually measured from one direction so only a part of the stem surface have been sampled.

The application was able to process the merged data from 38 scanning positions throughout the entire study area of 9.5 hectares in one session. The use of algorithms developed for exclusively single scans may be time consuming at so many scanning positions and special care should be taken to resolve the ambiguity resulting from the multiple detections of the identical trees.

The integration of data captured from multiple scanning positions enhances the accuracy of DBH estimates. The fragmentation of stem slice sections due to the occlusion effects or multi-directional scanning was managed by a merging procedure that utilizes a buffer zone to define the coherence among the fragments and yields disconnected image objects. Separate image objects of smaller stem fragments are also involved into the modelling that provides comprehensive and accurate representation of tree cross-sections even in the presence of data gaps.
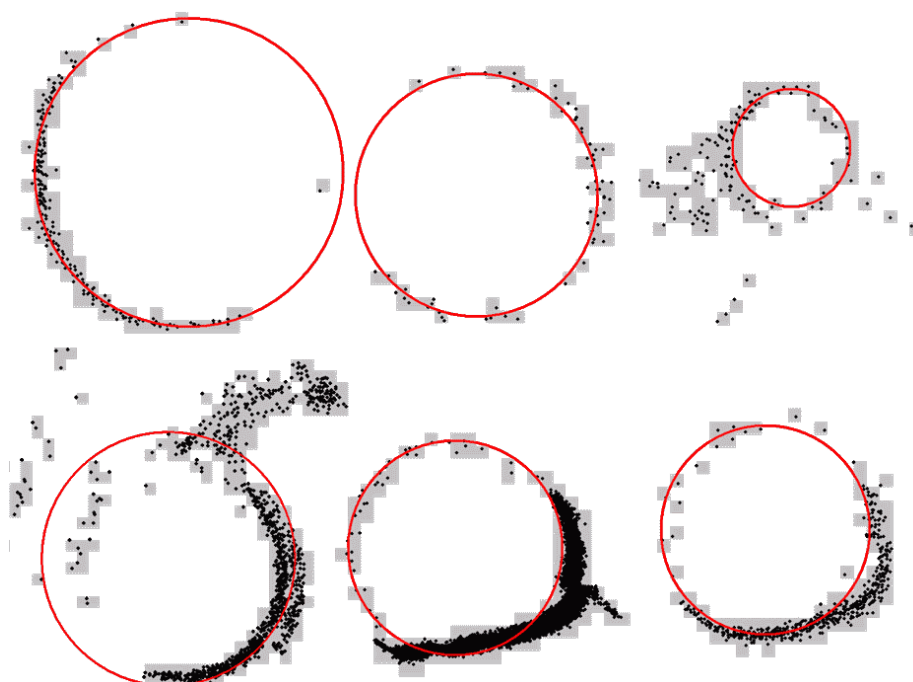
Figure 5-8. Examples on disconnected image objects identified as tree stems. (Mosaic, assembled of data from sample plot P0. Cell size: 2.5 cm)

5.2.3. Detection and modelling of mature trees in the voxel space

Voxel models hold more spatial information than classic tree maps as they present the tree structure in the vertical domain besides the stem position and attributes at a given reference height. This section is about the results of the automatic detection and architectural characteristics of the tree models. The accuracy assessment of the derived tree metrics is introduced in 5.3.2 and 5.3.3.

The outcomes of the tree detection routine are connected image objects that represent individual stems. As the image objects are contiguous, the relation between the target trees and image objects is unambiguous, thus the number of objects is equal to the number of target

trees (*Figure 5-9*). The routine detected 40 stems within the sample site H1 from the merged data of four scans. Out of 41 reference trees, the centre position of 39 stems (95%) was estimated within a horizontal tolerance of 30 cm at the reference height of 1.30 m. Two trees were omitted; both of them are thin shots sharing a common root with a larger stem. The detection of these shots was failed, as they composed of less voxels in the model space than the defined threshold. There was no misclassification; however, one tree was also detected that was not involved in the reference data as it did not exceed the minimum DBH of 10 cm.
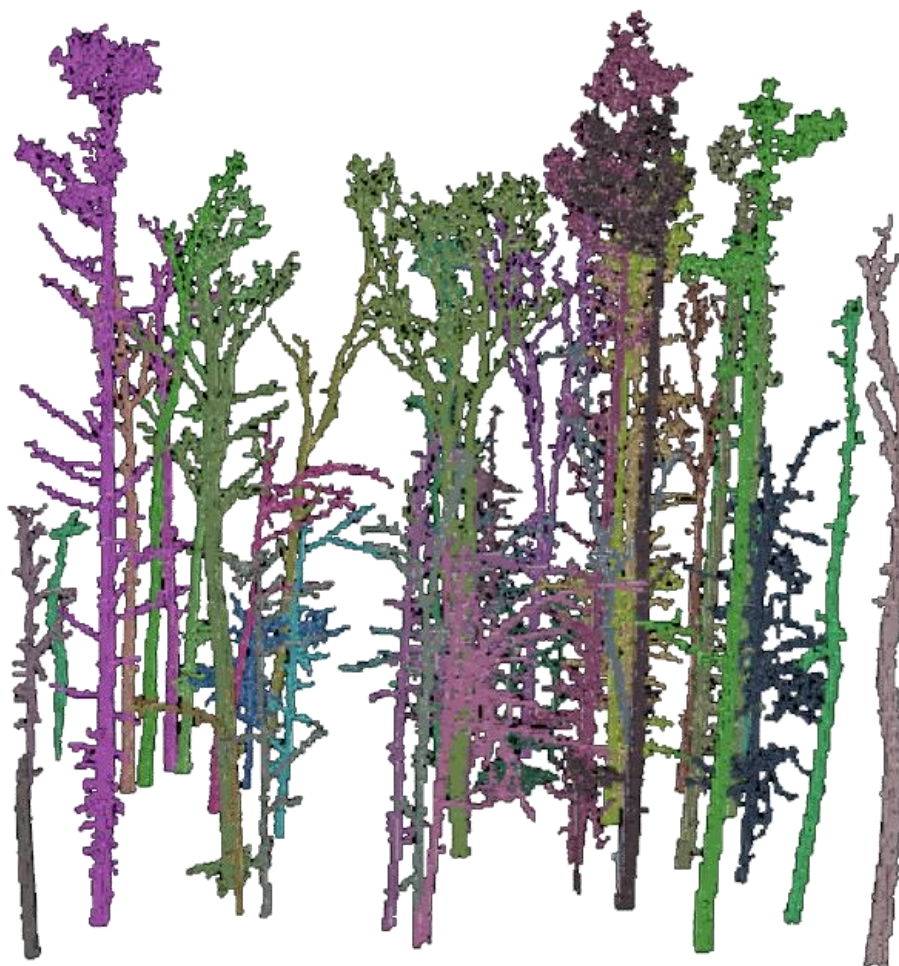
Figure 5-9. Stems were detected as connected voxel objects. (Data from sample plot H2. Perspective view. Individual objects are filled with distinct colours)

The complete tree structure, including the crown, was modelled by disconnected image objects (*Figure 5-10*). Each stem was represented by one connected image object having been extracted in the tree detection stage, to which separate objects of the crown fragments were assigned in the subsequent step. From the viewpoint of branching topology, this model is an aggregated type, namely the branches on different hierarchic levels cannot be distinguished if they are represented by a common connected image object. 73.8% of the total number of voxels could be assigned to the detected stems. Out of the 40 tree models, 25 ones being completely within the boundary of the sample plot were chosen for evaluating the distribution of voxels. The mean number of image objects composing the complete model of conifers, deciduous trees in the dominant canopy layer and deciduous trees in the lower canopy layer were 362, 501, and 127, respectively. The number of image objects depends on the tree size and the fragmentation degree of the tree model.
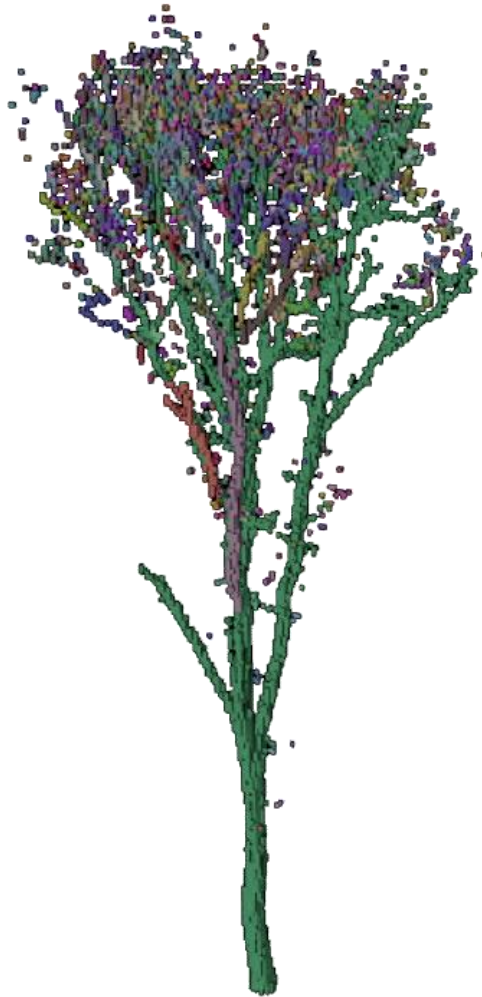
Figure 5-10. The complete model of a tree is an aggregation of many separate voxel objects, which resulted in accurate tree dimensions. (Data from sample plot H2. Perspective view. Individual objects are filled with distinct colours)

The size of the stem, crown and the complete tree is indicated by the mean counts of voxels according to the tree classes (*Figure 5-11*). Please note that the term 'size' or 'voxel counts' is related to the volume that the tree model occupies in the model space and it has to be differentiated to the tree metrics concerning tree parameter retrieval. It can be seen that the stems of the dominant trees are approximately the same size. The crown size is the half of the stems', but its proportion is slightly larger at the deciduous trees (32% against 27% with respect to the total tree size). Trees at the lower canopy layers have significantly smaller crown rate (18%). The fragmentation of the models is expressed by the mean object size i.e. the mean of the composing voxels. The most fragmented trees belong to the dominant deciduous class with 12.9 voxels per object, followed by the conifers (14.5) then the trees in the lower canopy layer (20.1). The high degree of compactness of the small trees is ascribed to the relative low crown proportion. The higher fragmentation of dominant deciduous trees in comparison to conifers may have physiological reasons: (1) The branches under leaf-less state are generally thinner and (2) The conifers have narrower and denser crown structure.

From methodological point of view, this algorithm succeeded in delineating crowns even in multi-layered stands with mixture of conifers and deciduous trees in the dominant canopy layer. The assignment of the objects representing the branches was based on the proximity of the nodal end point of the crown fragments. The validation of the models with respect to the derived tree metrics is given in 5.3.2 and 5.3.3.
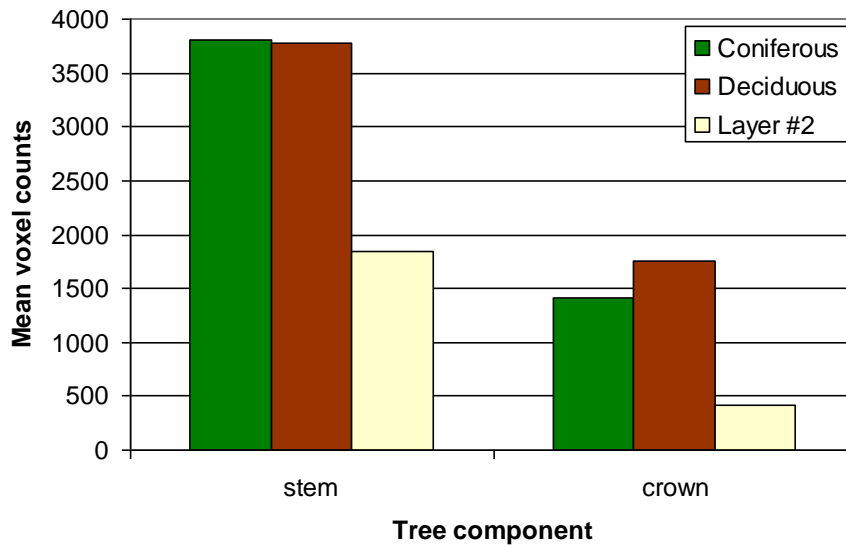
Figure 5-11. Mean voxel counts of objects according to species group and construction part

5.2.4. Detection of trees in regeneration phase

The algorithm for detecting juvenile trees provides the generalized axis of the stems, upon which the tree number within a regrowth patch can be estimated along with the location of the trees at a given reference elevation.

The generalized models are illustrated in *Figure 5-12*. The axes of the trees appear to consist of multiple objects aligned along a straight line. The tree stems are composed of the corresponding fragments as disconnected image object as a result of the aggregation procedure. In addition to the vertical ones, the algorithm managed to reconstruct the leaning trees as well.
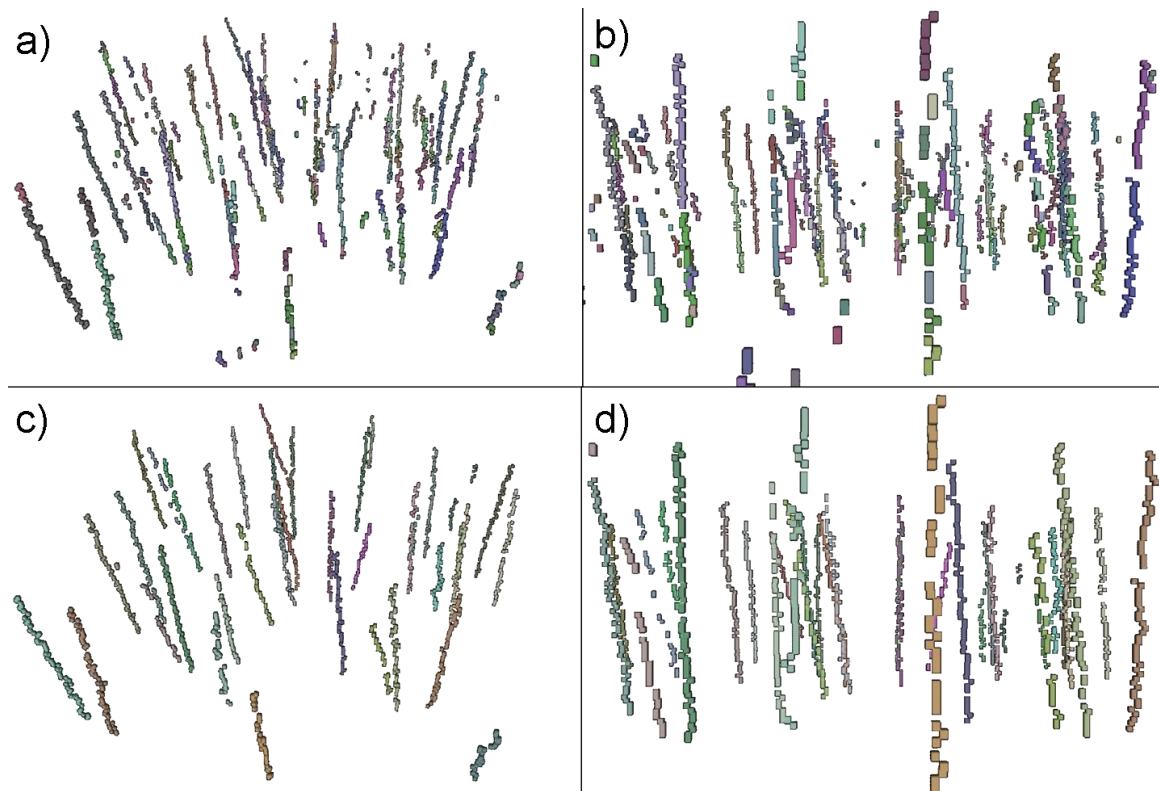
Figure 5-12. Stem fragments of juvenile trees a-b) before and c-d) followed by the aggregation procedure. (Data from sample plot P1. Perspective view)

The numbers of image objects in relation to the main stand characteristics are listed in *Table 5-2*. Tree models at the sample quadrates P1 and P2 are equally composed of 3.8 image objects in average, despite the significant difference in stem density. The maximum of object counts is 9. The models are less fragmented at the sample quadrate P3, where the stem density is moderated but the branching frequency is the highest.

Table 5-2. Relation between the degree of fragmentation and the stand characteristics.

Sample quadrate	P1	P2	P3
Detections	37	168	51
Mean object counts	3.8	3.8	2.9
Maximum object counts	9	9	8
Mean voxel counts (vertical axis)	45.4	38.8	47.7

Table 5-3 shows the comparison of tree centre estimates against the reference positions. The highest detection rate was achieved at the sample quadrate P1, where both the stem density and branching frequency was relatively low. Stem detection at sample quadrate P2 resulted in the highest rate in omission and misclassification, which confirms the assumption that the stem density has impact on the reliability. It has to be taken into account that the stem density at the sample quadrate P2 is larger by a factor of five than those at P1. In spite of this large variance, the difference in the detection rates was only 11%. As the average counts of component objects were almost the same in case of P1 and P2, the effect of stem density was reflected in the object size.

The tree detection implies regularity in the appearance of stems with respect to curvature, size and fragmentation when the image objects are assigned to each other to create complete models. The stand structure in the sample quadrate P3 is suboptimal in the sense the branching frequency is high and it could not be reduced through speckle filtering. This resulted in high degree of diversity at tree structures making the extraction of stems more complicated. With the generalization routine, each image object was thinned to its vertical axis to simplify the structure and highlight its vertical features. The detection rate of 87.9% supports that the generalization routine was effective in reducing the image objects to a one-voxel-thin axis, and the detection algorithm can be used efficiently even in case the target trees are of diverse architecture.

The detection of juvenile trees is especially challenging as the small stems are fragmented to multiple parts separated by data gaps. The tree detection was carried out with voxel-object-based concept. In order to simplify the structural diversity of the trees, the 3D objects were generalized to their vertical axis. In contrast to mature trees, the objects of stems and branches and low vegetation are of similar size, so the aggregation of the tree fragments was controlled by an iterative procedure that was optimized to result in straight, vertically extended disconnected image objects. The aggregation routine in combination with the generalization provides efficient tool to locate juvenile trees in regeneration patches even under dense stand conditions. As far as the author knows, this algorithm is the first one that supports the detection of juvenile trees in the voxel space (Brolly et al., 2011).

Table 5-3. The performance of the automatic detection of juvenile trees.

Sample quadrate	P1	P2	P3
Sample trees	41	212	58
Correct [%]	90.2	79.3	87.9
Omission [%]	9.8	20.7	12.1
Misclassification [%]	9.8	25.7	10.5

5.2.5. Comparison and combination of the tree mapping algorithms

This section approaches the challenge of stem mapping with the goal of exploring the advantages, limitations, as well as the possibilities in the synergetic use of the proposed algorithms. The use of the original point cloud seems straightforward as it ensures the highest degree of conformity with the physical surface of the target objects; consequently, it ensures the most accurate models. The point cloud based tree detection algorithm relies on the pattern of point measurements, more precisely the coherence of the point pattern and the hypothesised shape of the tree defined in parametric formula. The neighbourhood relations of the individual point measurements were disregarded. Raster algorithms delineate the fragments of vegetation through the neighbourhood relations of the cells resulting in image objects. Due to the discontinuity in the measured data, the stems are often represented by multiple image objects. The image object based stem detections include filtering of stem objects and assignment of the remaining fragments. This approach is more efficient in the presence of irrelevant isolated data than the pattern based one, as it is more convenient to specify shape properties in object level with regard to the simplified neighbourhood relations among the cells. The tree detection algorithms either locate stem centres in a constant elevation, or provide a structural model in the 3D domain. Algorithms using 2D data structure require less memory so they are proposed for surveying tree positions and stem diameter at larger area. The 3D methods have the potential for the specification of additional tree metrics such as tree height or crown projection area. As the shape of the crowns holds lower degree of symmetry as the shape of the stem cross-sections, data from multiple scanning positions are preferred for the creation of 3D tree models.

The question comes up: which tree detection method has the best performance? According to the results of the validation procedures, it can be stated that no algorithm among the proposed ones could be distinguished as superior in all respect. However, a guideline on their practical use may be suggested with regard to the complexity of stand structure.

For homogenous stands and plantations, the point cloud based clustering is recommended. The benefit of this algorithm is that it requires no gridding, and owing to the spatial indices the detection routine is time saving. It needs more parameters than the raster-based algorithms, but these have simple physical meaning so they can be tuned intuitively or followed by a quick visual exploration of the point cloud data. The clustering-based stem detection algorithm provides optimal performance where the stem diameters are in a narrow range thus the maximum cluster radius can be specified more exactly. The use of original point measurement coordinates ensures accurate tree centre positions, and stem diameter estimates. The absence of low vegetation is an important limitation of this algorithm.

Close-to-nature stands with diverse structure demand the combination of the proposed grid-based algorithms. Isolated data resulted from the low vegetation should be removed first by the raster-based filtering routine. Tree positions can be estimated for the mature trees using the raster object based stem detection. This algorithm contains a routine for filtering stem surface cells that moderate the effect of branches on DBH estimates. In case the estimation of additional tree metrics is required, subsets should be assigned, where the recording of target trees has been taken place from multiple directions. Raster objects yielded from the previous routine are compatible to voxel objects, thus they can be utilized as seed regions for the creation of 3D stem models within the subsets. Tree height and crown projection area can be estimated through the voxel models. Point measurements having been classified as mature trees cannot represent juvenile trees at the same time, thus they have to be removed from the point cloud before recreating the 3D model space of regrowth patches. Juvenile trees are detected directly in the 3D model space, which needs 3D approach to remove irrelevant data. For this reason, the use of anisotropic local filtering is recommended. The object-based detection of juvenile trees completes the proposed workflow.

5.3. Tree metrics

5.3.1. Stem diameter

Two algorithms (tree detections based on clustering and on raster image objects) provide means for assessing stem diameter at the reference height of the mapping. As the mapping elevation was identical to the so-called breast height (1.30 m above the ground), the stem diameters are referred to as DBH. The stem cross-sections were modelled by circles whose parameters were calculated by least squares adjustment. The input data for the circle fitting were the cluster points without additional filtering at the first method. The image object based stem detection includes a two-step filtering procedure, namely (1) selecting the inner bark surface cells and (2) querying stem point measurements using a ring buffer from the outer stem surface to get less biased DBH estimates.

The residual of each observation versus the corresponding reference data was calculated as follows:

$$\Delta d = d_{estimated} - d_{reference} \tag{5-1}$$

DBH estimates resulted from the stem detection algorithms were validated on distinct reference data. The main difference is that the sample plot H0 was scanned by a single instrument set up in contrast to sample site P0, which was captured from multiple scanning positions. Another relevant difference is the variation in the density of low vegetation that may adversely affect the accuracy of DBH estimates through irrelevant isolated data. The minimum stem diameter at the clustering-based method was 5 cm, while the geometric resolution of the raster limited the tree size to be detected by image objects to 10 cm. The surveying of the reference tree positions and the field measurement of the DBH were carried out separately at the sample site P0. Out of the 1110 tree positions, the DBH of 1041 were measured at the field.

Both data sets contained some outliers (gross errors) that are numerically distant from the value of other observations. Their counts are low relative to the sample size; however, they have heavy impact on the overall statistics. Most of the outlying deviations are resulted from the incomplete detection of stem surface points so these should be removed from the sample to get unbiased evaluation on the accuracy of DBH estimates. Observation errors with absolute value exceeding the triple of the standard deviation of the overall error statistics were considered as gross errors ('three-sigma rule') and they were excluded from the accuracy assessments (*Table 5-4*). This treatment of outliers is based on the investigation of Pueschel et al. (2013) that supports that the error distribution of the tree diameter estimates is quasi-normal if the cross-section is modelled through geometric circle fit of TLS data. The scatter plots of the DBH estimates against the reference data are shown in *Figure 5-13* and *Figure 5-14*. Observations outside the dashed boundary lines are outliers.

Table 5-4. Error statistics of the DBH estimates.

Sample site	H1	P0
Detection concept	Cluster based	2D image object
Outliers	5	16
Outliers [%]	3.8	1.5
Counts	128	1025
Bias [cm]	-1.3	-0.9
SD [cm]	2.1	2.5
Minimum [cm]	-6.6	-9.2
Maximum [cm]	6.3	9.4

Both methods utilized the original point measurements from the point cloud data to model the cross-section of the trees by fitted circle. The biases of the DBH estimates indicate systematic underestimation with 1.3 and 0.9 centimetres for the models achieved through the cluster based and image object based stem detection techniques respectively. It was pointed out in the study of Brolly and Király (2009a) that circles fitted to stem surface points tends to underestimate the actual stem diameter especially at trees with rough bark. This empirical observation was ascribed the fact that the stem diameter is practically measured along the outer bark surface at calliper or tape measurements, while the laser beam illuminates the rifts in the bark surface as well. Circles fitted to the point measurements are assumed to model the stem along the mid-line of the bark. There are larches with significant mixture rate in sample plot H0 having typically rough bark in their present age.
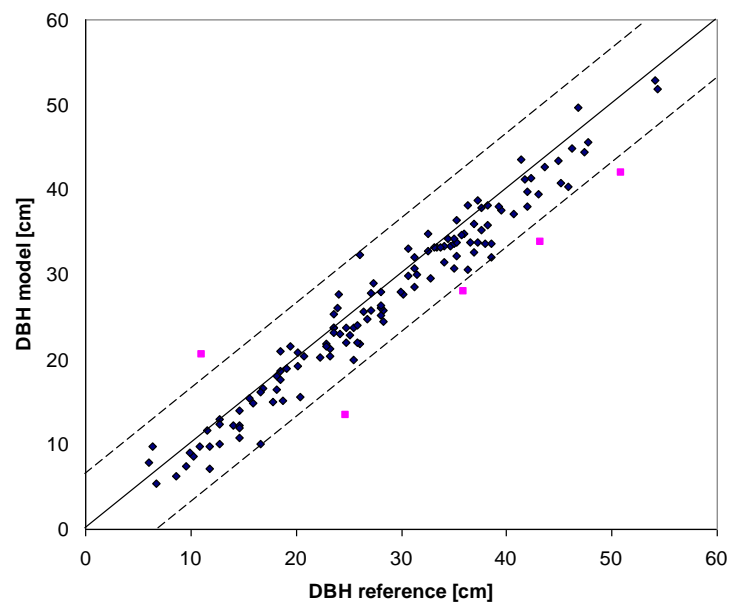
Figure 5-13. Scatter plot of DBH estimates derived from the data of sample site H1 by clustering-based stem detection against the reference measurements. Solid diagonal line depicts the 1:1 gradient. Observations outside the dashed boundary lines are outliers.
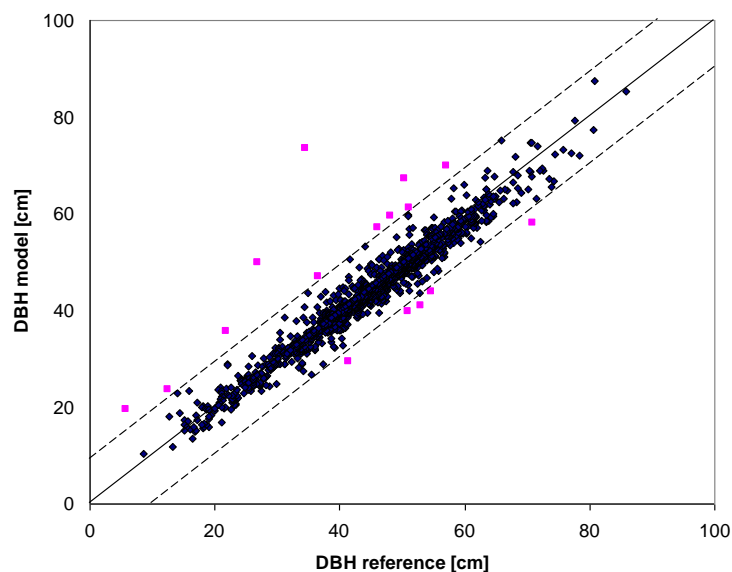
Figure 5-14. Scatter plot of DBH estimates derived from sample site P0 by image-object-based stem detection against the reference measurements. Solid diagonal line depicts the 1:1 gradient. Observations outside the dashed boundary lines are outliers.

The larger degree of DBH underestimation at this sample plot seems to confirm the relation between the DBH estimation accuracy and bark roughness. The cells representing the inner bark surface in the image objects were selected to reduce the effect of measurements reflected from other vegetation parts. This selection magnifies the bias towards the underestimation as it may disregard the cells from the outer stem surface. To quantify this systematic effect, the DBH estimation was carried out once again but using exclusively the stem surface cells as input for the circle fit. The underestimation increased by 0.5 cm indicating that the stem surface cells do not represent the whole extent of the stem cross-section. This supports the assumption that additional measurements need to be involved from the outer stem surface using the ring buffer to get less biased DBH. (*Figure 5-15*).
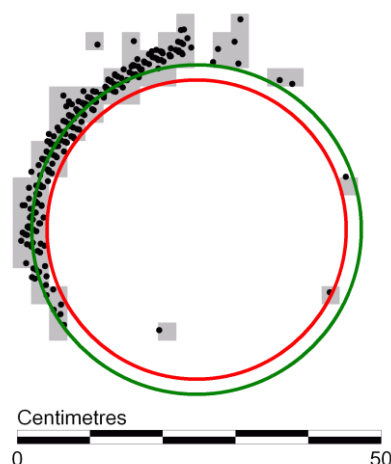
Figure 5-15. Result of circle fit using the stem surface cells (red) and the extended query of the stem point measurements (green). (Data from sample plot P0)

The estimation accuracy is quantified by the standard deviation (SD) of the residuals. In contrast to the bias, the random type error can not be eliminated by calibration so this constrains the limits of the actual application fields. The accuracy of the DBH estimates are ±2.1 and ±2.5 cm for the clustered point cloud and the image object based filtering routine, respectively. The higher SD found at the image object based method is partially ascribed to the variation in diameter increment over the two-year period between the laser scanning and the field measurements. The achieved accuracy is in agreement with previous studies as well as with those of classic devices used in the forestry practice (e.g. Bienert et al., 2007, Litkey et al, 2008, Huang et al., 2011). It should be remarked that the automatically filtered stem surface data and the fitted circles need to be submitted to visual check to ensure this level of conformity with the traditional methods.

The difference in the proportion of outliers reflects the efficiency of the filtering procedure aimed at the delineation of stem surface cells within the image objects. It is an additional benefit of the image object based method that it reloads the original measurements from the point cloud data for the DBH estimation. Stem surface points having been eliminated by unreasonable filtering are involved into the computation in this way.

5.3.2. Total tree height

Total tree heights were estimated through the voxel models created for the trees within the sample site H2. The estimates against the reference heights measured manually in the point cloud are depicted in *Figure 5-16*. The accuracy of the estimates is summarized by tree species groups and by canopy layers in *Table 5-5*. Trees at the lower canopy layer are all deciduous.
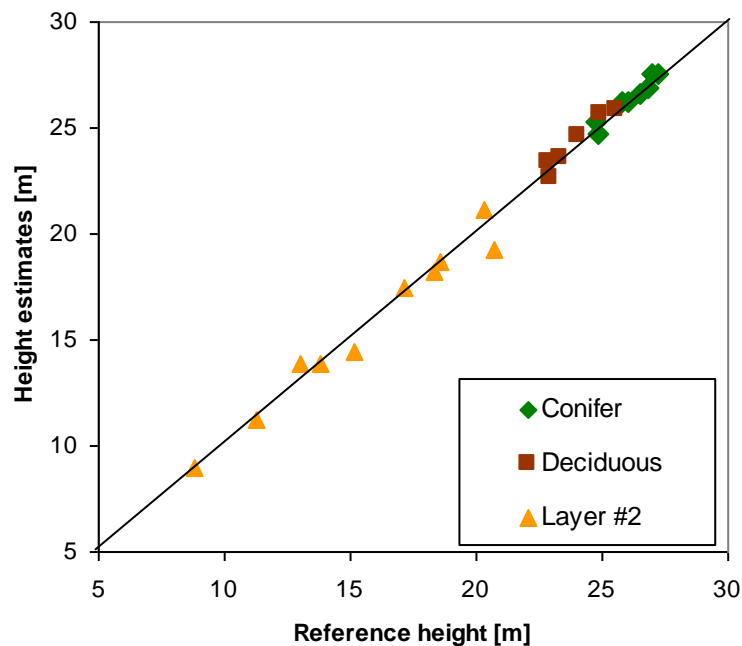
Figure 5-16. Scatter plot of total tree height estimates against the reference heights. Solid diagonal line depicts the 1:1 gradient.

Table 5-5. Descriptive statistics of the validation of tree height estimates.

Class	Canopy layer	Samples	Deviations [m]			
			Mean	SD	Min	Max
Conifer	Upper	9	0.24	0.23	-0.09	0.56
Deciduous	Upper	6	0.53	0.25	0.20	0.81
Deciduous	Lower	10	-0.11	0.62	-1.45	0.85
Total		25	0.17	0.49	-1.45	0.85

The bias of the height estimates seems negligible regarding the descriptive statistics of the complete data set. It can be pointed out that the estimates are biased towards opposing directions at the distinct canopy layers, which yields low resultant.

Estimates at the upper canopy layer tend to overestimate the actual tree height, which is quiet surprising, as the tree models do not extrapolate the crown surface beyond the point measurements. The accuracy of tree height estimates primarily depends on the accuracy of tree top location and secondary on the location of the terrain level. As the terrain is gently sloped at the sample plot H2, the difference in terrain elevation are expected to have no relevant impact on tree height estimates. Consequently, the systematic underestimation might be explained by the dissimilar tree top location technique used at the visual interpretation of reference trees. The interpretation had to consider whether an isolated point measurement above the upper region of the crown had been reflected from a branch or being data noise. As the branches are thin at the top of the canopy, partial reflection of the laser beam might be encountered in the upper region that resulted in gross errors at the laser ranging. To avoid the estimation errors caused by these ghost points, the operator at the interpretation marked the top point measurement in accordance with the crown shape. In contrast, the automated algorithm assigned the highest voxel within the maximum gap distance to the crown model disregarding its context.

The random errors in height estimates at the species groups presented in the upper canopy layer are of similar magnitude and propagate up to the 5% of the mean tree heights. The best

accuracy was achieved at the conifers being the highest members within the reference trees. This is rather unexpected, because the top of the highest trees have been sampled relative sparsely at the data acquisition as they were afar from the scanner. Moreover, these trees are mostly larches having no needles at the season of the data acquisition. It is assumed that the moderate curvature in the upper stem region along with the narrow crown shape resulted in reliable assignment of crown objects as the crown fragments were horizontally close to the stem.

The height estimates for the trees at the lower canopy layer introduce relatively small bias but the random error (62 cm) is about two times larger as in case of the dominant trees. This means that the overestimations und underestimations extinguish each other. Despite the small bias, the height estimates are less accurate for the trees at the lower canopy layer. In contrast to the dominant trees, the bias is negative that implies different kind of error sources in the estimation as it was in the upper canopy. The crowns of the subdominant trees consist of only a few branches that are too thin to be all along represented by point measurements. It has higher probability that the resulted image objects are separated by data gaps exceeding the allowed maximum gap distance. An incomplete crown model may lead to underestimates in tree height up to a magnitude of some meters. There are some overestimations as well, but they are of smaller degrees indicating that the crowns of the subdominant trees do not contain misclassified branches from the upper canopy layers. In other words, the assignment of crown fragments was reliable as the crown models are separated according to the canopy layers (*Figure 5-17*).
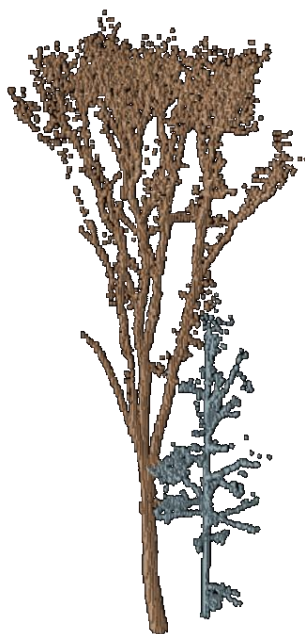
Figure 5-17. Trees from the lower canopy layers were delineated by the routine even in the presence of adjacent trees. (Data from sample plot H2. Perspective view)

5.3.3. Crown projection area

The crowns of the sample trees are located in the upper canopy layer in the sample site H2. The variation in crown projection area among the species groups is rather large as it ranges between $5.2 - 20.9$ m^2 for conifers and $11.4 - 75.9$ m^2 for deciduous trees. At such a high interspecific variation, the absolute residuals say little about the degree of conformity of the estimated crown sizes and the reference data. In order to account for the variation, the statistics of the residuals have been normalized with the average crown size of the corresponding species group yielding relative accuracy indices:

$$X_{RELATIVE} = \frac{X_{ABSOLUTE}}{A_{REFERENCE}} \cdot 100\% \qquad (5\text{-}2)$$

Where *X* denotes a given statistics of the residuals, and *A* denotes the crown projection area. The results of the crown projection area estimates in terms of absolute and relative accuracy are listed in *Table 5-6*.

The bias of the estimates regarding all the sample trees is 0.6 m^2. To give a more expressive interpretation on the measure of this area, it can be converted into linear error assuming circular crown shape, which corresponds to an overestimation of 0.39 m in crown radius. The all over relative bias implies overestimation of 12.5% at conifers, and underestimation of 2.5% at deciduous trees. The residuals of the estimates are similarly positive at the (needle-less) larch and spruce individuals denoting that the estimation of crown size of conifers is invariant under the phenological state. The scatter plot of the crown size estimates (*Figure 5-18*) points out that despite the all over underestimation of crown area, the overestimations are more frequent at deciduous trees similarly to the conifers. However, the estimate of the largest deciduous crown area introduces the maximum relative deviation of –90.4% having dominant impact on the bias of deciduous trees. This observation has not been removed as outlier from the sample because of two reasons. (1) The number of reference data is quite low. (2) Old growth deciduous trees with wide crown are underrepresented, as there are only two of them in the sample area. Discarding either would constrain the validity of the statistics to the younger age class. The modelling procedure is considered invariant to the crown size in present state, so this constrain would require reasonable geometric explanation and validation on higher samples.

The standard deviations of the residuals (SD) relative to the average crown areas are 32.0% and 44.3% for the conifers and deciduous trees respectively. It may seem unexpected that the all over SD exceeds that of both species groups with 45.7%. This is explained with the above-mentioned distance in the value of the biases between the species groups, which turned into higher SD value for the total set of samples. The highest deviations in crown projection area estimates are found to 9.2 m^2 (67.6%) for conifers and –30.4 m^2 (–90.4%) for deciduous trees.

The sum of crown projection areas is in close agreement regarding to the whole sample plot H1, as the relative difference is only 2.8%. The top view of the crown models shows realistic appearance of the higher canopy layer as the individual crowns are radially symmetric and the crown boundaries are well separated (*Figure 5-19*).

Table 5-6. Error statistics of crown projection area estimates. Relative indicators are normalized with the average crown projection area of the corresponding species group.

Class	Canopy layer	Samples	Deviations [m^2]			
			Mean	SD	Min	Max
Conifer	Upper	9	1.7	4.3	-3.0	9.2
Deciduous		6	-0.8	14.9	-30.4	9.8
Total		15	0.6	9.9	-30.4	9.8
			Relative deviations [%]			
Conifer	Upper	9	12.3	32.0	-21.9	67.6
Deciduous		6	-2.5	44.3	-90.4	29.2
Total		15	2.8	45.7	-140.8	45.4
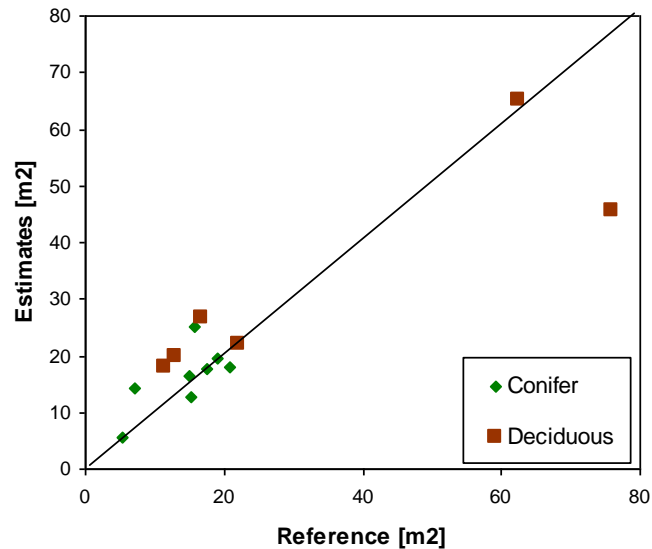
Figure 5-18. Scatter plot of horizontal crown projection area estimates against the reference measurements. Solid diagonal line depicts the 1:1 gradient.

The accuracy of the crown projection area estimates is lower as the accuracy of tree height estimates although both are crown-related metrics. The difference is partly ascribed to that the maximum gap tolerance being a substantial parameter for the crown architecture was calibrated by the tree height. From the viewpoint of the reference data, the crown delineation is less accurate conducted either with field measurements or on the screen digitization due to the occlusion of the neighbouring crowns. Nevertheless, of the moderated accuracy achieved at individual tree level, the crown projection area estimates are unbiased so the models may be useful in the assessment of plot-level canopy closure.
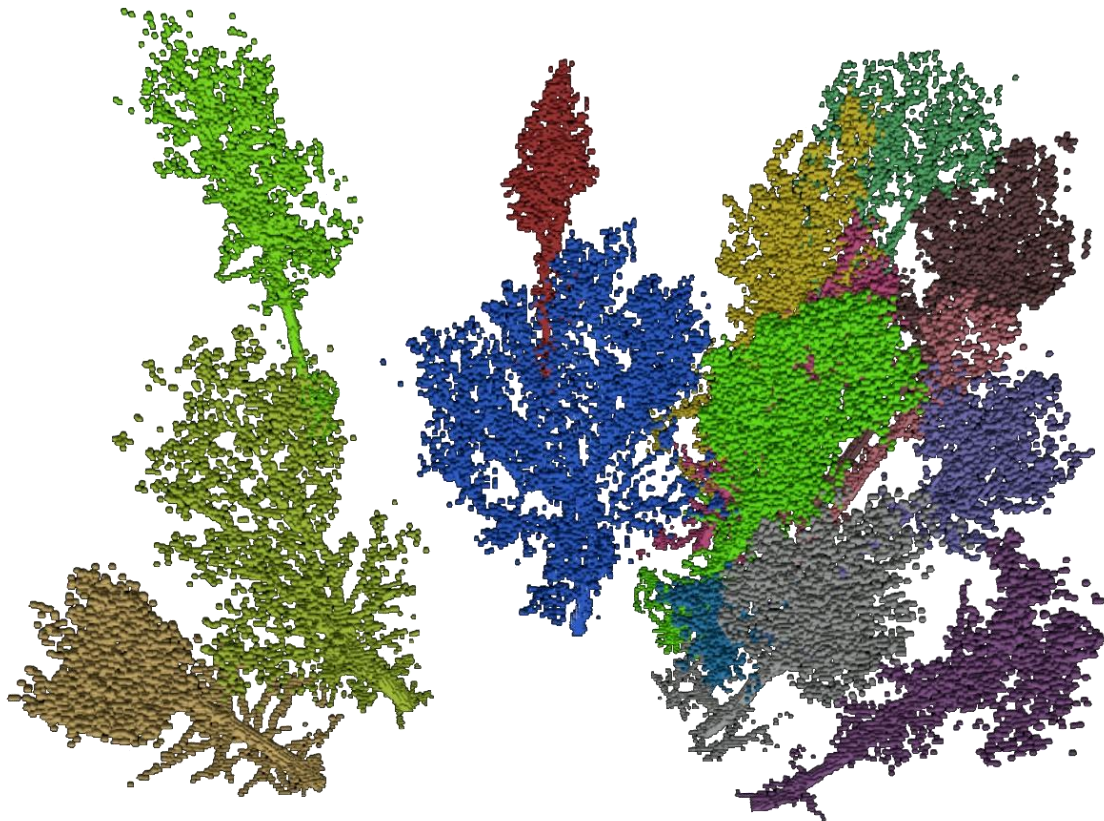
Figure 5-19. Perspective view of the tree crowns at the upper canopy layer. (Data from sample plot H2)

6. Conclusion

6.1. Potential and limitations of the algorithms

The characteristics of close-to-nature stand structures including irregular tree spacing, mixed species composition, uneven age-distribution, and multiple canopy layers make difficult to retrieve forest inventory parameters by means of classic instruments but open the door to remote sensing techniques. Specific attention was paid for that the developed estimation algorithms become powerful at processing the data of natural stands.

One of the most challenging features of the diverse stand structure is the presence of low vegetation, including trees at regeneration phase as they generate large amount of data that are irrelevant for stem mapping but make the stem detection more complicate. It has been shown that the reduction of irrelevant data has key role in suppressing the potential error sources of the subsequent tree detection. Low vegetation has additional constrain on tree detection through its shadowing effect. In order to manage the data gaps resulted from the occlusions, most of the algorithms were based on the concept of disconnected image objects, including routines for the filtering of tree fragments and for their aggregation to yield complete models.

Out of stem mapping applications with respect to mature trees, an algorithm was developed especially for the detection of juvenile trees. The image regions of juvenile trees within the regrowth patches are particularly fragmented due to the occlusion of the neighbouring low vegetation. The performance of the algorithm in term of detection rate was comparable to the results achieved at mature stands. The proposed stem detection algorithms provide automatic solutions for mapping trees from the juvenile age up to the mature state, which makes them especially suitable for surveying in stands under natural conditions such as in long-term-regeneration.

Tree height and crown projection area were estimated for both conifers and deciduous trees through complete tree models. The model creation procedure ensures reliable matching of stem positions and corresponding tree tops via the proximity-based aggregation of image objects without additional assumptions on stem straightness or crown symmetry. The routine for tree height estimates proved to be sufficient for parameter retrieval even at multi-layered stands.

The accuracy of DBH estimates and total tree height estimates were comparable to that of classic methods. The crown model is of aggregated type that means it does not account for the branch topology. The accuracy of crown projection area estimates is less than it is required for estimates at individual tree level. Although, the proposed method might be reasonable for the assessment of the mean canopy closure at a sample plot, by taking the union of the individual crown projection areas and normalizing it with the plot size.

The algorithms on parameter retrieval and even some of the stem mapping algorithms provide optimal performance followed by calibration with regard to the actual local forest state. The calibration may be carried out using in-situ field measurements on a small sample area or through acquiring reference data from visual interpretation on the point cloud. In addition to the calibration, visual assessment has further importance on the quality check of the results especially at the elimination of misclassified data and gross errors at DBH estimates.

All the algorithms are invariant under horizontal translation and rotation of the point cloud so they are appropriate for processing scans from single or multiple surveying points as well. This feature has practical value as forest inventories are based on plot-wise data capture that requires a processing method optimized for single scans, while other applications may demand surveying of trees in a comprehensive stand scanned from multiple directions.

Furthermore, neither of the stem detection algorithms requires sensor-specific parameters, which is beneficial at surveys conducted by instruments of different types or at the processing of data from time series of acquisitions. It has to be remarked that sensor parameters, especially the point density has influence on the performance of the algorithms. Nominal point density is an important parameter at the survey planning as it has influence on the number of scanning positions and, in this way, the cost of data acquisition. From the viewpoint of processing, a guideline can be given for optimising the horizontal point spacing at raster-based algorithms. Trees being represented as contiguous regions can be detected with higher reliability than those composed of separate regions. In order to avoid data gaps, horizontal point spacing below the cell size of 1–3 cm is required at the distance of the farthest tree to be detected.

6.2. Practical aspects

Terrestrial laser scans document the actual state of stand structure with explicit spatial information content and with high level of details, which allows for creating tree maps and estimate tree metrics through automatic data processing. From theoretic point of view, high accuracy and efficiency in parameter retrieval resulting from the automatic procedure assign potential for terrestrial laser scanning to be competitive with classic dendrometric devices in forest inventory applications.

From technical point of view, the instruments are still large for a person to carry over a distance of kilometres in the field. Although, the size and weight of the new instruments are keep decreasing and their usage may become more convenient in a few years. The active sensor is an important advantage of the laser scanning in comparison to close range photogrammetry, as poor light conditions under the canopy have less impact on data acquisition. Laser scanning provides directly 3D point measurements, so there is no need for using stereoscopic relations to retrieve 3D point coordinates, as is the case in photogrammetry. Moreover, the laser beam provide higher spatial resolution at long range measurements resulting in more accurate point location, which ensures larger surveying area and finer sampling in the upper crown.

From methodological point of view, the processing of laser scans can be automated on high level, therefore it is repeatable and consequently more objective than direct field measurements. Laser scanning records the complete structure of trees, from which the desired parameters are calculated through modelling and generalization. As the point cloud preserves the original state of the structure, additional parameters can be derived even some years after the data acquisition. Present thesis focused specifically on the methodological issues of using laser scanning in forested environment. The introduced algorithms have extended the possibility of the automatic processing of laser scans over semi-natural deciduous forests in the temperate zone. Many essential questions still remain open. For instance, future investigations have to find solution on how tree species can be classified using laser scanner data, how small trees and shrubs can be distinguished, how the saplings smaller than a few meters can be detected and how tree volume in the canopy can be calculated. The geometric concepts used are expected to be beneficial in the future; however, with the advent of full-waveform technique, physical-based approaches are also seem prosperous. The full-waveform information may contribute to tree species classification through the description of bark roughness and direct measurement of the reflectance properties of the vegetation surface.

From economic point of view, it is evident that the pricing of terrestrial laser scanners put limitation on the affordable use of this technique in the daily forestry practice. Accessories, data storage, regular calibration, and the license for the basic processing software further raise the costs of the technology. A comparative study on the benefits and actual costs of the

potential new technologies including TLS has not been conducted yet for forest inventory purposes. However, TLS is assumed expensive alternative of classic field surveying or even close-range photogrammetry for the retrieval of standard forest inventory parameters. Despite this constrain, the use of TLS could be reasonable in the existence of either the following conditions:

(1) Additionally to standard forest inventory parameters, such specific attributes are needed that cannot be obtained by competitive methods. These attributes are, for instance, the parameters in relation to crown structure, or the fine-scale spatial pattern of the forest regeneration.

(2) Objectivity of the data processing has priority over the costs. This is typically the case if data processing has to be exactly repeatable, for instance, in multi-level controlling of some data supply, or analysis of time series.

Now then, what are the realistic possibilities for the application of TLS technique along with the developed algorithms on tree mapping and forest parameter retrieval?

The spatially explicit information content of terrestrial laser scans might have primary importance for regional scale forest inventories based on airborne or spaceborne remote sensing techniques. Airborne laser scanning as well as satellite images need to be related to biophysical stand attributes, which requires spatially accurate ground-truth data as reference. One of the most challenging issues is the identification of reference trees in the ALS point cloud. Tree maps composed by classic field survey contain stem positions at ground level or at breast height, while the crowns delineated from the airborne data are located at the elevation of the canopy. Stems and crowns often introduce displacement making their matching ambiguous or even impossible. Tree models created from terrestrial laser scanner data could be appropriate for not only the retrieval of parameters but owing to the crown model, also for linking the ground position of the reference trees to the crowns delineated in the airborne data.

Forest monitoring is an additional possibility for the use of stem maps and tree models e.g. within the frame of Integrated Forest Monitoring System in Hungary. The main advantage of using laser scanner data is the objectivity in data capture and, in case of using automatic algorithms, the reproducibility of data processing. It is expected that a regional forest monitoring network across the European community come into existence with the goal of assessing forest health and forest estate. Establishment of a similar monitoring system on global scale has also reality for controlling the temporal changes in carbon absorption potential of forests. Through the subsidies and carbon credits, this assessment has important financial implications. In these cases, the techniques for parameter retrieval should be objective and standardized, for which the terrestrial laser scanning is prospective candidate.

The primary field of application for terrestrial laser scanning in forestry is the scientific research at the moment. Investigations on forest stand dynamics require location of stems and accurate metrics of trees at various ages under diverse site conditions. Algorithms on forest growth simulation make use of stem maps and tree models as input data with special regard to the location of juvenile trees because the competitive processes at juvenile age have especially strong impact on the stand structure in later age. Models of crown structure can be utilized for the prediction of wind spread or noise intensity in urban environment. The derived structural models are bases for realistic visualization of trees supporting also civil engineers in planning constructions within forested environment.

7. Summary

This thesis introduces the methodology and validation of proprietary computer algorithms developed to locate individual trees and obtain quantitative structural attributes by means of terrestrial laser scanner data. The algorithms have been optimised, focusing on the characteristics of the Hungarian forests with special regard to the challenges of diverse (semi-natural) stand structure. The proposed methods allow for filtering irrelevant data, detecting individual trees in the laser-scanned point cloud, modelling the tree structure in 2D and 3D space, locating the tree centre coordinates and providing estimates on biophysical attributes such as stem diameter, total tree height and horizontal crown projection area.

The stem mapping algorithms detect trees at wide range of growth state and thus are adequate for the automatic surveying of uneven-aged forests or stands under natural regeneration. Three variants for tree detection at the older growth stage (DBH>10 cm) have been introduced. The first one is a clustering technique operating on the horizontal section of the point cloud. The second – a raster-based stem detection algorithm – considers the geometric features and neighbourhood relations of disconnected image objects. The third variant produces stem models through morphologic filtering followed by simultaneous region growing in the 3D voxel domain. Trees at the age of regeneration phase (DBH<10 cm) are detected through generalized 3D image objects and their stem axes are reconstructed from fragments through an aggregation procedure.

The developed tree detection techniques are invariant under horizontal translation and rotation, so they require no auxiliary data beside the laser-scanned point coordinates such as the location of scanning positions or the nominal point spacing. They are equally appropriate for processing of single laser scans at forest inventory plots or surveying a complete forest stand from the combination of scans. Reduction of irrelevant data was achieved through local morphological operations, image pattern matching and structuring elements with anisotropic filtering effect.

Following the localization of tree positions, partial or complete models were created with the aim of deriving quantitative tree metrics. Detection techniques that locate the tree positions from two-dimensional data yield the stem diameter by modelling the stem cross section through geometric circle fit. A filtering procedure was developed that delineates the stem surface points in such a manner that it excludes the measurements from other vegetation parts and reduces the negative impact of bark roughness on DBH estimation. Complete tree models have been created in 3D grid structure, considering the proximity and neighbourhood relations of laser point measurements. The proposed technique has the ability to delineate tree crowns for both conifers and deciduous trees even in the lower canopy layers and at high canopy closure. The crown models were used for the estimation of tree height and crown projection area.

The developed algorithms were validated on terrestrial laser scans captured at a Forest Reserve and at a managed stand under natural regeneration. The filtering routines reduced the data pool by 37-87% by the elimination of irrelevant isolated measurements, which had key role in suppressing the rate of misclassifications in subsequent stem detection. In addition, the structuring element used at anisotropic filtering had an advantage in stem detection by highlighting stem surface points. In mature stands, it was possible to extract 69–77% of the trees automatically from the laser scans. The algorithm for the detection of juvenile trees in

regrowth patches succeeded in locating 79–90% of the samples. Treatment of data discontinuity is a special capability of this algorithm that enables tree detection despite data gaps caused by high stem density and heavy branching.

The DBH estimates were biased towards underestimation by 0.9 and 1.3 cm, with standard deviations of 2.5 and 2.1 cm respectively. The bias of the tree height estimates compared to the reference data obtained by visual interpretation was 0.2 meter with standard deviation of 0.5 meter. The relative bias of the crown projection area estimates was 3% with a relative accuracy of 46%. Consequently, the resulting models allow for DBH and tree height retrieval of similar accuracy as classic devices used in field practice. The method for estimation of crown projection area holds promise for the assessment of canopy closure at plot level as it introduced negligible systematic error, although it needs further improvement to be used at the individual tree level.

The algorithms deliver information on tree locations and structural metrics from terrestrial laser scanner data; visual interpretation, however, is still needed for the calibration of input parameters and for the quality control of the results. The algorithms have a potential primary in providing ground-based reference data for the calibration of airborne (spaceborne) remote sensing techniques in regional forest inventories. The created 3D tree models are prosperous for the simulations of forest growth and for the planning of construction within forested areas.

8. Thesis

1. Specific algorithms have been developed to reduce the data that are irrelevant from the viewpoint of tree mapping and modelling. The algorithms are efficient in the presence of low vegetation as well as in regrowth patches.

2. A partitioning method has been proposed for locating stem positions and DBH estimation from the horizontal section of the point cloud data. It has been proven that the algorithm is an efficient tool in the mapping of even-aged stands with sparse low vegetation.

3. A raster-based method has been developed that detects tree positions and delivers cross-sectional stem models in the presence of low vegetation following the aggregation of disconnected image objects in a two-level hierarchic structure. Geometric relations are used for selecting stem surface measurements to improve the accuracy of DBH estimates.

4. A voxel-based method has been developed for detecting and reconstructing juvenile trees in regrowth patches. The algorithm aggregates the tree fragments in the 3D voxel space through a parametric optimization procedure and delivers the tree positions and axes of stems as a disconnected set of generalized image objects.

5. An algorithm has been proposed for the creation of complete 3D structural models of conifers and deciduous trees in the voxel space. The delineation of individuals was achieved through a simultaneous region growing procedure that enables unambiguous segmentation even in case of multiple stems and high canopy closure. The models consider the data discontinuity in the upper crown region; thus, they provide an apparent basis for the estimation of tree height and crown projection area in multi-layered stands.

Acknowledgement

I would like to express my thank to

- my supervisor, Dr. Kornél Czimber for his guidance and valuable advices to the development of the algorithms
- Dr. Géza Király, who has supported this study in its all stages beginning from the project coordination, through the publications, as far as the review of the dissertation
- Dr. Tamás Lovas and Dr. László Bányai whose valuable remarks helped to improve the quality of this manuscript
- All my colleagues in the Institute of Geomatics and Civil Engineering for the peaceful and inspiring atmosphere.

I am also very grateful to Mária, Hore and Kimo for the proofreading.

Last but not least, I thank to my relatives and friends their encouragement.

Sopron, 03.05.2013

Brolly Gábor

References

AGCA, D. (2007): Least Squares 3D Surface Matching. Dissertation, Swiss Federal Institute of Technology Zurich. 92 p.

ÁLLAMI ERDÉSZETI SZOLGÁLAT (2002): Pilisszentkereszti Erdészet Erdőgazdálkodási Egység üzemterve. Állami Erdészeti Szolgálat, Budapesti Igazgatóság, Budapest.

ÁLLAMI ERDÉSZETI SZOLGÁLAT (2004): Soproni Erdészet Erdőgazdálkodási Egység üzemterve. Állami Erdészeti Szolgálat, Szombathelyi Igazgatóság, Szombathely.

ANDREW, A. M. (1979): Another Efficient Algorithm for Convex Hulls in Two Dimensions. Information Processing Letters 9: 216-219.

ASCHOFF, T. – SPIECKER, H. (2004): Algorithms for the automatic detection of trees in laser scanner data. In: Proceedings of the ISPRS working group VIII/2, "Laser-Scanners for forest and Landscape assessment". Freiburg, Germany. 3-6 October 2004. 71-75.

ASCHOFF, T. – THIES, M. – SPIECKER H. (2004): Describing forest stands using terrestrial laser-scanning. In: Proceedings of the ISPRS working group VIII/2, "Laser-Scanners for forest and Landscape assessment". Freiburg, Germany. 3-6 October 2004. 192-198.

AXELSSON, P. (2000): DEM generation from laser scanner data using adaptive TIN models. International Archives of the Photogrammetry, Remote Sensing and Spatial Information Sciences. 33 (B3/1): 119-126.

BAATZ, M. – BENZ, U. – DEHGHANI, S. – HEYNEN, M. (2004): eCognition Professional. User Guide. Definiens imaging, München, Germany. 486 p.

BAZSÓ, T. (2008): A Hidegvíz-völgy Erdőrezervátum kutatási eredményeinek térinformatikai feldolgozása. Diplomamunka, Budapesti Műszaki és Gazdaságtudományi Egyetem, Budapest. 56 p.

BENZ, U.C. – HOFMANN, P. – WILLHAUCK, G. – LINGENFELDER, I. – HEYNEN, M. (2004): Multi-resolution, object-oriented fuzzy analysis of remote sensing data for GIS-ready information. ISPRS Journal of Photogrammetry & Remote Sensing 58: 239- 258.

BERÉNYI, A. (2011): Földi lézerszkennelés mérnökgeodéziai célú alkalmazása. PhD értekezés, Budapesti Műszaki és Gazdaságtudományi Egyetem, Budapest. 103 p.

BIENERT, A. – MAAS, H. – SCHALLER, S. (2006): Analysis of information content of terrestrial laserscanner point cloud for the automatic determination of forest inventory parameters. In: "Proceedings of Workshop on 3D Remote Sensing in Forestry". Wienna, Austria. February, 2006. 44-49.

BIENERT, A. – QUECK, R. – SCHMIDT, A. – BERNHOFER, C. – MAAS H.G. (2010): Voxel space analysis of terrestrial laser scans in forests for wind field modeling. International Archives of Photogrammetry, Remote Sensing and Spatial Information Sciences. 38, (5)

BIENERT, A. – SCHELLER, S. – KEANE, E. – MOHAN, F. – NUGENT, C. (2007): Tree detection and diameter estimations by analysis of forest terrestrial laserscanner point clouds. International Archives of Photogrammetry, Remote Sensing and Spatial Information Sciences 36 (3/W52)

BIENERT, A. – SCHELLER, S. – KEANE, E. – MULLOOLY, G. – MOHAN, F. (2006): Application of terrestrial laser scanners for the determination of forest inventory parameters. International Archives of Photogrammetry, Remote Sensing and Spatial Information Sciences. 36 (5)

BROLLY, G. – CZIMBER, K. – KIRÁLY, G. (2011): Fiatalkorú faállományok voxel alapú térképezése földi lézeres letapogatás adatai alapján. In: "NYME, EMK Tudományos konferencia". Sopron, 05.10.2011. 40-45.

BROLLY, G. – KIRÁLY, G. (2009a): Algorithms for stem mapping by means of Terrestrial Laser Scanning. Acta Sylvatica et Lignaria Hungarica 5: 119-130.

BROLLY, G. – KIRÁLY, G. (2009b): Lézeres letapogatás feldolgozása erdei környezetben. In: "Erdészeti, Környezettudományi, Természetvédelmi és Vadgazdálkodási Tudományos Konferencia". Sopron, 12.10.2009. 29-34.

BROLLY, G. – KIRÁLY, G. (2010): Algorithm for individual stem mapping from terrestrial laser scanning. Proceedings of 10th International SilviLaser Conference on "LiDAR Applications for Assessing Forest Ecosystems". Freiburg, Germany, 14-17.09.2010. 641-657.

BUCKSCH, A. – FLECK, S. (2011): Automated detection of branch dimensions in woody skeletons of fruit tree canopies. Photogrammetric Engineering and Remote Sensing 77 (3): 229-240.

CORMEN, T. H. – LEISERSON, C.F. – RIVEST, R.L. (1990): Algoritmusok. Műszaki Könyvkiadó, Budapest. 884 p.

COTE, J.F. – WIDLOWSKI, J.L. – FOURNIER, R.A. – VERSTRAETE, M.M. (2009): The structural and radiative consistency of three-dimensional tree reconstructions from terrestrial lidar. Remote Sensing of Environment 113: 1067-1081.

COTE, J.F. – FOURNIER, R.A. – EGLI, R. (2011): An architectural model of trees to estimate forest structural attributes using terrestrial LiDAR. Environmental Modelling & Software 26: 761-777

CZIMBER, K. (1997): Geoinformatika. Egyetemi jegyzet, Soproni Műhely, Sopron. 110 p.

CZIMBER, K. (2009): Új, általános célú képosztályozó kifejlesztése nagyfelbontású, textúrával rendelkező digitális képek feldolgozására. Geomatikai közlemények 12: 249-259.

DANSON, F.M. – HETHERINGTON, D. – MORSDORF, F. – KOETZ, B. – ALLGÖWER, B. (2007): Forest Canopy Gap Fraction From Terrestrial Laser Scanning. IEEE Geoscience and remote sensing letters 4 (1): 157-161.

DUCEY, M. – ASTRUP, R. – SEIFERT, S. – PRETZSCH, H. – LARSON, B. – COATES, D. (2013): Comparison of forest attributes derived from two terrestrial Lidar systems. Photogrammetric Engineering & Remote Sensing 79 (3): 245-258.

ELMQVIST, M. – JUNGERT, E. – LANTZ, F. – PERSSON, A. – SÖDERMAN, U. (2001): Terrain Modelling And Analysis Using Laser Scanner Data. International Archives of Photogrammetry and Remote Sensing 34 (3/W4): 219-226.

FOGARAS, A. – LUKÁCS, A. (2005): Klaszterezés. In: IVÁNYI, A. (ed): Informatikai algoritmusok 2. ELTE Eötvös Kiadó, Budapest. 1397-1423.

FRÖHLICH, C. – METTENLEITER, M. (2004): Terrestrial laser scanning - new perspectives in 3d surveying. International Archives of Photogrammetry and Remote Sensing 36 (8/W2): 7-14.

GORTE, B. – PFEIFER, N. (2004): Structuring laser-scanned trees using 3d mathematical morphology. ISPRS- International Archives of Photogrammetry, Remote Sensing and Spatial Information Sciences. Vol 35, Part B 39-45.

HAALA, N. – REULKE, R. – THIES, M. – ASCHOFF, T. (2004): Combination of terrestrial laser scanning with high resolution panoramic images for investigations in forest applications and tree species recognition. Proceedings of the ISPRS working group V/1, "Panoramic Photogrammetry Workshop". Dresden, 19-22 Feb. Vol 34, Part 5/W16.

HENNING, J.G. – RADTKE, P.J. (2006a): Detailed Stem Measurements of Standing Trees from Ground-Based Scanning Lidar. Forest Science 52 (1): 67-80.

HENNING, J. G. – RADTKE P. J. (2006b): Ground-based laser Imaging for Assessing Three-dimensional Forest Canopy Structure. Photogrammetric Engineering and Remote Sensing 72 (12): 1349-1358.

HENNING, J.G. – RADTKE, P.J. (2007): Multiview range-image registration for forested scenes using explicitly-matched tie points estimated from natural surfaces. ISPRS Journal of Photogrammetry and Remote Sensing 63: 68-83.

HENRICI, P. (1985): Numerikus analízis. Műszaki Könyvkiadó, Budapest. 366 p

HOPKINSON, C. – CHASMER, L. – YOUNG-POW, C. – TREITZ, P. (2004): Assessing forest metrics with a ground-based scanning LIDAR. Canadian Journal of Forest Research. 34: 573-583.

HORVÁTH, F. – BIDLÓ, A. – HEIL, B. – KIRÁLY, G. – KOVÁCS, G. – MÁNYOKI, G. – MÁZSA, K. – TANÁCS, E. – VEPERDI, G. – BÖLÖNI, J. (2012): Abandonment status and long-term monitoring of strict forest reserves in the Pannonian biogeographical region, Plant Biosystems - An International Journal Dealing with all Aspects of Plant Biology: Official Journal of the Societa Botanica Italiana, DOI:10.1080/11263504.2011.650728: 1-12

HUANG, H. – LI, Z. – GONG, P. – CHENG, X. – CLINTON, N. – CAO, C. – NI, W. – WANG, L. (2011): Automated methods for measuring DBH and tree heights with a commercial scanning lidar. Photogrammetric Engineering and Remote Sensing 77 (3): 219-229.

HUSCH, B. – BEERS, T. – KERSHAW, J.A. (2003): Forest mensuration. Fourth edition, John Wiley & Sons, Inc, Hoboken, New Jersey. 439 p.

JAIN, R. – KASTURI, R. – SCHUNCK, B.G. (1995): Machine Vision. McGraw-Hill, Inc., ISBN 0-07-032018-7; 549 p.

KIRÁLY, G. (2006): ERDŐ+h+á+l+ó létesítése a Hidegvíz-völgy Erdőrezervátum magterületén és a védőzóna kiválasztott területein. MTA ÖBKI. Report (with map). p. 3

KIRÁLY, G. – BROLLY, G. – MÁRKUS, I. (2007): Földi lézerszkenning alkalmazása egyesfák vizsgálatára. Geomatikai közlemények 10: 241-251.

KIRÁLY, G. – BROLLY, G. (2007): Tree height estimation methods for terrestrial laser scanning in a forest reserve. International Archives of Photogrammetry, Remote Sensing and Spatial Information Sciences. 36 (3/W52): 211-215.

KIRÁLY, G. – BROLLY, G. (2008): Modelling single trees from terrestrial laser scanning data in a forest reserve. The Photogrammetric Journal of Finland 21 (1): 37-50.

KIRÁLY, G. – BROLLY, G. (2010): Volume calculations of single trees based on terrestrial laser scanning. Proceedings of 10th International SilviLaser Conference on "LiDAR Applications for Assessing Forest Ecosystems". Freiburg, Germany, 14-17.Sep.2010. 629-640.

KISS, B. (2009): Geodéziai előkészítő munkálatok lézeres felméréshez a Pilisszentlélek 25A Pro Silva Bemutató Területen. MSc Thesis, University of West Hungary, Sopron. 57 p.

KRAUS, K. – PFEIFER, N. (1998): Determination of terrain models in wooded areas with airborne laser scanner data. ISPRS Journal of Photogrammetry & Remote Sensing 53: 193-203.

KU, N.W. – POPESCU, S.C. – ANSLEY, J.R. – HUMBERTO, P.L. – FILIPPI, A.M. (2012): Assessment of available rangeland woody plant biomass with a terrestrial LIDAR system. Photogrammetric Engineering and Remote Sensing 78 (4): 349-361.

LÉBER, A. (2012): Megalapozó faállomány-szerkezeti vizsgálatok a Pilisi Parkerdő Zrt. Pilisszentkereszti Erdészetének területén lévő szálaló erdőben. Diplomamunka, Sopron. 65 p.

LITKEY, P. – LIANG, X. – KAARTINEN, H. – HYYPPÄ, J. – KUKKO, A. – HOLOPAINEN, M. (2008): Single-scan TLS methods for forest parameter retrieval. In: Proceedings of SilviLaser 2008, 8th international conference on LiDAR applications in forest assessment and inventory, Heriot-Watt University, Edinburgh, UK, 17-19 September, 2008. 295-304.

LOVAS, T. – BERÉNYI, A. – BARSI, Á. – DUNAI, L. (2009): Földi lézerszkennerek alkalmazhatósága mérnöki szerkezetek deformáció mérésében. Geomatikai közlemények 12: 281-291.

LOVAS, T. – BERÉNYI, A. – BARSI, Á. (2012): Lézerszkennelés. Terc Kiadó, Budapest. 166 p.

MANDLBURGER, G. (2005): Derivation of Terrain Models from ALS data. Lecture notes. "University Course Laser scanning - Data acquisition and Modeling." Vienna, Feb. 2005.

MCGAUGHEY (2010): Fusion/LDV Software (Version 2.90) for LIDAR Data Analysis and Visualization. United States Department of Agriculture. 154 p.

MOKOS, B. (2008): Felmérési módszerek alkalmazása az erdőrezervátum kutatásban. Diplomamunka, Budapesti Műszaki és Gazdaságtudományi Egyetem, Budapest. 35 p.

PFEIFER, N. (2007): Overview of TLS systems, overall processing and applications. Presentation: ISPRS Summer school "Theory and Application of Laser Scanning". Ljubljana, Slovenia.

PFEIFER, N. – BRIESE, C. (2007): Laser Scanning - Principles and Applications. "III Geo-Sibir International Scientific Confernece". Nowosibirsk, 25-27 April 2007. ISBN: 978-5-87693-229-7; 93-112.

PFEIFER, N. – GORTE, B. – WINTERHALDER, D. (2004): Automatic reconstruction of single trees from terrestrial laser scanner data. ISPRS- International Archives of Photogrammetry, Remote Sensing and Spatial Information Sciences. 35 (B): 114-119.

PiLINE Kft (2006): Sopron - két erdei mintaterület (05_11 és 08_10 pont) lézerszkenneres felmérése és feldolgozása. Műszaki leírás, 10 p.

PiLINE Kft (2009): 3D lézerszkenneres felmérés és feldolgozása a Pilis hegység - Pro Sylva erdei mintaterületen. Műszaki leírás, 5 p.

PRO SILVA (2012): Pro Silva Principles. Pro Silva Europe. 69 p.

PUESCHEL, P. – NEWNHAM, G. J. – ROCK G. – UDELHOVEN, T. – WERNER, W. – HILL, J. (2012): The influence of scan mode and circle fit algorithms on the extraction of stem diameter and volume from TLS data. Proceedings of SilviLaser 2012., Vancouver, Canada, 16-19 September 2012. 148-156.

PUESCHEL, P., NEWNHAM, G., ROCK, G., UDELHOVEN, T., WERNER W., HILL, J. (2013): The influence of scan mode and circle fitting on tree stem detection, stem diameter and volume extraction from terrestrial laser scans. ISPRS Journal of Photogrammetry and Remote Sensing 77 (1): 44–56.

RESHETYUK, Y. (2007): Self-calibration and direct georeferencing in terrestrial laser scanning. Doctoral thesis in Infrastructure, Geodesy. Royal Institute of Technology, Stockholm. 174 p.

SCHILLING, A. – SCHMIDT, A. – MAAS, H.-G. (2011): Automatic Tree Detection and Diameter Estimation in Terrestrial Laser Scanner Point Clouds. In: "Proceedings of the 16th Computer Vision Winter Workshop". Mitterberg, Austria, 2011. 75-83.

SCHILLING, A. – SCHMIDT, A. – MAAS, H-G (2012): Tree topology representation from TLS point clouds using depth-first search in voxel space. Photogrammetric Engineering and Remote Sensing 78 (4): 383-392.

SIMONSE, M. – ASCHOFF, T. – SPIECKER, H. – THIES, M. (2003): Automatic determination of forest inventory parameters using terrestrial laser scanning. In: "Proceedings of the ScandLaser Scientific Workshop on Airborne Laser Scanning of Forests". Umea, Sweden. 2-4 September, 2003. 271-257.

SOILLE, P. – VOGT, P. (2009): Morphological segmentation of binary patterns. Pattern Recognition Letters 30 (4): 456-459.

SOININEN, A. (2005): TerraScan User's Guide. Terrasolid Ltd, Finland. 169 p.

SOPP, L. (Ed., 1974): Fatömegszámítási táblázatok fatermési táblákkal. Mezőgazdasági Kiadó, Budapest. 420 p.

STRAHLER, A.H. – JUPP, D.L.B - WOODCOCK, C.E. – SCHAAF, C.B. – YAO, T. – ZHAO, F. – YANG, X. – LOVELL, J. – CULVENOR, D. – NEWNHAM, G. – NI-MIESTER, W. – BOYKIN-MORRIS, W. (2008): Retrieval of forest structural parameters using a ground-based lidar instrument 'Echidna®'. Canadian Journal of Remote Sensing 34: 426-440.

THIES, M. – PFEIFER, N. – WINTERHALDER, D. – GORTE, B. (2004): Three-dimensional reconstruction of stems for assessment of taper, sweep and lean based on laser scanning of standing trees. Scandinavian journal of forest research 19: 571-581.

THIES, M. – SPIECKER, H. (2004): Evaluation and future prospects of terrestrial laser scanning for standardized forest inventories. In: Proceedings of the ISPRS working group VIII/2, "Laser-Scanners for forest and Landscape assessment". Freiburg, Germany. 3-6 October 2004. 192-198.

VITÁLIS, A. – ZAKARIÁS, É. (2005): A Hidegvíz-völgy Erdőrezervátum faállomány-szerkezeti felvétele és vizsgálata. Diplomamunka, Nyugat-magyarországi Egyetem, Sopron. 75 p.

VOSSELMAN, G. (2000): Slope Based Filtering of Laser Altimetry Data. International Archieves of Photogrammetry and Remote Sensing 33 (B3/2): 935-942.

WAGNER, W. (2005): Physical principles of airborne laser scanning. Lecture notes. "University Course Laser scanning - Data acquisition and Modeling." Vienna, Feb. 2005. 40 p.

WATT, P.J. – DONOGHUE, D.N.M. (2005): Measuring forest structure with terrestrial laser scanning. International Journal of Remote Sensing 26 (7): 1437-1446.

WEINACKER, H. – KOCH, B. – WEINACKER, R. (2004): TreesVis - A Software System for Simultanious 3D-Real-Time Visualization of DTM, DSM, Laser Row Data, Multispectral Data, Simple Tree and Building Models. International Archives of Photogrammetry and Remote Sensing 36 (8/W2): 90-96.

WEZYK, P. – KOZIOL, K. – GLISTA M. – PIERZCHALSKI, M. (2007): Terrestrial laser scanning versus traditional forest inventory first results from the polish forests. ISPRS Workshop on Laser Scanning and SilviLaser, Espoo, Finland, September 12-14.

WULDER, M. – HANA, T. – WHITEA, J. – SWEDAB, T. – TSUZUKI, H. (2007): Integrating profiling LIDAR with Landsat data for regional boreal forest canopy attribute estimation and change characterization. Remote Sensing of Environment 110 (1): 123-137.

ZÁVOTI, J. (2001): A geodézia korszerű matematikai módszerei. Geoamtikai közlemények II. MTA Geodéziai és Geofizikai Kutató Intézet, Sopron. 149 p.

http://www.leica-geosystems.com/en/HDS7000_90337.htm (accessed: Dec., 2012)

http://www.riegl.com/nc/products/terrestrial-scanning/produktdetail/product/scanner/5/ (accessed: Dec., 2012)

http://www.riegl.com/products/terrestrial-scanning/produktdetail/product/scanner/4/ (accessed: Dec., 2012)

List of figures

List of tables